

CRANFIELD UNIVERSITY

School of Engineering

Group Design Project

Academic Year: 2019-2020

Barcelo, Marc - Maldonado, Julio - Moudir, Erwan - Valade,  
Léa - Warnakulasuriya, Tharindu

**Fluid-Structural Analysis with Finite Element Modelling  
of an Aircraft Wing**

Supervisor(s):

Dr. László Könözsy

© Cranfield University, 2020.  
All rights reserved. No part of this publication may be reproduced  
without the written permission of the copyright holder.

Except where acknowledged in the customary manner, the material presented in this thesis is, to the best of our knowledge, original and has not been submitted in whole or part for a degree in any university.

# Abstract

In this research project, the Fluid Structure Interaction problem for the Onera M6 wing in a transonic flow is investigated. The Onera M6 wing geometry is chosen because it is a common validation test case in the aerospace industry. In this study, two CAD models of the Onera M6 wing are used. One model is taken from Grabcad. The structure of this CAD model is only composed of the skin. The second model is designed in CATIA V5 and has structural elements such as ribs and spars in addition to the skin. To validate our CAD models, the numerical results of the Onera M6 wing are presented and compared with results found in the literature. Several RANS turbulence models are used for this Fluid Structure Interaction problem: the Spalart-Allmaras, the standard  $k-\varepsilon$ , the realizable  $k-\varepsilon$ , the standard  $k-\omega$  and the SST  $k-\omega$ . The flow problem is solved in ANSYS-FLUENT and combined with the structural problem. Then it's solved with the finite element code ANSYS-WORKBENCH for the only skin-CAD and in ABAQUS for the self-designed CAD. For the structural problem different types of analysis are performed: a static structural analysis (total deformation, equivalent stress, equivalent strain), a modal analysis (natural frequencies, mode shape), an eigenvalue buckling analysis (buckling factor) and a transient dynamic analysis. For these analyses, each turbulence model and several materials commonly used in the aerospace industry are tested for the Onera M6 wing skin: the Al 2024 T3, the Epoxy Carbon UD and the Epoxy S-Glass. Satisfactory results have been achieved through this study that could be helpful in future investigations.

# Acknowledgements

We would like to thank Dr. László Könözsy, our supervisor who provided good advice and encouraged us all during this project. He was available and helped us keep on the right track but also granted us much autonomy.

We are grateful to the Cranfield University that allowed us to do this Group Design Project and for providing us access to research works.

We also want to thank Michael Emeribe who provided a literature review during the preliminary part of this work.

# Contents

<b>Abstract</b>	<b>v</b>
<b>Acknowledgements</b>	<b>vi</b>
<b>List of Figures</b>	<b>xii</b>
<b>List of Tables</b>	<b>xiii</b>
<b>Abbreviations</b>	<b>xiv</b>
<b>Symbols</b>	<b>xvi</b>
<b>1 Introduction</b>	<b>1</b>
1.1 Background and Motivation . . . . .	1
1.2 Problem Statement . . . . .	2
1.3 Structure of the M.Sc. Thesis . . . . .	2
1.4 Literature Review . . . . .	3
<b>2 Theory fundamentals</b>	<b>7</b>
2.1 Governing Equations (Julio) . . . . .	7
2.1.1 Flow Dynamics Governing Equations . . . . .	7
2.1.2 Structural Governing Equations . . . . .	9
2.2 Structural Problem (Léa, Erwan) . . . . .	11
2.2.1 Static Analysis . . . . .	12
2.2.2 Modal Analysis . . . . .	14
2.2.3 Buckling Analysis . . . . .	15
2.2.4 Transient Dynamic Analysis . . . . .	18
2.3 Aerodynamic Flow Problem (Marc) . . . . .	19
2.3.1 Turbulence Modelling . . . . .	21
2.3.1.1 Spalart-Allmaras model (Léa, Erwan) . . . . .	22
2.3.1.2 k- $\varepsilon$ turbulence models (Léa, Erwan) . . . . .	23

2.3.1.3	Wilcox's standard k - $\omega$ (Julio)	25
2.3.1.4	Shear Stress Transport k - $\omega$ (Marc)	26
<b>3</b>	<b>Simulation Setup</b>	<b>30</b>
3.1	Physical Problem (Marc)	30
3.2	Aircraft characteristics - ONERA M6 Wing (Marc)	31
3.2.1	CAD Modelling (Julio)	33
3.3	FEM Modelling	35
3.3.1	Motivation and Definition of Finite Element Methods (Marc)	35
3.3.2	Elements (Marc)	37
3.3.2.1	1-D Elements	37
3.3.2.2	2-D Elements	37
3.4	Boundary conditions (Marc)	39
3.5	Applied Loads (Marc, Julio)	39
3.6	ANSYS-FLUENT Setup (Marc)	41
3.7	ANSYS-Workbench Setup (Léa, Erwan, Marc)	43
3.8	ABAQUS Setup (Julio)	44
<b>4</b>	<b>Results</b>	<b>49</b>
4.1	Materials (Marc)	49
4.2	Coarse Mesh. Validation and Verification of the Results (Marc)	50
4.2.1	Flow Problem	50
4.2.2	Structural Problem	58
4.2.2.1	Static Analysis	58
4.3	Grid Convergence Study (Léa, Erwan, Marc)	65
4.4	Only Skin CAD	68
4.4.1	Static Analysis (Léa, Erwan)	68
4.4.2	Modal Analysis (Léa, Erwan)	69
4.4.3	Buckling Analysis (Marc)	72
4.4.4	Transient Dynamic Analysis (Tharindu)	77
4.5	Loading analysis (Tharindu)	80
4.6	Self-designed CAD (Julio)	84
4.6.1	Static Analysis (Julio)	84
4.6.1.1	Aluminium 2024 T3	84
4.6.1.2	Epoxy-Carbon unidirectional (UD)	87
4.6.1.3	Epoxy E-Glass	87
4.6.1.4	Epoxy S-Glass	88
4.6.2	Modal Analysis (Julio)	89
4.6.3	Buckling Analysis (Julio)	91

<b>5 Conclusions</b>	<b>94</b>
<b>6 Future Work (Marc, Julio)</b>	<b>98</b>
<b>Bibliography</b>	<b>100</b>
<b>7 Appendix</b>	<b>106</b>
7.1 Appendix 1: Individual Contribution . . . . .	106
7.2 Appendix 2: Materials (Marc) . . . . .	110
7.2.1 Aluminium 2024 T3 . . . . .	110
7.2.2 Composite Materials . . . . .	111
7.2.2.1 Epoxy-Carbon UD . . . . .	113
7.2.2.2 Epoxy-Glass . . . . .	114
7.3 Appendix 3: Wing Drawings (Julio) . . . . .	115

# List of Figures

2.1	Wing Structure (Venkatesan et al.,2018) . . . . .	11
2.2	Stress strain Diagram of a mild steel beam element (SIMSCALE) . . . . .	12
2.3	Stress strain Diagram of a AL2024-T3 (Gunes,R and Arslan, K, 2016) . .	13
2.4	Static structural analysis results (Das, S K and Roy, S, 2018) . . . . .	14
2.5	Comparison of the stress behaviour with different materials of buckling load factor for the conventional wing. (Ravi Kumar B, 2018) . . . . .	17
2.6	Deformation angle of the wing around the Z axis (Xueyan Zhang et al.,2018)	19
3.1	ONERA M6 Wing geometry definition . . . . .	32
3.2	ONERA M6 CAD - Inner Structure . . . . .	34
3.3	ONERA M6 CAD - Skin . . . . .	34
3.4	Triangular Lift Scheme . . . . .	40
3.5	ANSYS simulation scheme: inheritance of values for the FSI problem .	44
3.6	Inner structure mesh generated with Abaqus . . . . .	45
3.7	Skin mesh generated with Abaqus . . . . .	46
4.1	Residuals of the turbulence models . . . . .	51
4.2	Static Pressure Distribution along the wing . . . . .	52
4.3	Static Pressure Distribution for the 3 selected sections . . . . .	53
4.4	Q criterion of value $197565\ s^{-2}$ to represent the wingtip vorticity for the SST and Spalart-Allmaras turbulence models . . . . .	53
4.5	Validation of the airfoil in $z= 60\ %$ of the wing with experimental values from [1] . . . . .	54
4.6	Mach Contours in medium section, $Z=50\%$ . . . . .	55
4.7	Static pressure distribution along the ONERA M6 wing . . . . .	57
4.8	Coarse Mesh for the Structural Analysis . . . . .	59
4.9	Imported Pressure from the CFD . . . . .	59
4.10	Pressure distribution along the AGARD 445.6 wing from [2] . . . . .	60
4.11	Total Deformation of the ONERA M6 Coarse mesh for Al 2024 T3 . . .	61
4.12	Equivalent stress of the ONERA M6 Coarse mesh for Al 2024 T3 . . .	62

4.13	Equivalent Elastic Strain of the ONERA M6 Coarse mesh for Al 2024 T3	63
4.14	Refinement of factor 5 to the whole structural domain (skin) . . . . .	63
4.15	Static Results for the SST $k-\omega$ FSI interaction with fine mesh, Al 2024 T3 alloy . . . . .	64
4.16	Norms of the deviations between the turbulence models for the Total Deformation . . . . .	65
4.17	Chosen points to conduct the Grid Convergence Study, Fine Mesh . . . . .	67
4.18	First six modes for the SST $k - \omega$ with the Al 2024-T3 . . . . .	72
4.19	Buckling Modes: Total Deformation plot for the SST $k - \omega$ , Al 2024-T3	75
4.20	Buckling Modes: Total Deformation plot for the SST $k - \omega$ , Epoxy S-Glass	76
4.21	AL 2024 T3 (left) and S-glass (Right) produced Total deformation of Transient analysis . . . . .	79
4.22	AL 2024 T3 and S-glass produced by von-Mises stress of Transient analysis	79
4.23	AL 2024 T3 (left) and S-glass (Right) produced von-Mises strain of Transient analysis . . . . .	79
4.24	von Mises Stress (Left) and displacements (Right) produced by punctual load load AL 2024 T3 . . . . .	80
4.25	von Mises Stress (Left) and displacements (Right) produced by distributed load AL 2024 T3 . . . . .	81
4.26	von Mises Stress (Left) and displacements (Right) produced by triangular load AL 2024 T3 . . . . .	81
4.27	von Mises Stress (Left) and displacements (Right) produced by triangular load Carbon Epoxy UD . . . . .	82
4.28	von Mises Stress (Left) and displacements (Right) produced by triangular load Epoxy E-glass . . . . .	83
4.29	von Mises Stress (Left) and displacements (Right) produced by triangular load Epoxy S-glass . . . . .	83
4.30	von Mises Stress (Left) and displacements (Right) produced by punctual load for Al 2024 T3 . . . . .	85
4.31	von Mises Stress (Left) and displacements (Right) produced by Uniform load for Al 2024 T3 . . . . .	85
4.32	von Mises Stress (Left) and displacements (Right) produced by triangular load for Al 2024 T3 . . . . .	86
4.33	von Mises Stress (Left) and displacements (Right) produced by triangular load for Epoxy-Carbon UD . . . . .	87
4.34	von Mises Stress (Left) and displacements (Right) produced by triangular load for Epoxy E-Glass . . . . .	88

4.35 von Mises Stress (Left) and displacements (Right) produced by triangular load for Epoxy S-Glass . . . . .	88
4.36 Deformations of first modes of Modal Analysis for aluminium alloy . . . .	91
4.37 Deformations of first modes of Buckling Analysis for aluminium alloy . .	93
7.1 Aviation materials evaluated in specific modulus and strength. Source: [3]	112

# List of Tables

2.1	Results of the modal analysis (El Maani et al.,2016) . . . . .	15
3.1	Wing geometry aerodynamic parameters . . . . .	33
3.2	Flow parameters setup . . . . .	42
3.3	Numerical definition of the flow solver . . . . .	43
4.1	Mechanical properties of the materials to be evaluated . . . . .	50
4.2	Configuration of the coarse mesh for the flow domain . . . . .	50
4.3	Grid Convergence Study . . . . .	67
4.4	Static structural results for the Aluminium 2024 T3 . . . . .	68
4.5	Static structural results for the Epoxy-Carbon UD . . . . .	68
4.6	Static structural results for the Epoxy S-Glass . . . . .	68
4.7	Worst case scenario for the static structural . . . . .	69
4.8	Natural frequency (Hz) of the wing for each turbulence model assessed and wing material . . . . .	70
4.9	Maximum amplitude of vibration (mm) for each mode shapes for each turbulence model assessed and wing material . . . . .	70
4.10	Buckling Load Factor for each turbulence model assessed and wing material	73
4.11	Transient analysis maximum total deformation . . . . .	77
4.12	Transient analysis maximum stress . . . . .	78
4.13	Transient analysis maximum strain . . . . .	78
4.14	AL 2024 T3 results on Punctual, Distributed, Triangular loads . . . . .	82
4.15	Triangular loading on 4 different materials . . . . .	84
4.16	Static analysis results comparison with different load approximations . . .	86
4.17	Static analysis results comparison with each material for triangular loads .	89
4.18	Natural frequencies (Hz) of the wing for each material . . . . .	90
4.19	Buckling Load Factor for each wing material . . . . .	92

# Abbreviations

<b>2D</b>	Two Dimensions
<b>3D</b>	Three Dimensions
<b>AoA</b>	Angle of Attack
<b>BC</b>	Boundary Conditions
<b>BF</b>	Buckling Factor
<b>CAD</b>	Computer Aided Design
<b>CFD</b>	Computational Fluid Dynamics
<b>CFL</b>	Courant-Friedrichs-Levy Number
<b>GCI</b>	Grid Convergence Index
<b>CPU</b>	Central Processing Unit
<b>DOF</b>	Degrees of Freedom
<b>DNS</b>	Direct Numerical Simulation
<b>ENO</b>	Essentially Non-Oscillatory method
<b>FAR</b>	Federal Aviation Regulations
<b>FEA</b>	Finite Element Analysis
<b>FEM</b>	Finite Element Method
<b>FDS</b>	Finite Difference Splitting Scheme
<b>FSI</b>	Fluid-Structure Interaction
<b>LES</b>	Large Eddy Simulations
<b>LF</b>	Load Factor
<b>LST</b>	Linear Strain Triangular element
<b>MTOW</b>	Maximum Take Off Weight
<b>MUSCL</b>	Monotonic Upstream-Centered Scheme for Conservation Laws
<b>NACA</b>	National Advisory Committee for Aeronautics
<b>NASA</b>	National Aeronautics and Space Administration
<b>NSE</b>	Navier-Stokes Equations
<b>PDE</b>	Partial Derivative Equation
<b>Pr</b>	Prandtl Number
<b>RAM</b>	Random Access Memory
<b>RANS</b>	Reynolds Average Navier-Stokes

## **Abbreviations**

---

<b>Re</b>	Reynolds Number
<b>RNG</b>	Re-Normalisation Group method
<b>SST</b>	Shear Stress Transport model
<b>UDL</b>	Uniform Distributed Load
<b>UMIST</b>	University of Manchester Institute of Science and Technology
<b>WENO</b>	Weighted Essentially Non-Oscillatory

# Symbols

$A$	Area
$C_D$	Drag coefficient
$C_L$	Lift coefficient
$C_P$	Pressure coefficient
$D$	Drag force
$E$	Young Modulus
$E_T$	Energy
$\epsilon$	Strain tensor
$F$	Force
$\nabla$	Nabla Operator
$q$	Heat Flux
$I$	Moment of Inertia
$J$	Jacobian
$l$	Length
$L$	Lift force
$\Lambda$	Sweep angle
$\lambda$	Taper ratio
$M$	Structural mass matrix
$\mu$	Kinematic viscosity
$\partial$	Partial derivative operator
$p$	Pressure
$\pi$	Pi number
$\rho$	Density
$S$	Surface
$\sigma$	Cauchy stress tensor
$t$	Time
$\tau$	Reynolds stress tensor component
$u$	Flow speed X component
$v$	Flow speed Y component

---

$v$	Poisson ratio
$w$	Flow speed Z component
$\omega$	Natural frequency
$x$	First spatial component
$y$	Second spatial component
$z$	Third spatial component

# **Chapter 1**

## **Introduction**

### **1.1 Background and Motivation**

The whole performance of the operation of modern aircrafts is considered to be an enormous challenge as it involves so many elements that apparently no one is able -within a lifetime- to conduct it with enough solvency and expertise. The flight mechanics field, specially the knowledge we own about it, has changed extremely from the first flight achieved from with the Montgolfier and Wright brothers, with respective prototypes of rudimentary balloons and aircraft. Therefore the stretch collaboration and merge of different professionals and environments is needed to success in this process. From manufacturing to the economic section, with specialists in aerodynamics, structure, combustion and electricity work intensively being the echelon of a huge development chain. In this process, specifically in the design stage, the calculus and mathematical model of the real element is done and then studied facing the expected conditions. Here, the model of the ONERA M6 Wing geometry is conducted and studied under one of the most demanding situations faced during the cruise: the transonic conditions, where non-linear waves (shocks) take place and suppose a challenge to mathematically describe in order to predict them accurately. The influence of these phenomena will be evidently noted in the structure, as the gradient of adverse pressure done by the fluid in the full surface will be significant. The mathematical description - accurate to the real problem- of this evaluation will be the aim of this research by applying the Finite Element Model Methodology, performing precise and appropriate numerical schemes to simulate the whole operation. Recent techniques used by the nowadays industry and academia research such as the Fluid-Structure Interaction Study will be accordingly applied here as a result of their proximity to the real problem in contrast of the analytical and classical means of facing the problem, which will be also commented. Another interesting insights such as turbulence approach -which is still a problem to be solved of classic physics- and materials

## **1. Introduction**

---

to be used in the skin , amongst other considerations, will be also developed within this document.

### **1.2 Problem Statement**

A wing is a structural element that may bend, twist and break under high pressures. To avoid failures, its design must be carefully done: the shape of the skin, the number of ribs and spars, the size of the wing or the material chosen. The Onera M6 wing is a widely used test case but not many papers were available to check the behavior of the wing when an aircraft is cruising at a transonic flow, whereas tools are accessible. The finite element method is the most common one because it gives very accurate results and predicts well the behavior of element systems. Across this study, the aim will then be to see how will act the wing with different materials and with two different designs, one simplified with only the skin and the other with ribs and spars, and using different turbulence models which will simulate the flow around the aircraft.

### **1.3 Structure of the M.Sc. Thesis**

This document will be developed through the following scheme. In this section, the motivation of our study and the existing publications of previous similar researches will be accordingly explained. The second chapter will introduce an initial and first theory background of the mathematical governing equations that will hold the numerical computations applied. Both fluid and structure endeavours are carefully reviewed explaining from the general formulation to the individual and particular case studied. This is where details of the turbulent models and structural insights will be accordingly detailed. Then, the methodology is presented, giving special attention to the creation of the model (CAD), setting up the operational, initial and boundary conditions and later solution process of the flow and structural problem using ANSYS package and ABAQUS FEM software. Special detail is given to the Finite Element Modelling, revealing its behaviour and differences with other available approaches of the continuous problem.

The results of the research have been gathered in Chapter 4 and deeply discussed, commenting the special differences noted for each turbulence model, mesh, CAD and material separating the flow problem from the structural. Afterwards, conveniently, all our findings and final deductions for this research have been summarized in Chapter 5: Conclusions, where the overview of the whole investigation can be seen.

Given the current time (which was limited) and world-wide exceptional circumstances

## **1. Introduction**

---

during the elaboration of the present work, several interesting additional research could be done by conducting a further investigation serving this document as a basis. Hence, a section of "Future Work" is also specified where the authors give ideas of the most interesting applications and possible research to conduct in a later time. After this chapter, the references and bibliography of all the materials reviewed and considered for the creation of this document are posted.

Finally, the last chapter represents the annex or appendix documentation, where in the first subsection the materials used for the simulations are largely detailed. Then, it is followed by the engineering plans of the own-developed ONERA M6 CAD in case it would be interesting to later manufacture and construct it.

## **1.4 Literature Review**

Wide range of studies have analysed the wing structure with FEM methodologies, however only few of them have centered in studying the Onera M6 wing, which is the one analysed in this study. As a consequence of this, research works with similar wings have been considered, such as the thesis performed by (Hoang; 2015) [4] in which a simplified commercial aircraft wing is analysed. The author uses similar materials to the ones used in our study such as aluminium alloy or carbon fiber. Moreover, he applies the triangular load lift approximation in the Abaqus software. Due to these reasons, this thesis will be useful to validate the results.

We tried to find relevant literature which were the closest to this present work. We focused on four different papers for each structural analysis: "*Finite element analysis of aircraft wing using carbon fiber reinforced polymer and glass fiber reinforced polymer*" (Das, S K and Roy, S, 2018) for the static structural, "*Validation numérique d'un modèle aérodynamique*" (El Maani et al.,2016) for the modal, "*Investigation on buckling response of the aircraft's wing using finite-element method*" (Ravi Kumar B, 2018) for the buckling and "*Analysis of wing flexure deformation based on ANSYS*"(Xueyan Zhang et al.,2018) for the transient.

Moreover, we read many works to understand the fundamentals of the structural analysis or the turbulence modelling. Several papers which deals with Fluid-structure interaction have been read to have a better understanding of the whole problem. Therefore, we have considered the following research papers.

In [5]: "*Fluid-Structure Interaction Over an Aircraft Wing*" (G.Vigneshwaran, M.Vijayaraghavan,

## 1. Introduction

---

K.Sivamanikandan, K.Keerthana, K.Balaji, 2017), G.Vigneshwaran, M.Vijayaraghavan, K.Sivamanikandan, K.Keerthana, K.Balaji, were interested in the one way fluid-structure interaction problem and strongly coupled flow field, for the NASA SC(2)-0412 airfoil. In this study they looked for the best performances and deformation limit of the wing with several Mach numbers. The geometrical model is generated with Catia and for the fluid-structure interaction, they have used ANSYS. This paper is based on the study of T.Sai Kiran Goud, and also Chowla Sangeetha, which explains the analysis of fluid structure interaction for the AGARD 445.6 wing for a transonic flow.

In [6] : "*Fluid Structure Interaction on AGARD 445.6 wing at transonic Speeds*" (Sangeetha, Chowla and Veeranjaneyulu, Mr and Guptha, MSN, 2015), Chowla Sangeetha , Mr. Veeranjaneyulu , Dr. MSN Guptha, focused their research on understanding the structural behaviour and the elastic properties of the AGARD 445.6 wing for strongly coupled fluid-structure system, under load conditions which reflect realistic flying conditions. In this sense, they illustrate the fluid-structure interaction problem by predicting the initial boundary conditions of the AGARD 445.6 wing which is a common benchmark test for aero-elastic analysis. They classify three different type of fluid-structure interaction: The Zero strain interactions, the Constant strain steady flow interactions and the Oscillatory interaction which is the one which is consider in this study. The wing is created in CATIA and the mesh is generated in the CFX software. They have analysed the contour of total deformation the wing at different Mach numbers in ANSYS Workbench. They noticed that, for each Mach number, it exists a dynamic pressure at which the wing tip displacement remains constant. This phenomenon is called Flutter Boundary of the wing. In addition to this it is observed that, the deformation increases in the area over the flutter boundary and the deformation decrease in the area under the flutter boundary.

In [2] : "*Three-dimensional fluid–structure interaction simulation with a hybrid RANS–LES turbulence model for applications in transonic flow domain*" (Bojan Šekutkovskia, IvanKostic, AleksandarSimonović, Philip Cardiff, VladimirJazarević, 2016), Bojan Šekutkovskia, IvanKostic, AleksandarSimonović, Philip Cardiff, VladimirJazarević, have presented different numerical modelling methods and solutions for turbulent flow over the Onera M6 wing in a transonic flow at different angles of attack. Also, the FSI problem is considered for a turbulent flow over the AGARD 445.6 wing in a transonic flow for an angle of attack of 0 degree and several Mach number. In this study an improved RANS-LES turbulence model of the k-w SST model, which is the k-w SST SA IDDES, is tested and compared with two different RANS turbulence models: the Spalart-Allmaras and the k-w SST. This novel turbulence model is also validated with the Onera M6 wing. The strongly coupled 3D FSI solver is combined with the turbulence model and a large deformation finite vol-

## 1. Introduction

---

ume structural solver is implemented in OpenFOAM. In this study they were interested in the FSI problem for the AGARD 445.6 wing. A 3D hexahedral mesh with 321 360 tetrahedrons is used for the CFD mesh and a 3D hexahedral mesh with 760 hexahedrons is used for the structural mesh. For the three turbulence models considered, they have compared the displacement vector magnitude of the point at the top of the wing trailing edge for two Mach numbers: 0.96 and 1.141. They have observed that flutter occurred for each Mach number they have tested. After that, for each turbulence model, they have compared the flutter data measured in air for the AGARD 445.6 wing.

The scope of this document, as it can be seen, involves a wide variety of aspects to face thence the need of documenting ourselves in those.

The Finite Element treatment has been documented serving as basis for the study the general books of [7] and [8]. The application of the methodology in wings has been found in [9]. The main outcome of this last research is the construction of a satisfactory template for an aircraft wing geometry creation and FEM model based on the parametric treatment of the wing's characteristics and optimized mechanical procedures for the wing skeleton generation. The languages used to program these guidelines have been Visual Basic and PCL for the well-known engineering softwares of CATIA and PATRAN, in which this model is created considering that they may be one of the most globally used. Additionally, MSC Nastran is also used for the Finite Element treatment of the generated mesh. With this template, a significant reduction of time and effort is aimed yet also the validity of the process as it performs largely accepted operations and optimizations as a preliminary stage of the study of the aircraft structure. Specifically, the most important contributions of this process are the efficient generation of a skeleton model, the inclusion of operation conditions in the process of geometric mesh segmentation, the Finite Element treatment automatically implemented and the fact that it runs in the widely used commercial software of CATIA, as the PATRAN procedures that were before necessary are already encapsulated in the template.

The materials in the simulation have been previously analyzed by [10] for a different geometry, which presented evidently some minor differences with the results obtained in this document. Books such as [11], [12], [13] have been reviewed to understand the basis of the mechanics of aluminium alloys and specifically, in composites, to understand the mission of the matrix and the reinforcement material. In [14] provides the characterization and investigation of the Epoxy S-Glass under various types of simulations and experimental tests. Yildiz, in [15] provides the study of the substitution of steel from shipping containers for carbon fiber laminates, acquiring in his results a reduction in weight of 80% whilst maintaining decent mechanical properties. It is more positive than previous

## **1. Introduction**

---

studies ran by [16] where a reduction in weight of 20% was achieved and entailing a 7% improvement in fuel consumption of airplanes, which is significant.

# Chapter 2

## Theory fundamentals

### 2.1 Governing Equations (Julio)

#### 2.1.1 Flow Dynamics Governing Equations

The study of the flow dynamics plays major roles in the development of vehicle aerodynamics, and this is the reason of the importance of its study. The Navier-Stokes equations (NSE) predicts the behaviour of the flow for all cases. They are obtained by applying the principles of mechanics and thermodynamics to a finite volume of fluid, obtaining this way the integration formulation of the NSE. Applying some considerations such as the Newton viscous law, the differential formulation is obtained, which is the generally used for problem solving.

NSE are capable to describe the pressure, temperature and density of a fluid flow for every time instance. They consist of time dependant continuity equations for the mass conservation, a momentum conservation equation and an energy conservation equation, which are defined below [17].

Continuity Equation:

$$\frac{\partial \rho}{\partial t} + \frac{\partial(\rho u)}{\partial x} + \frac{\partial(\rho v)}{\partial y} + \frac{\partial(\rho w)}{\partial z} = 0 \quad (2.1)$$

X-Momentum Equation:

$$\frac{\partial(\rho u)}{\partial t} + \frac{\partial(\rho u^2)}{\partial x} + \frac{\partial(\rho uv)}{\partial y} + \frac{\partial(\rho uw)}{\partial z} = -\frac{\partial p}{\partial x} + \frac{1}{Re} \left( \frac{\partial \tau_{xx}}{\partial x} + \frac{\partial \tau_{xy}}{\partial y} + \frac{\partial \tau_{xz}}{\partial z} \right) \quad (2.2)$$

## 2. Theory fundamentals

---

Y-Momentum Equation:

$$\frac{\partial(\rho v)}{\partial t} + \frac{\partial(\rho uv)}{\partial x} + \frac{\partial(\rho v^2)}{\partial y} + \frac{\partial(\rho vw)}{\partial z} = -\frac{\partial p}{\partial y} + \frac{1}{Re} \left( \frac{\partial \tau_{xy}}{\partial x} + \frac{\partial \tau_{yy}}{\partial y} + \frac{\partial \tau_{yz}}{\partial z} \right) \quad (2.3)$$

Z-Momentum Equation:

$$\frac{\partial(\rho w)}{\partial t} + \frac{\partial(\rho uw)}{\partial x} + \frac{\partial(\rho vw)}{\partial y} + \frac{\partial(\rho w^2)}{\partial z} = -\frac{\partial p}{\partial z} + \frac{1}{Re} \left( \frac{\partial \tau_{xz}}{\partial x} + \frac{\partial \tau_{yz}}{\partial y} + \frac{\partial \tau_{zz}}{\partial z} \right) \quad (2.4)$$

Energy Equation:

$$\begin{aligned} \frac{\partial E}{\partial t} + \frac{\partial(uE)}{\partial x} + \frac{\partial(vE)}{\partial y} + \frac{\partial(wE)}{\partial z} &= -\frac{\partial(up)}{\partial x} - \frac{\partial(vp)}{\partial y} - \frac{\partial(wp)}{\partial z} - \frac{1}{RePr} \left( \frac{\partial q_x}{\partial x} + \frac{\partial q_y}{\partial y} + \frac{\partial q_z}{\partial z} \right) + \\ &+ \frac{1}{Re} \left[ \frac{\partial}{\partial x}(u\tau_{xx} + v\tau_{xy} + w\tau_{xz}) + \frac{\partial}{\partial y}(u\tau_{xy} + v\tau_{yy} + w\tau_{yz}) + \frac{\partial}{\partial z}(u\tau_{xz} + v\tau_{yz} + w\tau_{zz}) \right] \end{aligned} \quad (2.5)$$

Where the  $x$ ,  $y$  and  $z$  are the spatial coordinates,  $t$  the time,  $p$  the pressure,  $\rho$  the density,  $E$  the energy, and  $u$ ,  $v$ ,  $w$  the components of the velocity for the three spatial directions.  $Re$  is the Reynolds number,  $Pr$  the Prandtl number,  $q$  the heat flux and the  $\tau$  variables are the components of the Reynolds stress tensor, which has an important relationship with the turbulence of the flow. The left terms represent the variation of the flow variable of the NSE with the non-stationary term (evolution in time across the flow volume) and the convective terms (spatial variation) due, they are related with the properties transportation because of the ordered motion of the fluid. By the other side, the right term of the equations are known as diffusive terms, due these terms are related in the properties transportation by a random flow motion. This diffusive part is related with the turbulence and the generation of the boundary layers [17]. However, there is not a general solution for the equations, just for some particular cases, and for this reason it is necessary to apply numerical methods for solving these equations.

It exists a variety of methodologies for solving NSE which are mainly the Reynolds Average Navier-Stokes (RANS) method, the Large-Eddy Simulations (LES), the Direct Numerical Simulation (DNS) and Hybrid modelling, which is mix of RANS and LES methodologies [18].

RANS is one of the most used approaches in the industry due it is quick and provides good quality results of the flow motion simulation. In this case, the turbulent flow is de-

## **2. Theory fundamentals**

---

composed into average and fluctuations, which represents the turbulence of the fluid that are computed in the Reynolds stress tensor [19]. The main problem of this approach is that it can not describe complex flow structures with high quality, and also can have problems with unsteady flows.

With LES the large scale motions of turbulence are directly calculated and solved for time and space, and only small scales are modeled, producing this way that the computational time increases respect RANS approach, but is still quicker than the computation time of a DNS simulation, and achieving always a very high quality results [20].

DNS simulations are a complete time and space independent solutions for all the fluid domain, and with the capability of solving the instantaneous flow speed in function of time and space in all the domain. This method is valid for all scale problems, however it has a very high computational cost, which makes it unfeasible for the industry use [18].

The hybrid RANS-LES approach achieve to integrates in one methodology the benefits of RANS and LES methods. It is capable of improving the accuracy in comparison with RANS simulations and perform it with less time than a LES simulation [21].

### **2.1.2 Structural Governing Equations**

The study of the structures behaviour is one of the major topics in the development of any vehicle, and more when it is submitted to aeroelastics efforts, like is the case in the present study, however lets start with the basics. The continuum mechanics, which is the branch of mechanics that is going to be used, is the one that deals with those materials that modeled as a continuous mass, and not as discrete elements [22].

This approach usually used for length scales problems bigger than inner-atomic distances, provides high accurate results. Going deeper, it is going to be considered the elastic solid mechanics branch, inside the continuum mechanics, this is because it is only going to be considered the elastic part of solid materials, as they are the interesting for the study. Of course, this consideration, is an approximation to the reality, but in this report, any material that overcome the maximum elastic strength will be considered a break of the material, so this approach is good enough for the study.

The linear elastic model is then, a mathematical model in which the solid object suffers "small" deformations where there are linear relationships between the stresses and strain [23]. These assumptions, as said before, is reasonable for multiple engineering cases, and

## 2. Theory fundamentals

---

as a consequence, widely used for structural analysis.

The governing equations that predicts the linear elastic model are based on three tensor PDE for the balance of linear momentum, and the infinitesimal relationships between the strain and displacements [24]. Those relationships, are presented in the following lines.

Equation of motion:

$$\frac{\partial^2 u}{\partial t^2} = \frac{1}{\rho} \nabla \cdot \sigma + F \quad (2.6)$$

Where  $u$  is the displacements vector,  $t$  is the time,  $\rho$  is the material density,  $\sigma$  is the Cauchy stress tensor,  $F$  the body force, and  $\nabla$  the nabla operator. This equation is also known as Cauchy momentum equation, written in Lagrangian form, comes from the Newton 2nd law, and describes the deformation of any continuum material either solid or fluid [24].

Strain-Displacement equation:

$$\varepsilon = \frac{1}{2} [\nabla u + (\nabla u)^T] \quad (2.7)$$

Where  $\varepsilon$  is the infinitesimal strain tensor, and T the transpose. This equation uses the infinitesimal strain theory to describe the relationship between the strain and displacements.

Hooke's Law:

$$\sigma_{ij} = C_{ijkl} \varepsilon_{kl} \quad (2.8)$$

Where  $C_{ijkl}$  is the stiffness tensor presented in Cartesian form notation. This equation connects by a linear relationship, the stress and the strain tensors [23].

With the equations presented, and specifying the boundary conditions, the system of equations is completely defined, and can be solved. Exist then, several methodologies to solve these types of problem, and a big number of equations are involved, computational methods are usually used. Further details of several structural computational methods can be found on section 3.3 FEM Modelling of this report.

## 2. Theory fundamentals

---

### 2.2 Structural Problem (Léa, Erwan)

A wing is comparable to a cantilever beam: one side is attached to the fuselage while the rest can move freely. A normal wing is composed of ribs in the front, middle and rear that can be made of different materials such as wood or metal. Also, there are spars, crossing the wing from the fixed side to the wing tip, which will carry the all the weight [25]. The structure of the wing is shown in figure 2.1.

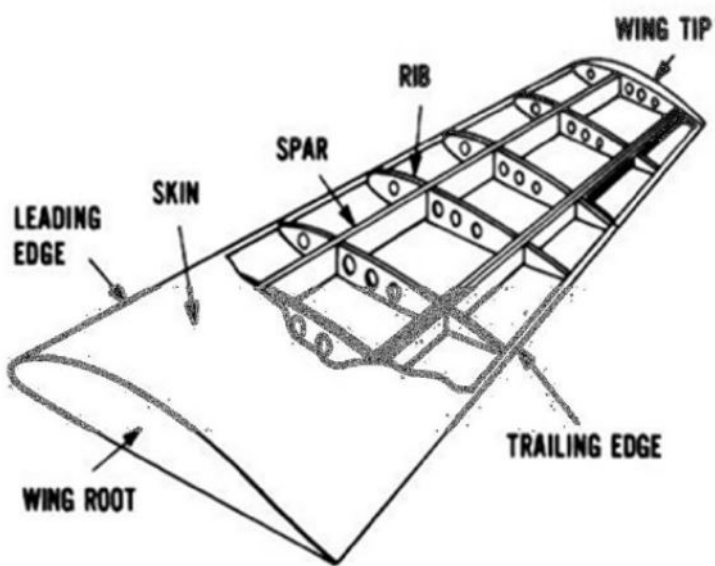


Figure 2.1: Wing Structure (Venkatesan et al.,2018)

During the flight of an aircraft, the wing is subjected to pressures on its bottom and top. This difference of pressure generates lift and will have repercussions on the structure of the wing. Most of the wings are made with aluminum alloy [26]. To design an aircraft, the study of the physical phenomena must be done. We will perform different analysis: static structural, modal, transient and buckling. In most papers, the geometry of the wing is simplified. No more ribs or spars.

## 2. Theory fundamentals

---

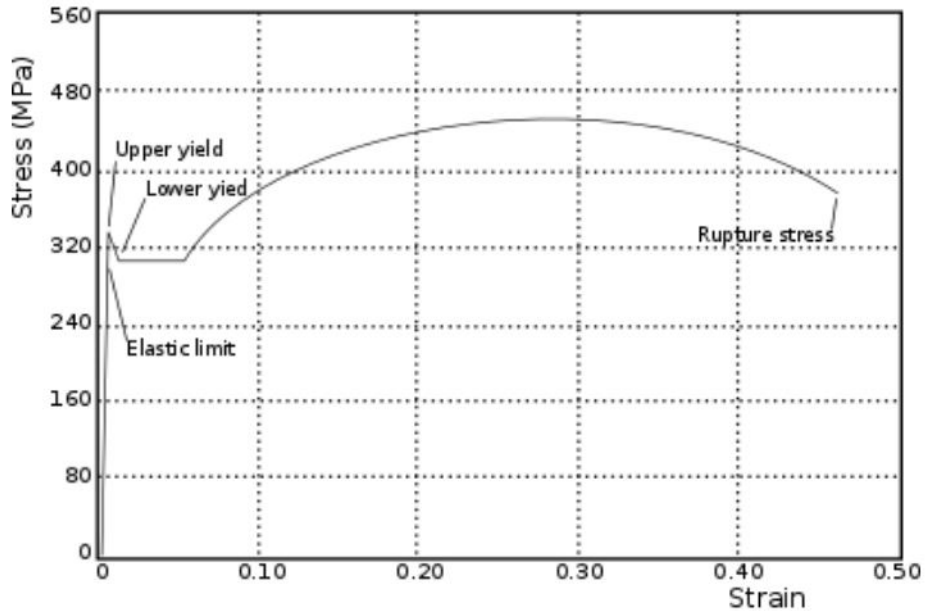


Figure 2.2: Stress strain Diagram of a mild steel beam element (SIMSCALE)

### 2.2.1 Static Analysis

When an object like a wing is subjected to a load, it will deform, either to find a mechanical or a deformation equilibrium. Stress will be defined by the external load, and strain by the body deformation. For example, a beam element made of mild steel subjected to an axial compression force will first enter the elastic limit region. If we remove the load, the beam will return to its original form. However, if we increase the stress above the elastic limit, also called yield stress, we enter into the plastic deformation region, where the deformations become irreversible. At the upper yield limit, the deformation will suddenly drop to the lower yield limit. With higher stress, the deformation will keep going until it reaches a rupture point [27]. On figure 2.2, we see the deformation of a mild steel beam element.

Depending on the material properties, the curve will not be exactly the same. In their study, Gunes R and Arslan K (Gunes, R AND Arslan, K, 2016) worked on aluminium sandwich plates, using aluminium alloy Al 2024-T3 for the facesheets and Al 3003-H19 for the honeycomb core [28]. On figure 2.3, we see the difference of deformation between the two aluminium alloys. Compared to the diagram of the steel element, there is no lower yield or upper yield.

## 2. Theory fundamentals

---

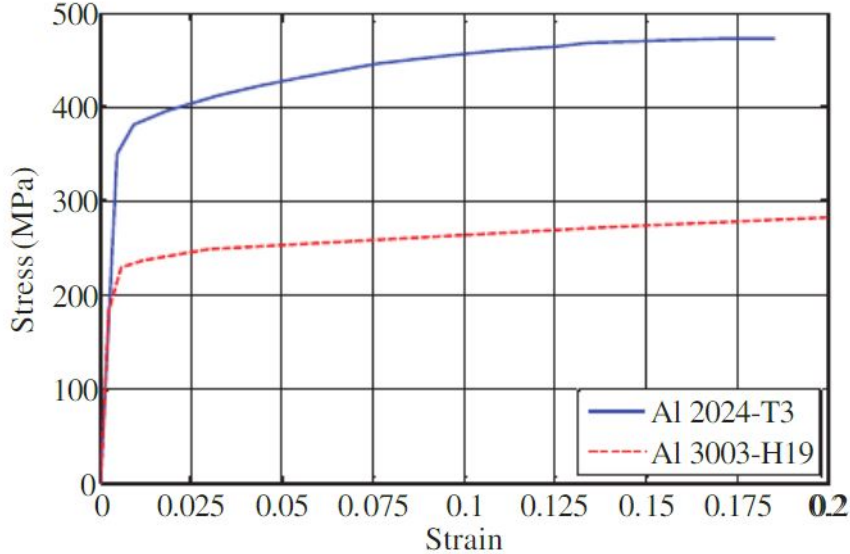


Figure 2.3: Stress strain Diagram of a AL2024-T3 (Gunes,R and Arslan, K, 2016)

In static structural analysis, important values such as the von Mises stress, the equivalent strain and the deformation will be plotted. The von Mises stress is a value used to see if the material will yield. This lead to the von Mises yield criterion [27]. In its simplest mathematical form, the von Mises yield criterion is the relation between the distortion strain energy  $J_2$  and the yield stress of the material when in pure shear  $k$  (2.9).

$$f(J_2) = J_2 - k^2 = 0 \quad (2.9)$$

Where  $k = \frac{\sigma_y}{\sqrt{3}}$ .

Or, in its more general form (2.10), we transform  $J_2$  using the Cauchy stress tensor components and we assume that the von Mises stress  $\sigma_v$  is equal to the yield strength  $\sigma_y$ . Depending on the boundary conditions, this formula will change [29].

$$\sigma_v = \sqrt{\frac{(\sigma_{11} - \sigma_{22})^2 + (\sigma_{22} - \sigma_{33})^2 + (\sigma_{33} - \sigma_{11})^2 + 6(\sigma_{12}^2 + \sigma_{23}^2 + \sigma_{31}^2)}{2}} \quad (2.10)$$

The yield will then occur when the  $\sigma_v > \sigma_y$  [27].

In their study, Salu Kumar Das and Sandipan Roy (Das, S K and Roy, S, 2018) performed a structural analysis on a wing composed of 2 spars and 15 ribs, with the following dimensions: Exposed Length of wing =4750mm, Root chord =2400mm, Tip chord =700 mm and Semi span length =5500mm. A pressure of 500 Pa is put at the center of pressure at the surface under the wing [26]. They did the simulation with several materials, and

## 2. Theory fundamentals

---

found the maximum equivalent strain, stress and total deformation as shown in 2.4.

Materials	Total deformation (mm)	Equivalent stress (Mpa)	Equivalent strain
Epoxy-carbon UD	4.223	16.225	0.00016508
Epoxy S-glass UD	9.8794	16.145	0.00040288
Aluminum 2024 T3	6.7377	16.034	0.00022722
Epoxy-carbon Woven	7.9845	15.709	0.00030371
Epoxy E-glass	10.943	15.943	0.00044117

Figure 2.4: Static structural analysis results (Das, S K and Roy, S, 2018)

### 2.2.2 Modal Analysis

The modal analysis works on the mechanical structures behavior when subjected to dynamics excitation. It will find the dynamic characteristics of the system, mainly the natural frequency and the modes shapes. It can be used in reducing the noise travelling from the system to the environment [30]. As a wing is comparable to a cantilever beam, the natural frequency of the beam is:

$$\omega_n = (\beta l)^2 \sqrt{\frac{EI}{\rho Al^4}} \quad (2.11)$$

Where I is the length of the beam in meters, E is the Young's modulus of the beam in Pascals, I is the second moment of area in  $m^4$  (EI is defined as the flexural rigidity),  $\rho$  is the mass density of the beam in  $kg/m^3$ , and A is the cross section of the beam in meters. To find  $(\beta l)^2$ , we use the displacement general solution (2.12), where  $c_1, c_2, c_3$  and  $c_4$  are coefficients found with the boundary conditions and x is the position of the beam.

$$w(x) = c_1(\cos\beta x + \cosh\beta x) + c_2(\cos\beta x - \cosh\beta x) \\ + c_3(\sin\beta x + \sinh\beta x) + c_4(\sin\beta x - \sinh\beta x) \quad (2.12)$$

In simply supported boundary conditions, the displacement and the bending moment are equal to zero, which leads to  $\sin\beta l = 0$ . Moreover, for a beam free to move at both ends, the bending moment and the shear force will be also zero at the both ends, which leads to  $\cos\beta l \cosh\beta l = 0$ . With these two equations,  $(\beta l)^2$  can be calculated [31].

In their study, R. El Maani, B. Radi, A. El Hami (El Maani et al., ) worked on the modal analysis of the Onera M6 wing. In fluent Ansys, they created a distributed load in setting a fluid with a Mach number M=0.8395, an angle of attack  $\alpha = 3.06$  and a Reynolds number Re=11.72e6. To perform their simulations, they did a fluid structure interactions

## 2. Theory fundamentals

---

to keep the same load distribution. The wing is made of aluminium alloy (Young Modulus  $E = 7.1 \times 10^10$  Pa, density  $\rho = 2770 \text{ kg.m}^{-3}$ , Poisson ration  $\nu = 0.32$ ). The results of the prestressed modal analysis are presented in 2.1. They show the four first modes with its natural frequency values [32].

Table 2.1: Results of the modal analysis (El Maani et al.,2016)

Mode	Frequency
1	31.414
2	103.338
3	142.073
4	232.695

### 2.2.3 Buckling Analysis

The buckling analysis is an essential part of a Structural analysis. Indeed, one of the most important issues for the wing design is the definition of the response of the wing structure subjected to different types of loads.

The Buckling is defined in [33] as a sudden failure of a mechanical component such as material failure and structural instability. Moreover, buckling is a tendency of the slender compression elements to bow, which causes bending. It's independent of the material strength, but it depends on the stiffness of the components. Also, it is affecting all the compression members, for example, the columns, truss bars or bracing.

To see if the buckling will occur, we can use the buckling factor (BF). The formula of the buckling factor is:

$$BF = \frac{p_{cr}}{p_{app}} \quad (2.13)$$

Where:

- $p_{cr}$  is the critical buckling load also called Euler's critical load
- $p_{app}$  is the applied load

When:

- $BF > 1$  and  $BF < -1$ , the structure will not buckle
- $BF \in (0, 1)$  , the structure will buckle
- $-1 < BF < 0$ , the structure can buckle

## 2. Theory fundamentals

---

The critical buckling load is the greatest load that will not cause buckling effect. We can obtain the critical buckling load by deriving the Euler buckling theory. The critical buckling load  $p_{cr}$  is calculated with the following formula:

$$p_{cr} = \frac{\pi^2 \cdot E \cdot I}{(L \cdot K)^2} \quad (2.14)$$

Where:

- E is the Young's modulus of the components (in GPa),
- I is the minimum area moment of inertia of the cross section of the components, (in  $m^4$ ),
- L is the length of the slender members (in m)
- K is the effective length factor (for a Pin ended column K=1)

Shivaraj, Ranganatha S R, V S Ramamurthy and K E Girish carried out the buckling analysis on a fuselage, that they created on Catia V5 [33]. They evaluated on the fuselage if the bottom skin of the wing could endure the load without buckling. For the boundary conditions, the fuselage was fixed on the wing axis, and a uniform load was applied on the upper half skin of the fuselage. In order to calculate the load for the fuselage, they used the following formula:

$$UDL = \frac{Totalload}{\pi \cdot r} \quad (2.15)$$

Where UDL is the uniform distributed load and r is the radius of the fuselage. After that, they made a local buckling analysis on the critical panel of the fuselage. They calculated the load for the panel with the stress around the panel. It was observed that when the Eigen buckling load values were higher than the distributed load applied to the structure, the analysed structure became unstable and buckled immediately. Also, after reaching a critical point, the investigated structure had displayed a snap-through behaviour.

Sruti Deshpande, studied the buckling and post buckling effects of structural components subjected to heavy loads, such as shallow arch, shallow truss, cylindrical panel and so on [34]. Also, he used ANSYS APDL and ANSYS Workbench in order to perform simulations. In this study, buckling is defined by a sudden and large deformation of the structure at the point of critical load value. Because of that, the structure loses its ability to carry the load. Another phenomenon is also defined: the post buckling. This phenomenon occurs after a buckling failure. When it happens, the deformation on the structure can continue to increase. This can create a second buckling failure.

## 2. Theory fundamentals

---

The studied structure displayed a rupture behaviour at a critical point. In order to identify the nonlinear behaviour of the models, they plotted the load reaction at the central node against the displacement, and the load reaction against the horizontal reaction. Sruti Deshpande noticed that, under specific loaded conditions, the buckling effects do not appear immediately. And when the Eigen Buckling load values were higher than the applied load, the buckling appeared immediately, and the structure became also unstable immediately.

Ravi Kumar B, performed a structural analysis and a finite methods analysis for a wing structure [10]. He focused on the Buckling analysis of an standard aircraft wing with a simplified structure. Moreover, he used different thicknesses for the bulkhead which has different critical buckling loads. For this, he compared the stress behaviour of various material such as aluminium alloy, Kevlar, S-glass and Boron fiber. He plotted the buckling load factors against the applied load in (Kpa) for each material, this is what we can see on the figure 2.5:

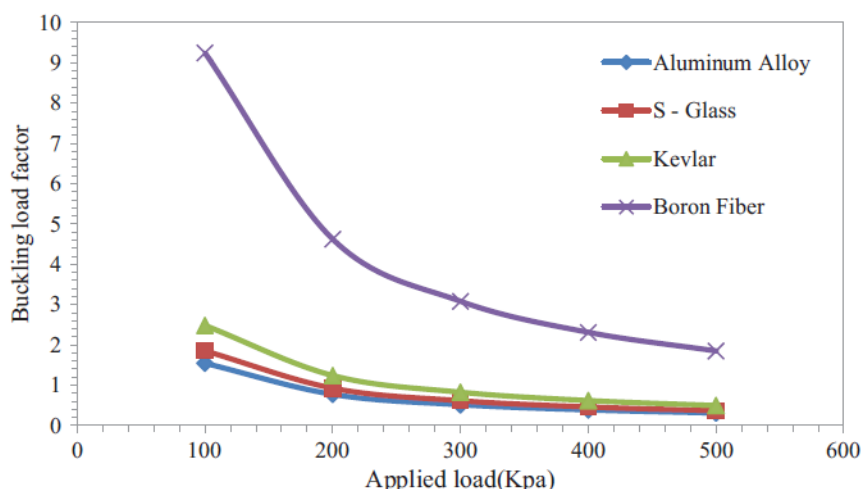


Figure 2.5: Comparison of the stress behaviour with different materials of buckling load factor for the conventional wing. (Ravi Kumar B, 2018)

In conclusion to this study he found, thanks to the calculation of the buckling loads and factor of safety, that for the design of the wing, it's better to have a conventional design. Also, for the material, the aluminium is safer than the carbon fiber. However, the other materials such as the Kevlar had better results: the strength to weight ratio of composite materials were higher.

## 2. Theory fundamentals

---

### 2.2.4 Transient Dynamic Analysis

The transient dynamic analysis is used to determine the dynamic response of a structure under any time varying load [35]. This analysis is also called time-history analysis. Thanks to this analysis, we can calculate the time-varying displacements, stresses, strains, and forces in a structure as it responds to any combination of static loads, transient loads, and simple harmonic loads. Moreover, this analysis can include inertia, damping and non-linear effects.

The semi-discrete equations of dynamic equilibrium of a structural system for a transient dynamic problem at time t can be written as [36]:

$$[M] \{ \ddot{x} \} + [C] \{ \dot{x} \} + F_{int} \{ x \} = F_{ext}(t) \quad (2.16)$$

Where:

- M is the structural mass matrix
- {  $\ddot{x}$  } is the nodal acceleration vector
- C is the structural damping matrix
- {  $\dot{x}$  } is the nodal velocity vector
- $F_{int}$  is the internal resisting force vector
- { x } is the nodal displacement vector
- $F_{ext}$  is the external force vector
- t is the time

Xueyan Zhang, Yan Zhao and Fan Si (Xueyan Zhang et al., 2018) have studied, the effects of the aerodynamic loads and turbulences during a flight on the NACA2412 wing, using ANSYS [35]. They perform a modal analysis in order to obtain the natural frequencies and the modal shape of the first four orders. Thanks to the modal analysis, the designer of the wing can minimize the excitation of the natural frequencies and prevent the wing from the flutter. After that, a transient dynamic analysis is achieved. Moreover, the wing structure is in aluminium alloy and the two spars and the six ribs are made of titanium alloys. With the modal analysis, they found that the spars mainly bear the bending deformation, and the skin and the ribs mainly bear the torsional deformation. Thereafter, they focus on the transient structural analysis. This analysis is based on the results of natural frequencies of the wing obtained in the modal analysis. In the transient structural

## 2. Theory fundamentals

---

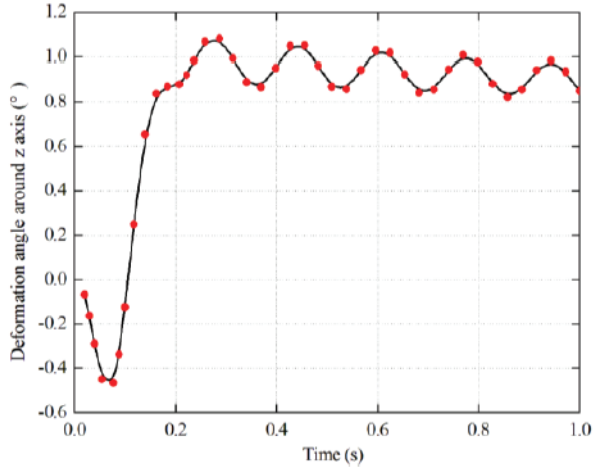


Figure 2.6: Deformation angle of the wing around the Z axis (Xueyan Zhang et al.,2018)

analysis, they consider, the flexure deformation of the wing around the Z axis, which we can observe on the figure 2.6:

Also, they used this analysis to calculate time-varying displacement, stress and strain of the structure subjected to random combinations of static loads, transient loads, and simple harmonic loads.

In Ansys, they have used the Elastic Modulus reduction method to calculate the total deformation of the wing. As a result, they found that, as for the modal analysis, the wing mainly produces bending deformation for the modal shapes of the first three order. Moreover, the largest deformation is at the wingtip and the smallest, is at the wing root. Thanks to this analysis, they explain that it is necessary to reinforce the wing root properly to improve the safety performances of the aircraft.

## 2.3 Aerodynamic Flow Problem (Marc)

From the first basic aircraft introduced by the Wright brothers circa 1908, the development of aerodynamics science has suffered a huge enhancement, specially sharp in war times where efficient belligerent machinery was considered as an essential need. After these unfortunate times, the huge development, expansion and settlement of civil aviation has motivated the consideration of using aircrafts as a first need and usual mean of transport. This fact has lead most aviation manufacturing companies, such as Airbus, Boeing, Embraer, etcetera to construct models that are able to operate a significant number of times a day without jeopardizing the performance either the safety of the flight. Thence, the need of strong use of mathematic model and physics derivations to ensure the satisfaction and optimization of the flight variables that must be controlled.

## 2. Theory fundamentals

---

However, the aerodynamic problem was already present years before the first aircraft could lift several meters from the ground. We are not only referring to aerostatic balloons, cars, but to any vehicle or object which was subject to very strong velocities or to a big adverse pressure difference between its top and bottom surface.

Here, the main fluid problem to investigate is the flow over a 3-D wing -particularly ONERA M6 Wing- and as it is not infinite and as the turbulence in the wingtip is significant, it cannot be simplified to the 2-D airfoil problem. According to aerodynamics' basic theory, which is enclosed and backed up by the Fluid Mechanics Theory, a difference of pressures between two points of a solid element creates a force with a direction from the minor pressure point to the greater pressure point (along the minimum distance between them). This force is known as lift. When this force, for angle of attack (AoA) 0, overpasses the weight of an element, the object -still immersed in the fluid- is able to rise precisely from the current position.

However, and unfortunately as it will be explained, the lift force is not the only main aerodynamic outcome of the flow. Depending on the geometry of the aircraft, the flow regime and the flight parameters, a considerable force called drag is also derived on the direction of the incident flow. It is specially sensitive to the geometry immersed in the flow and strongly depends on the flow velocity. It can be splitted into different subforces -depending on the cause and effect- such as parasite drag (formed at the same time by the form drag and the skin-friction drag), the lift-induced drag and the wave drag. Its main and basic effect highly reduces the performance of the thrust force (which moves the aircraft into the desired direction), and therefore implies consumption of more fuel and the reduction of the theoretically expected air flow.

The vectorial contribution of both forces is known as the aerodynamic force. In the rigid solid analysis, it is applied as a point load applied to the pressure centre. In the real flow, it is a distributed and vectorial load. The calculations of both forces follow a similar structure:

$$\begin{aligned} L &= \frac{\rho v^2}{2} \cdot S \cdot C_L \\ D &= \frac{\rho v^2}{2} \cdot S \cdot C_D \end{aligned} \tag{2.17}$$

The equations from above have been dimensioned with the dynamic pressure of the downstream flow and evidently focus the importance of the formula on the parameters  $C_L$  and  $C_D$ . In these terms, all the wide variety of sources (geometry, flow attributes, etc) that affect each force are included. Although several attempts of considering the most pre-

## **2. Theory fundamentals**

---

dominant contributions have been done and described so as to obtain an approximate function, actually, the modelling is so complex that experimental values are mostly used.

The only main basic force to mention, apart from the aircraft's weight, is the thrust, which moves the aircraft forward. It is created as a result of Newton's third law, and directly depends on the action of the propeller. These forces, must be in equilibrium at each direction considered. This is why, translated into the fluid mechanics, the Navier-Stokes equations, continuity equations and other derivations must be equally satisfied. Analytical solutions for most problems, mainly subsequent of non-linearity, enforces the scientific community to model the terms with discretized, approximated and quantified functions and to solve it with iterative means.

As it is evident, the external loads that will incur into structural stress and deformation of the wing will be caused by the flow behaviour, and this input can be obtained by nodal analytical assumptions and formulas or more accurately with Fluid-Structure Interaction (FSI) setups. Hence, structural simulations with point approaches and FSI will be equally reviewed in this document. For the last ones, the fluid problem is needed to be solved beforehand.

The terms of the Fluid Mechanics Equations will be modelled, schemes will be used and iterative procedures are required as well.

The most conflictive in the aircraft operation takes place during transonic environments, in which most of the cruise is held, where no theory from subsonic and supersonic is merged and non-linear waves such as shocks take place. In this case, the use of special flow approximations for compressible assumptions will be critical, as non-physical results would be obtained otherwise. These flux "computers" are known as Riemann Solvers and the one that will be predominant in this research is the ROE-FDS Riemann Solver.

However, the most challenging term to model is turbulence as it will be detailed now. The approach in which it is faced will entail a significant effect on the solution. This is why, several turbulence models will be described - emphasizing its advantages and cons - and used in the flow simulation to determine the incidence in the structural solution.

### **2.3.1 Turbulence Modelling**

Richard Feynman, one of the best 20th century physicists, once quoted 'Turbulence is the most important unsolved problem of classical physics.' Until now, and without any evidence of changing in the near future, this statement has remained unfortunately true. Due to this fact, the description of the fluid behaviour is still challenging and uncertain.

## 2. Theory fundamentals

---

Numerical solvers, which lack a hundred percent reliability in the results they provide, are still required to achieve hints or data of any fluid problem faced.

However, strong efforts have been made and are currently being made to achieve further understanding of turbulence, into what is actually called as the Turbulence Closure Problem. The most powerful entities to describe it mathematically are the Navier-Stokes Equations and The Reynolds Stress equations, hence a coupling of these hostile expressions is believed to work as the initial required step. Experience has demonstrated several issues in this first process in which non-linearity stands as the most problematic obstacle. It cannot be omitted due to its significant influence to the fluid behaviour. Other strategies, such as the average of non-linear terms of fluctuating quantities such as occasional procedures in RANS simulations will only lead to the creation of new unknown variables without adding governing equations, and therefore resulting in the enlargement of the undetermined system. As a result, current turbulence models provide new set of equations through the implementation of semi-empirical expressions or even developments for specific environments. The general solution, then, is not still established. Specifically RANS simulations take advantage of the development and model of the viscosity parameter to partially overcome the Turbulence Closure Problem, which has proven to be a quick approach yet entails subsequent problems.

### 2.3.1.1 Spalart-Allmaras model (Léa, Erwan)

The Spalart–Allmaras model uses one equation of the transport equations, for the kinematic eddy viscosity parameter  $\tilde{\nu}$ . The Eddy viscosity is calculated as following:

$$\mu_t = \rho \tilde{\nu} f_{v1}. \quad (2.18)$$

Where  $\mu_t$  and  $f_{v1}$  is the wall-damping function

It also needs to define the length scale. For models with two transport elements added like the k– $\varepsilon$  model, the length scale can be found in linking the two quantities  $\varepsilon$  and k:

$$l = \frac{k^{\frac{3}{2}}}{\varepsilon}. \quad (2.19)$$

Thus, for the Spalart–Allmaras model, this value needs to be determined in order to find the rate of dissipation used in the transported turbulence quantity. This model is known to give good results for stalled flows because it captures well the adverse pressure gradients in boundary layers. However, it's not a suitable model with complex geometries because it has difficulties to evaluate the length scale. Also, this model has issues in capturing sudden changes of the flows [37].

## 2. Theory fundamentals

---

### 2.3.1.2 k- $\varepsilon$ turbulence models (Léa, Erwan)

The k- $\varepsilon$  model solves two transport equations to find the kinetic energy  $\varepsilon$  and specific dissipation rate  $k$ . The turbulence can adapt itself in case of slow changes in the flow direction such as in thin shear layers for 2D problems. However, this case does not work for too complex flow problems, leading to unreliable results. So, we only look at the statements about the turbulence dynamics. The k-epsilon model will work more especially on what disturbs the turbulent kinetic energy [37].

Depending on the fluid flow problem, the best turbulence model is not always the same. The RNG and Realizable k- $\varepsilon$  models are often better in representing the gas dispersion while the Standard model has lower performances. Different explanations were given, such as difficulties of the Standard k- $\varepsilon$  model to represent the flow structure [38] or the fact that it gives poor results with low Reynolds number [39].

The Standard k- $\varepsilon$  is a robust and quite accurate model for many turbulence models which can explain its popularity. The turbulent viscosity is set constant which means that it's independent of the flow [40]. For the Standard k- $\varepsilon$  model, the turbulent kinetic energy is defined with:

$$\frac{\partial}{\partial t}(\rho k) + \frac{\partial}{\partial x_i}(\rho k u_i) = \frac{\partial}{\partial x_j}[(\mu + \frac{\mu_t}{\sigma_k}) \frac{\partial k}{\partial x_j}] + G_k + G_b - \rho \varepsilon - Y_M + S_k \quad (2.20)$$

And the specific dissipation rate is computed with:

$$\frac{\partial}{\partial t}(\rho \varepsilon) + \frac{\partial}{\partial x_i}(\rho \varepsilon u_i) = \frac{\partial}{\partial x_j}[(\mu + \frac{\mu_t}{\sigma_\varepsilon}) \frac{\partial \varepsilon}{\partial x_j}] + C_{1\varepsilon} \frac{\varepsilon}{k} (G_k + C_{3\varepsilon} G_b) - C_{2\varepsilon} \rho \frac{\varepsilon^2}{k} + S_\varepsilon \quad (2.21)$$

Where  $S_\varepsilon$  and  $S_k$  are source terms defined by the user,  $C_{1\varepsilon}, C_{2\varepsilon}, C_{3\varepsilon}$  are constants. The Prandtl numbers for  $k$  and  $\varepsilon$  are respectively  $\sigma_k$  and  $\sigma_\varepsilon$ .  $Y_M$  is the part of fluctuation dilatation.  $G_b$  is the turbulence kinetic energy created because of the buoyancy. The mean velocity gradients produced turbulence kinetic energy  $G_k$ .

The Realizable k- $\varepsilon$  model is flow dependent, the turbulent viscosity is not constant. This model has better predictions of the spreading rate for, axisymmetric, round or planar jets. It also performs well simulations containing recirculation, boundary layers or rotations. However, this model may generate non-physical turbulent viscosities if there are stationary and rotating fluid areas in the computational domain [41].

For the Realizable k- $\varepsilon$  model, the turbulent kinetic energy is defined with:

$$\frac{\partial}{\partial t}(\rho k) + \frac{\partial}{\partial x_j}(\rho k u_j) = \frac{\partial}{\partial x_j}[(\mu + \frac{\mu_t}{\sigma_k}) \frac{\partial k}{\partial x_j}] + G_k + G_b - \rho \varepsilon - Y_M + S_k \quad (2.22)$$

## 2. Theory fundamentals

---

And the specific dissipation rate is computed with:

$$\frac{\partial}{\partial t}(\rho \varepsilon) + \frac{\partial}{\partial x_j}(\rho \varepsilon u_j) = \frac{\partial}{\partial x_j}[(\mu + \frac{\mu_t}{\sigma_\varepsilon}) \frac{\partial \varepsilon}{\partial x_j}] + \rho C_1 S_\varepsilon - \rho C_2 \frac{\varepsilon^2}{k + \sqrt{v\varepsilon}} + C_{1\varepsilon} \frac{\varepsilon}{k} C_{3\varepsilon} G_b + S_\varepsilon \quad (2.23)$$

Where:

$$C_1 = \max[0.43, \frac{\eta}{\eta + 5}], \quad \eta = S \frac{k}{\varepsilon}, \quad S = \sqrt{2S_{ij}S_{ij}} \quad (2.24)$$

The RNG model in ANSYS FLUENT can take into account the effects of rotation and swirl, if the turbulent viscosity is well-chosen. It gives better performances than the Standard k- $\varepsilon$  in certain flow problems because it represents better the effects of curvature and strain [42].

For the RNG k- $\varepsilon$  model, the turbulent kinetic energy is defined with:

$$\frac{\partial}{\partial t}(\rho k) + \frac{\partial}{\partial x_j}(\rho k u_j) = \frac{\partial}{\partial x_j}(a_k \mu_{eff} \frac{\partial k}{\partial x_j}) + G_k + G_b - \rho \varepsilon - Y_M + S_k \quad (2.25)$$

And the specific dissipation rate is computed with:

$$\frac{\partial}{\partial t}(\rho \varepsilon) + \frac{\partial}{\partial x_j}(\rho \varepsilon u_j) = \frac{\partial}{\partial x_j}(a_\varepsilon \mu_{eff} \frac{\partial \varepsilon}{\partial x_j}) + C_{1\varepsilon} \frac{\varepsilon}{k} (G_k + C_{3\varepsilon} G_b) - C_{2\varepsilon} \rho \frac{\varepsilon^2}{k} + S_\varepsilon - R_\varepsilon \quad (2.26)$$

The main difference between the standard k- $\varepsilon$  and the RNG k- $\varepsilon$  is the term  $R_\varepsilon$  defined in equation (2.27) which will allow the RNG model to have a better response to fast strain variations or streamline curvatures than the Standard k- $\varepsilon$ .

$$R_\varepsilon = \frac{C_\mu \rho \eta^3 (1 - \eta/\eta_0)}{1 + \beta \eta^3} \frac{\varepsilon^2}{k}, \quad \eta \equiv Sk/\varepsilon, \quad \eta_0 = 4.38, \quad \beta = 0.012 \quad (2.27)$$

ANSYS FLUENT can always generate the effects of buoyancy on k if there is a non-zero gravity field and a non-zero temperature (or density) gradient. Whereas for the generation of  $\varepsilon$ , these effects are neglected because its effects are not well understood [43]. All k- $\varepsilon$  models represent the turbulence kinetic energy production and the dilatation dissipation term (which takes into account the compressibility affects turbulence) in the same way [44]. To calculate the effective thermal conductivity, the standard and realizable k- $\varepsilon$  models use a constant Prandtl number, Prt=0.85 . For the RNG k- $\varepsilon$  model, Prt = 1/alpha, where alpha is the inverse effective Prandtl numbers and can vary. With high Reynolds numbers in Ansys, alpha =1.393. This model can calculate heat transfer in low-Reynolds-number

## 2. Theory fundamentals

---

zones [45].

### 2.3.1.3 Wilcox's standard k - $\omega$ (Julio)

The k- $\varepsilon$  models entail a very good approximation in a wide range of simulations. However, for aeronautical environments in which aerodynamic phenomena such as complex vorticity are important and the turbulence source strongly affects the flow behaviour, their accuracy is compromised. Although the flow is generally, inviscid, the influence of viscous and turbulent boundary layers and wakes makes it possible that vorticity in very small lengths of scales introduce a significant change in the overall flow nature.

According to [37], the most important drawbacks of the k- $\varepsilon$  model in aerodynamic environments involve the following facts:

A systematic overprediction of turbulent shear stress is captured by the k- $\varepsilon$  models, specially when there are adverse pressure gradients within the domain. Similarly, turbulence is also excessive under the presence of impingement either stagnation regions resulting in overprediction of heat transfer in the flow reattachment.

As a result, [46] tried to overcome these issues particularly notorious in the aerospace field. Similarly to the k- $\varepsilon$  models, two additional equations are used. The turbulent kinetic equation "k" equation remains barely equal, following Granshaw's assumption. Nonetheless, instead of serving the specific dissipation rate as second variable, Wilcox defines and derives the turbulent frequency  $\omega = k/\varepsilon$ . From this variable, the eddy viscosity is easily obtained with the equation:

$$\mu_t = \rho k / \omega \quad (2.28)$$

The two variables of this turbulence model are evaluated through a partial differential equation - particularly known as transport equation - such that the time evolution and transport of both is conserved through its source and dissolution . The scheme followed for these equations can be described as: rate of change of the variable + Convective transport of it = its turbulence diffusion + rate of production + rate of dissipation. Hence, the equations will be derived as: · Turbulent kinetic energy

$$\frac{\partial(\rho k)}{\partial t} + \nabla \cdot (\rho k U) = \nabla \cdot ((\mu + \frac{\mu_t}{\sigma_k}) \cdot \nabla k) + P_k - \beta^* \rho k \omega \quad (2.29)$$

$$\tau_{i,j} = 2\mu_t S_{ij} - \frac{2}{3} \rho k \delta_{ij} \quad (2.30)$$

## 2. Theory fundamentals

---

The stresses to be computed follow Reynolds' stress formulation, using Bousinessq expression:

$$\frac{\partial(\rho\omega)}{\partial t} + \nabla \cdot (\rho\omega U) = \nabla \cdot ((\mu + \frac{\mu_t}{\sigma_\omega}) \cdot \nabla \omega) + P_k + \gamma_1 (2\rho S_{ij} \cdot S_{ij} - \frac{2}{3}\rho\omega \frac{\partial U}{\partial x_j} \delta_{ij}) - \beta_1 \rho\omega^2 \quad (2.31)$$

and therefore biases the transport equations with the rate of production for both. Is it important to take a look of its influence in the term of the rate of the turbulent kinetic energy production hidden within the variable  $P_k$ .

$$P_k = 2\mu_t S_{ij} - \frac{2}{3}\rho k \frac{\partial U_i}{\partial x_j} \delta_{ij} \quad (2.32)$$

Furthermore, the constants used in this procedure have the following magnitudes:  $\gamma_1 = 0.553$ ,  $\beta_1 = 75/1000$ ,  $\beta^* = 9/100$ ,  $\sigma_k = 2.0$ ,  $\sigma_\omega = 2.0$

The use of this formulation or turbulence modelling entails a series of advantages in comparison with  $k-\epsilon$  methods. The first evident, is the fact that wall distance is not needed to be computed anymore. Theoretically, the parameters  $k$  and  $\omega$  have been set to 0 and to  $\infty$  respectively, yet Wilcox suggests approaching  $\omega$  with the hyperbolic function  $\omega_p = 6v/(\beta_1 y_p^*)$ . Experience has demonstrated that these value do not have a relevant impact on the final simulation.

Additionally,  $k$ -omega outstands for near-wall flow interactions. It demonstrates good performance with strong vorticity phenomena, swirling flows and complex boundaries, though slightly overpredicts separation too.

On the other hand, several weaknesses are also noticed. The mean flow is worsely predicted than in the  $k-\epsilon$  model, probably as a result of high sensitivity to inlet boundary conditions, initial conditions and with bad performance on free-stream flows. As it equally happened with the  $k-\epsilon$ , the shear stresses are overpredicted in adverse pressure regions, although its solution convergence is sometimes seriously slowed. As a result, several modifications and proposals have been done to Wilcox's method.

### 2.3.1.4 Shear Stress Transport $k$ - $\omega$ (Marc)

This turbulence model was created by [47] due to the limitations of the  $k$ -omega standard model. An over-prediction of shear stresses and bad performance in free-stream

## 2. Theory fundamentals

---

flows were the main responsible for the development of the Shear-Stress Transport k-omega model. Additionally, compared to k-epsilon models, the standard k-omega model displayed bad convergence ratio and special sensitivity to inlet boundary conditions and initial conditions as well.

Menter realized that the drawbacks of the standard k-omega model were overcome with the advantages of the k-epsilon model and vice versa, hence, a merge of both turbulence models could exhibit the best features of both. This last idea was the main motivation of the k-omega SST. Therefore, he developed a switch selector (transitioned by a blending function) that chooses which of these approaches conveniently prevails depending on the flow region and conditions faced. Besides, it follows Bradshaw assumption in which the principal shear stress is directly proportional to the kinetic turbulent energy such that  $\tau = \rho a_1 k$  or, in two-equations turbulence models,  $\tau = \mu_t \Omega$ .

Overall, the k-omega SST model exhibits better accuracy than both “father” models in determining the flow separation and reattachment. As said, it combines the good prediction of the k-epsilon model for free stream and main flow and the accurate performance of k-omega in boundary and near-wall behaviour. Although it is slower, its high accuracy is able to solve complex fluid phenomena in which the Spalart-Allmaras struggles. However, it may occasionally produce large turbulence levels in regions where large strain takes place, such as stagnation and highly accelerated regions. Nevertheless, this trait is much milder than the effect produced by the k-epsilon model.

This turbulence model includes two supplementary transport equations to predict the turbulent behaviour of the flow which will be presented immediately. As it is expected, the mathematical expressions do not hugely differ from the equations introduced in both reference turbulent models. The one with which most similarities are devised is with Wilcox’s k-omega, although the constants specified vary, but share even more traits with Menter’s baseline model (only the turbulent eddy viscosity and the parameter  $\sigma_K 1$  are not common)

The first of the two equations, the turbulent kinetic energy, is defined with:

$$\frac{\partial k}{\partial t} + U_j \cdot \frac{\partial k}{\partial x_j} = P_K - \beta^* \cdot k_\omega + \frac{\partial}{\partial x_j} ((v + \sigma_k \cdot v_T) \cdot \frac{\partial k}{\partial x_j}) \quad (2.33)$$

Similarly, specific dissipation rate can be derived:

$$\frac{\partial \omega}{\partial t} + U_j \cdot \frac{\partial \omega}{\partial x_j} = \alpha S^2 - \beta \omega^2 \cdot k_\omega + \frac{\partial}{\partial x_j} ((v + \sigma_\omega \cdot v_T) \cdot \frac{\partial \omega}{\partial x_j}) + 2(1 - F_1) \cdot \sigma_{\omega 2} \cdot \frac{1}{\omega} \frac{\partial k}{\partial x_i} \frac{\partial \omega}{\partial x_i} \quad (2.34)$$

## 2. Theory fundamentals

---

These equations are supported by the Reynolds' Shear Stress Equations:

$$\begin{aligned} P &= \tau_{ij} \cdot \frac{\partial u_i}{\partial x_j} \\ \tau_{ij} &= \mu_t (2S_{ij} - \frac{2}{3} \frac{\partial u_k}{\partial x_k} \delta_{ij}) - \frac{2}{3} \rho k \delta_{ij} \\ S_{ij} &= \frac{1}{2} \frac{\partial u_i}{\partial x_j} + \frac{\partial u_j}{\partial x_i} \end{aligned} \quad (2.35)$$

The kinematic eddy viscosity is modelled as:

$$v_T = \frac{a_1 k}{\max(a_1 \omega, SF_2)} \quad (2.36)$$

The closure entities are given by:

$$\begin{aligned} \cdot \text{Blended constant function } \phi &= F_1 \phi_1 + (1 - F_1) \phi_2 \\ \cdot F_1 &= \tanh((\min(\max(\frac{\sqrt{k}}{\beta^* \omega_y}, \frac{500v}{y^2 \omega}), \frac{4\sigma_{\omega 2} k}{CD_{k\omega} y^2}))^4) \\ \cdot F_2 &= \tanh((\max(\frac{\sqrt{k}}{\beta^* \omega_y}, \frac{500v}{y^2 \omega}))^2) \\ \cdot CD_{k\omega} &= \max(2\rho \sigma_{\omega 2} \frac{1}{\omega} \frac{\partial k}{\partial i} \frac{\partial \omega}{\partial i}, 10^{-10}) \end{aligned} \quad (2.37)$$

The constants used within the SST k-omega turbulence model account for the magnitudes of:  $\alpha_1 = 5/9$ ,  $\alpha_2 = 0.44$ ,  $\beta_1 = 3/40$ ,  $\beta_2 = 0.0828$ ,  $\beta^* = 9/100$ ,  $\sigma_{k1} = 0.85$ ,  $\sigma_{k2} = 1$ ,  $\sigma_{\omega 1} = 0.5$ ,  $\sigma_{\omega 2} = 0.856$

Additionally, according to (Menter, 1993), the implementation of a production limiter should improve the accuracy of the turbulence model. The most basic function recommended stands for the expression of:  $P = \min(P, 20\beta^* \rho \omega k)$

It is important to notice that the flow near the wall is different from the mean. In the normal direction of the wall, the flow is highly constrained and eddies are mainly anisotropic, and when flow is near to it, the flow shows laminar traits at the viscous sub-layer. This fact is incompatible with most of the linear turbulence models (such as the two-equation models seen), where turbulent and isotropic behaviour is predicted instead. In order to solve it, algebraic stress models and non-linear turbulence models have been developed by NASA and UMIST, which remain more trustworthy to real physics but demand significantly higher computational cost and time.

Although the k- $\omega$  SST has succeeded treating the adverse pressure gradients environ-

## **2. Theory fundamentals**

---

ments where the rest of the two-equations families have struggled, several proposals of enhancing this model have been done since its initial formulation. According to [48], in [49] the proper Menter proposed using the strain rate in the eddy viscosity instead of the term of vorticity. Besides, collaborating with Smirnov in [50] -and interestingly enough having the publication in the same year- Menter suggested an improvement by correcting the rotation and streamline curvature of the model. Finally, in [51], apart from these insights, two minor corrections are raised. The first one is a methodology to boost the blending function. The other poses a proper boundary treatment of the solid-wall behaviour of the parameter  $\omega$ .

# **Chapter 3**

## **Simulation Setup**

### **3.1 Physical Problem (Marc)**

The physical problem represents the aircraft operation in cruise conditions, where the air moving surround creates an adverse gradient of pressure and flow variables across the wing surface. This scenario induces different forces, stresses and momentum distributed along the aircraft geometry which can lead to deformation or even fracture of the structures depending on the material used and structural elements disposed. Furthermore, the deformation or displacement of the solid surface simultaneously perturbs the flow over it and hence a feedback between both structural and fluid insight is continuously made.

Here, as the problem is considered to be steady, the fluid problem will be solved and the pressure distribution along the wing will be imported as load to the structural problem as a 1-way scheme. However, a 2-directional feedback scheme has been designed as well and correctly tested in case an unsteady simulation is aimed. Since most of past flow problems were approached through analytical assumptions -validated by the aerodynamic theory-, in this research the most common point forces according to rigid solid mechanic theory and triangular lift theory will be also reviewed.

Once the fluid solution is approached, the structural problem will be subsequently solved with ANSYS or ABAQUS simulations held by the newtonian mechanic principles.

In this sense, the fluid and structural problem of the wing operation is coupled and adequately evaluated. This accurate approach is known as the Fluid-Structure Interaction (FSI) and its investigation is quite recent, since earlier computers could not cope with the memory and CPU power required.

### **3. Simulation Setup**

---

#### **3.2 Aircraft characteristics - ONERA M6 Wing (Marc)**

No details of current aircrafts using this CFD benchmark wing have been found in literature as it is mainly used for CFD algorithm validations. Therefore, the total simulation of the aircraft cannot be done, then the wing will be considered as the main element.

In case the total aircraft for a different commercial wing was aimed, the wings are the most representative and predominant element for lift generation - since the horizontal stabilizer is, as its name reveals, mainly significant for control issues. The lift distribution could be obtained and multiplied per two (wings), the total weight of the fuselage could be easily obtained and applied in the center of forces and a whole simulation could be in this sense set.

The geometry of the ONERA M6 wing can be described with the following image 3.1, which has been served as a scheme to create the CAD geometry.

### 3. Simulation Setup

---

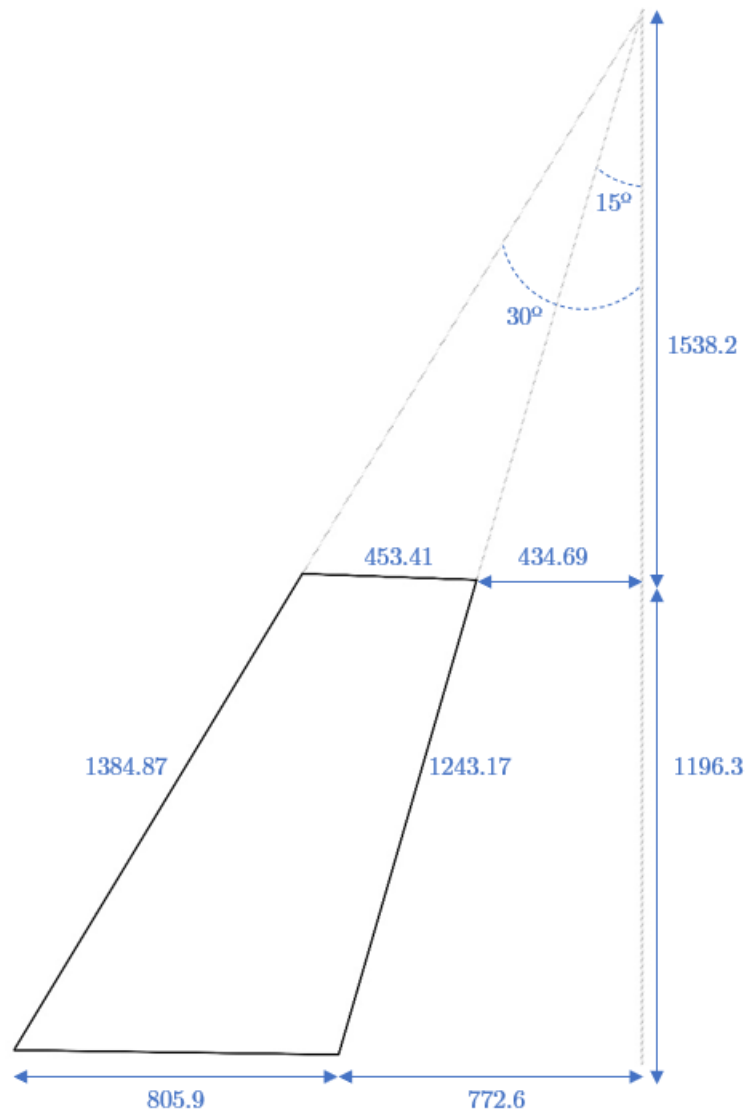


Figure 3.1: ONERA M6 Wing geometry definition

Besides, the aerodynamic usual parameters of wing design have been included in Table 3.1.

### 3. Simulation Setup

---

Table 3.1: Wing geometry aerodynamic parameters

Semi-wing Span (b)	1.19 m
Mean Aerodynamic Chord (c)	0.65 m
Aspect Ratio (AR)	3.8
Taper Ratio ( $\lambda$ )	0.562
Sweep Angle ( $\Lambda_{25\%}$ )	26.7
Leading Edge Sweep	30°
Trailing Edge Sweep	15.8°

#### 3.2.1 CAD Modelling (Julio)

In order to perform the simulations that are going to be described in the following sections, it has been necessary to create a CAD model. To do this, it has been used the well known CAD software CATIA V5, which is one of the most used CAD software in the industry.

The wing CAD model created is composed by 8 ribs, 2 spars, and the skin that covers all the internal structure. The geometry of the wing has been created by following the geometrical indications that describes the ONERA M6 wing in 3.1. The ribs have been created with the airfoil described by the points extracted from the references, and an extrusion of 3 mm has been done from that. As the wing has a sweep angle of about 30 degrees, each rib has had to be rescaled, and positioned according the geometrical conditions. For the beams, it has been positioned one near the leading edge at the 15% of the chord, and the other one near the trailing edge at 30% from it. Those beams has "UPN" normalized section with a height of 20 mm. Finally, the skin created for the wing has been performed with the surface mode of the CATIA V5 software. To do so, a multiple-surface tool has been used to extrude the skin from one rib to the following one, until all the skin is created. After that, it has been given a thickness of 1 mm to the created skin. All the drawings with the measurements of all the parts are included in the annex of the present study.

### 3. Simulation Setup

---

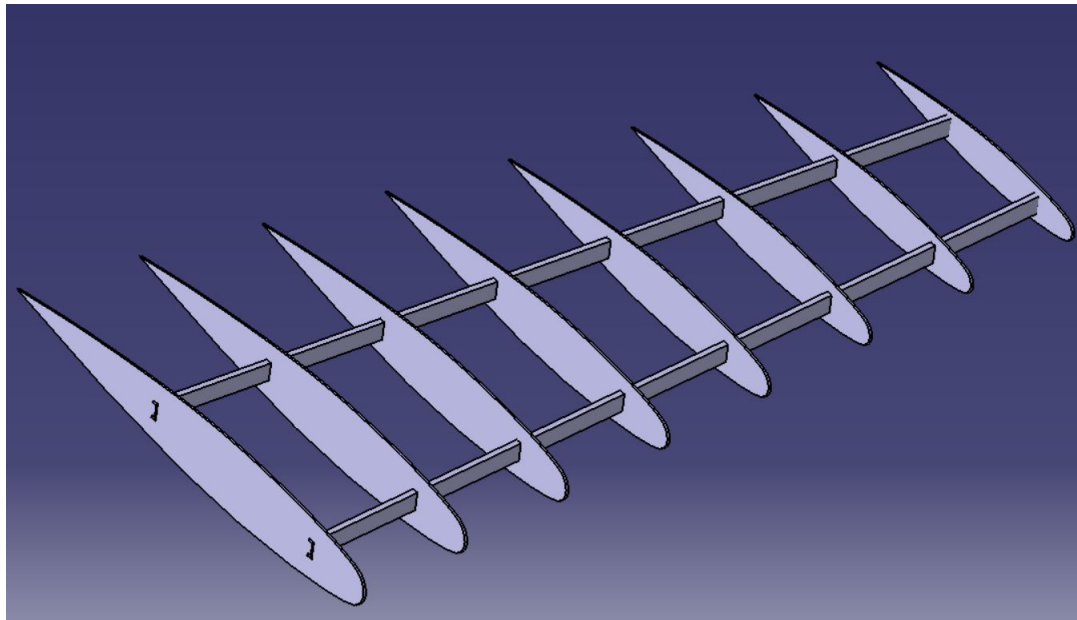


Figure 3.2: ONERA M6 CAD - Inner Structure

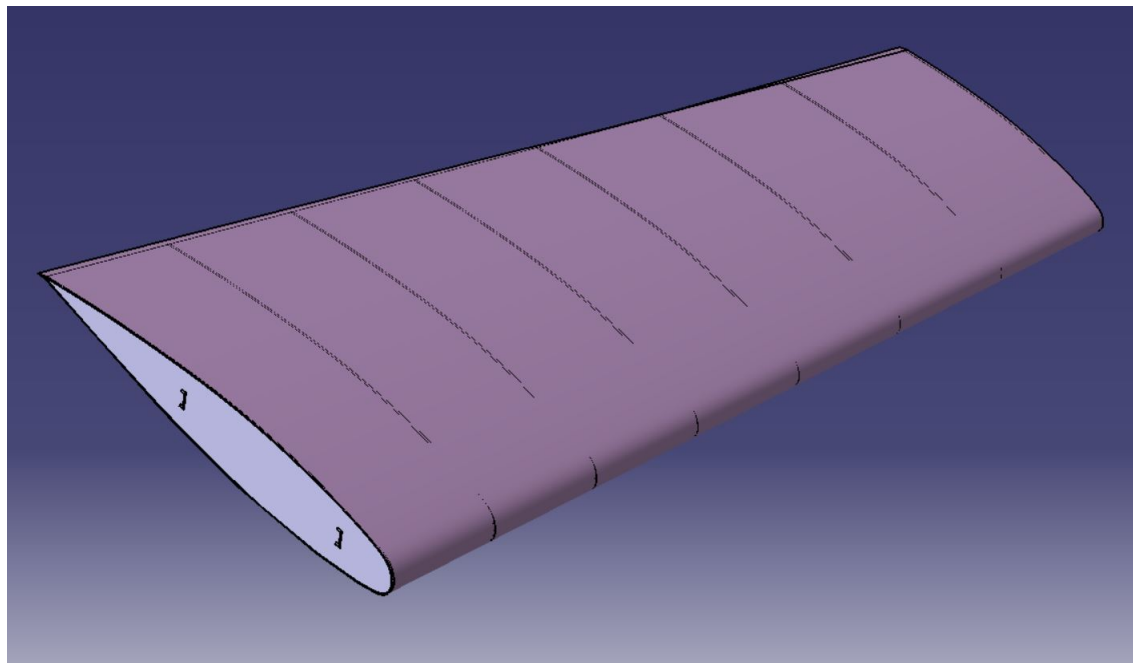


Figure 3.3: ONERA M6 CAD - Skin

### **3. Simulation Setup**

---

## **3.3 FEM Modelling**

### **3.3.1 Motivation and Definition of Finite Element Methods (Marc)**

The aim of the computational approaches is to translate the continuous (and therefore, somehow, "infinite") problem into the computational and discretized domain without loss of generality. However, this process entails a not evident yet large succession of problems and incompatibilities which will strongly compromise the accuracy of the solution. One example of it is the fact that, as it seems logical, the more elements and higher resolution considered, the more accuracy should be expected. However, as it has been proved by [52], some further studies and considerations about the stability of the discretizations (specifically in their publication, the CFL number relating spatial and time resolution). In the end, a general method that satisfies and guarantees the accuracy in all the variables and insights is not achieved and it is not likely to happen in a near future.

This is why, depending on the objectives of our study and considerations of the approach, several methods are available and new can be developed by attacking the same problem through different approaches or techniques.

As said, we are dealing with "nodes" or "points" that involve cells between them with n-dimensions (being n the number of variables to be solved) creating a grid or mesh structure where every node can be identified and is surrounded by more of them until the boundaries are reached. This formulation is known as Finite Element Analysis (FEA). The number of nodes is limited although the most attending to the judgement of how the differences and integrals of the governing equations (usually PDEs) are modelled and met, several methods standout as the most interesting ones to solve the differential equations: Finite Difference Schemes, Finite Element Methods and Finite Volume Methods. A detailed comparison of the features and performance of each of these procedures has been documented in [53], nonetheless, the basics and applications of each method will be introduced in this section.

Regarding the first ones, the Finite Difference Schemes, they attack the finite discretization of the solution by evaluating the evolution in space and time with increments of the variables. This is why they are called difference, by a uniform increment you can pass from one node to another. In this ambit, stencils are normally examined, as they give a quick representation of the dependencies of a determined grid value regarding their neighbouring values. In many procedures and calculations the Taylor Series are used within this methodology as they can approach values in other points by acknowledging the analytical derivation of the functions, or it can be calculated through the difference schemes

### **3. Simulation Setup**

---

as well. As it is evident, this approach is the most easy that can be considered and may work well under conditions of structured mesh, steady grid and boundary conditions and non-curvilinear geometries. If these assumptions do not match with the physical problem, artificial results will be obtained.

Another approach which is specially useful in the Structural ambit is the Finite Element Modelling. The mathematical formulation behind it is stronger than the found in the Finite Difference Schemes and subsequently acquires more generality. It assumes that the values of the solution can be approached through a finite summatory of the discretized values of that solution over a function that distributes the solution over the whole domain. The scalar product between different function vectors is known as the usual and it is given by the integral of both functions over a determined region. Depending on the attributes of these vectors, Galerkin methods are correctly derived, which are commonly used nowadays. With this approach, when evaluating the derivatives of these functions, a linear system of "n" equations is faced and it is solved by matrix numerical computation (for example, iteratively). Attending to the Elastic theory and specifically Hooke's Law, it is an efficient method of relating the displacements and nodal forces by solving the  $F_n = [K]_{nxn} \cdot x_n$  equation where K is the stiffness local or global matrix depending on the element to be solved. The other magnitudes can be easily obtained by formula application of these solutions, which need the implementation of boundary and initial conditions in order to not have a singular matrix. This is the suitability of FEM to describe structural problems and why it is the most used in this environment. With this approach, it is now able to consider more complex and unsteady geometries.

Finally, the Finite Volume Methods are widely used in CFD assumptions as they are capable of considering non linear phenomena and discontinuities in the variables which do take place in the physical problem. It assumes that the partial differential equations (as it happens with the Euler Equations) derive from conservation laws and hence fluxes -over defined volumes- for these conservative variables can be obtained. With the evaluation of these fluxes (averaging the integral value), the solution can be advanced in space and time. This is the most complex yet mathematically strong approach of the finite methods that have been described here. Specifically, in our FSI simulation, it will be used with the ROE-FDS Flux Riemann Solver for predicting the flow field over the ONERA M6 geometry in the operation conditions described. Therefore, it suits the most complex geometries and most general problems without incurring in an excessive loss of accuracy. However, the mathematical approach for each problem is really complex and the other modelling steps (discretizations, schemes, resolutions) that have not been described here do have an important influence on the solution.

### 3. Simulation Setup

---

Although the most complete approach is the Finite Volume Methods as it can be seen, for structural models, it is found that the FEM approach does provide an excellent performance and accurate results. Then, this approach will be the one applied in our ABAQUS and ANSYS Mechanical software. Depending on the structural features of each modelled part of the wing (skin, ribs, spars, etc even screws), modelled elements of different properties will be set according to the physical behaviour. These have been explained in the following section.

#### 3.3.2 Elements (Marc)

##### 3.3.2.1 1-D Elements

**Bar Element:** Modelled with 3 translation stiffnesses (no rotational) at each end so that it can only consider axial loads. If its cross section is circular, it is also known as rod element. As a result of its DOF, it is not subject to bending or torsion.

**Beam Element:** It adds 3 rotational DOF per node to the Bar Element, then, it has stiffness in all six directions. With this configuration, it can now deal with axial force, bending, and torsional loads. However, in order to be fully able to model an element with beam, several assumptions must be made: the length of the element is predominant to the other dimensions (width, depth). Besides, the cross section must remain constant for the whole element. In terms of the behaviour of the physic element, it must be able to transfer moments through the whole structure and also to resist a distributed load along its length.

##### 3.3.2.2 2-D Elements

**Plate Element:** The first conditions to fulfil to be able to consider a particular geometry as a plate element accounts for the fact that initially, the geometry must be flat in one plane and also the thickness of the real 3-D element must be smaller than the other 2 spatial dimensions.

Attending to the formulation of Plate Elements, they state three DOF per node (1 out-of-plane translation + 2 in-plane rotations) translation. This configurations makes them suitable for their use in research projects such as in pressure vessels.

Load forces must be perpendicular to the element plane, and moment must act around an axis contained in the element plane.  $\sigma_{zz} = 0$ . Direct stress component perpendicular to the plane is 0 so that the plane stress condition is fulfilled. The normal of the element plane remain straight after the deformation, but by definition, they do not have to be perpendicular to the element plane. The displacement perpendicular to the plane does not vary along the thickness.

**Membrane Element:** the membrane element is similarly defined as the plate element

### 3. Simulation Setup

---

with the main difference that the DOF are set contrary. This element also possesses Membrane elements also have three degree of freedoms, being two of them in-plane translation and one out-of-plane rotation. Due to this, the transmission of moment loads is not possible. A reasonable and interesting example would be considering the effects present in a balloon interface.

**Shell Element:** They are considered to be mainly a 2-D element since the first assumption is the fact that width and length must be larger than the thickness dimension.

Generally, membrane elements, plate and shell elements are commonly confused, but the main difference between them is that the combination of the first two can define the shell element behaviour. Therefore 6 DOF per node (3 translations + 3 rotations) are considered in the shell element. From the "2-D elements" (actually 3 but thickness in the mathematical approach is neglected) they are probably the best at capturing bending as a result of the discrete Kirchoff approach applied, which remains accurate to plate bending, by making use of Batoz's interpolation functions. Subsequently, the Kirchoff constraints are satisfied throughout the boundary layer. Besides, it also entails the linear development of the element's curvature. Depending on the number of nodes defined per element, triangular (3 to 6 nodes) or quadrilateral (4 to 8 nodes) geometries are usually used as main cells. For plane elements, by using the Linear Strain Triangular element (commonly known as LST, the Allman triangle is developed for triangular elements but the configuration of the same for quadrilaterals is easily derived as well. Thanks to this, curved elements can be approached as a result of the merge of the planes defined by the element's nodes.

It must be said that shell elements are usually computationally defined by their nodes or by their area in conjunction with a normal vector that indicates the orientation and configuration of shell elements. There are several procedures or criterions to treat this data then mesh will likely be -and it is needed to be- high quality For this reason a well-refined mesh is necessary. It must be said that, the less number of nodes per element, the finer mesh is needed as they must converge to a solution of displacement and stress by taking into account the out-of-plane bending.

Similarly to plate elements, the moments must act in the plane, and forces can be perpendicular or inside the plane. If they are flat, they can be computed as a combination of plane shane elements and plane plate elements. In order to compute the bending motion, Mindlin-Reissner theorem is applied and then the Mindlin element is modelled. It must be said that, for plane shell elements, the computation of values through integration can only be done through the reference surface.

### **3. Simulation Setup**

---

#### **3.4 Boundary conditions (Marc)**

The root airfoil is fixed to the fuselage thence the boundary conditions to be applied will remain as solid fixed. The airfoil of the tip, in the other hand, will be set free in its 6 DOF.

#### **3.5 Applied Loads (Marc, Julio)**

Due to the simplifications made during the modelling procedure, the applied loads must be dimensionalized as the worst-case scenario the aircraft can face. In this case -as the total weight of the aircraft and load due to aerodynamic forces is variable during the different stages of a flight- it is normally believed that the maximum take of weight may imply the most conflictive weight in terms of structural analysis. Besides, each engineering step must guarantee high standards of safety and durability, fulfilling each of the strict requirements held by aviation regulations and normative. Thence this total estimated weight may be equally multiplied by a safety factor such as the normative FAR 25.303 regulation indicates (the current value recommended is actually 1.25). Once the Lift Load is grossly reckoned, it will be assumed that it is entirely held by both wings, as the contribution made by the horizontal plane is negligible as its main functionality remains for stability purposes. Then, if problem is reduced to the study of a single wing this lift load will be reduced to its half.

Exist several methodologies to approximate the lift applied to the wing in order to the implementation of it into the FEM solvers. The first one, which is the simplest one, consist in apply all the load into one node located in the center of pressures of the wing. This method is very easy and quick to implement, and it is useful in a first preliminary study to know the order of magnitude of the stresses and displacements, however is not accurate. A clear example of it is (Kumar Das, Roy ; 2018), where a total force of 500 Pa is applied to this particular point. Here, in this research paper, the worst case scenario will be always considered as reference and studied in order to satisfy the minimum safety of the operation according to aviation regulations.

A second approximation that is also easy to implement, and gives more slightly accurate results, is the uniformly distributed lift load. This model provides a better approximation as the total load is distributed uniformly along all the surface of the wing, making this way, a more realistic approximation, however the loads of the wingtip and trailing edge will be overestimated, and it will be considered as a conservative approach.

Another important trait to bear is, according to the aerodynamic theory, the approach of how this load is geometrically applied to the wing. The most accepted yet basic approx-

### 3. Simulation Setup

---

imation, given the lift distribution, is a triangular load distribution which will be revised in the following lines.

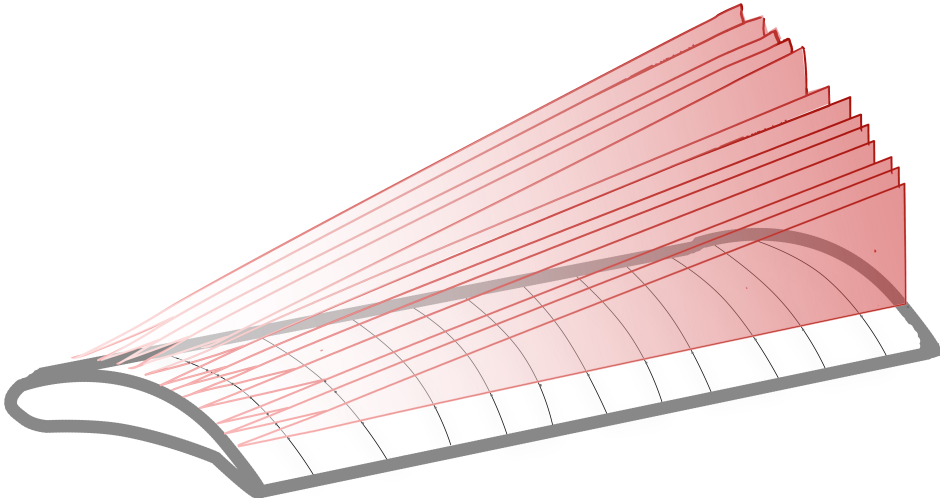


Figure 3.4: Triangular Lift Scheme

Triangular lift distribution is a simplification of the behaviour of the lift that aims to facilitate the problem of applying a real pressure distribution over the wing. This distribution is usually used for wing structural simulations, as can be observed in reference (Hoang; 2015) [4], and produce accurate results in comparison with real pressure distribution for typical subsonic and transonic flight regimes, with an easier implementation into the FEM solvers. This simplification is applied by creating a triangle, with a value of 0 at the wingtip, and increasing its value until reaching the maximum load value  $P$  at the root of the wing. In the same way, a triangle is created in the chord direction, with a value of 0 at the trailing edge and the maximum load value  $P$  at the leading edge. The combination of this two type of triangles create the triangular distribution of load over the surface of the wing that is used to simplify the lift, which can be seen in Figure 3.4.

Nonetheless, this approach may not represent the current problem as it only supposes an ideal approach, still simple and fast to compute which can actually give an interesting overall result. As a consequence of this, exist one methodology that allows to study the

### **3. Simulation Setup**

---

structural problem of the wing directly with the results obtained from the wing fluid simulation. This method is known as Fluid-Structure Interaction (FSI).

The FSI simulations allows to couple the CFD and FEM simulations by exporting the pressure results of CFD solver to the FEM one, and performing the structural simulation with that input. However as both solvers use different codes, the transfer of the boundary conditions from one code to the other, as well as the mesh are some of the main issue of the method. In this study, the CFD study is going to be performed with ANSYS Fluent software, and the FEM analysis with ANSYS Workbench and Abaqus. The coupling of both software Fluent and Workbench to perform the FSI method is simply to perform as it will be explained in this study, because both codes are developed by the same company, however the coupling of Fluent with Abaqus software is a way more complex, because the bad compatibility of both software.

### **3.6 ANSYS-FLUENT Setup (Marc)**

In order to achieve the FEM simulation based on Fluid-Structure Interaction we have chosen the ANSYS Workbench software.

The geometry to be simulated has been provided by Dr. László Könözsky in the assignment of "Modelling Approaches for Aerospace Applications" and reused within this investigation as the structural geometry -ONERA M6 wing- is the same for both studies.

A ".cas" file has been imported to the program ANSYS-Fluent where it includes the fluid zones of far-field, interior fluid, symmetry and wall, where will be served as an imported layer to the structural simulation. There is where will be important to correctly predict the fluid phenomena.

The conditions assumed to carry out the simulation are the following:

### 3. Simulation Setup

---

Table 3.2: Flow parameters setup

Density	Ideal
Cp	1006.43
Thermal Conductivity	0.0242
Viscosity	Sutherland
Molecular weight	Constant

As it can be seen the density is modelled with the ideal gas law in order to relate pressure, temperature and volume according to the principle of the state equation. The specific heat at constant pressure is considered to be constant along the whole domain such as the thermal conductivity of air, which is set to 0.0242. Besides, the viscosity is modelled with the two-coefficient Sutherland law which provides, according to [54], given by the following expression:

$$\mu = \frac{C_1 \cdot T^{3/2}}{T + C_2} \quad (3.1)$$

where  $C_1$  and  $C_2$  are coefficients whose values are, respectively,  $1.48 \cdot 10^{-6}$  and 110.4. These have been the definitions of the thermodynamic variables that are involved within the movement equation, nevertheless, the flow must be equally defined. The operation takes place in a transonic regime of  $M=0.858$  where most of commercial aircrafts develop their cruise stage. Although it is not as severe as the conditions suffered during take-off and landing where high lift devices are deployed, then the modelling of them was not the aim of the investigation therefore the study under transonic environment, when special fluid phenomena take place -such as non-linear waves and boundary layer detachment - that strongly influence the flow but the structure as well. In the same manner, the flow is supposed to be with an angle of attack (AoA) respect to the leading edge of  $5^\circ$ , then the X and Y components are accordingly  $\cos(5^\circ)=0.9993537$  and  $\sin(5^\circ)=0.035946$ .

The governing equations are solved through numerical means, which entails a necessary last setup of the approach followed. The flow will be implicitly solved, aiming for stability and worsening the time to converge. The Riemann Solver used to model the flow will be the ROE-FDS which bases is defined as a Godunov-type flow solver using its good performance to predict and capture non-linear waves by the treatment of discontinuities. The convective term will be defined as a 2nd order Upwind scheme which is accurate enough for this solver, even though more precision could be obtained by using a higher order scheme (MUSCL,ENO,WENO) but severely increasing the time of computation. However, it must be taken into account that so little literature is conducted in FSI (Fluid-

### 3. Simulation Setup

---

Structure Interactions) and most structural studies of wings are based in distributed loads or nodal forces application, hence the adequacy of the stated approach. Besides, the convergence monitor will be set to 1e-05 for all the flow parameters, in case they are achieved before completing 1000 iterations. This case, however, it is not likely to happen as the flow problem is complex enough to need more than 10.000 iterations to reach this convergence threshold, nevertheless, the stabilization of the residuals will be sighted. Feel this information gathered in the following table:

Table 3.3: Numerical definition of the flow solver

Method	Implicit
Flux	ROE-FDS
Flow	2nd Order Upwind
Courant Number	5

## 3.7 ANSYS-Workbench Setup (Léa, Erwan, Marc)

In this study, we are using the one-way FSI on ANSYS Workbench if we are dealing with static results or two-way when transient dynamics are aimed. In this sense, the static structural analysis is developed under the assumption of for small deformation theory in the structure. In order to perform the FSI, we calculate the flow field by using Fluent software as it is explained above. Then we import the solutions we have, to the structural analysis FEA code, which is composed of a static structural analysis, a modal analysis, an eigenvalue buckling analysis and a transient dynamic analysis. In Workbench, it can be done by transferring the solution data provided by fluent, to the setup of the static structural analysis system.

For the static structural analysis, the first step is to define the materials used in the Engineering Data component. This materials have been specified by our own as they are not gathered in the ANSYS default library of materials. Done this, it is necessary to import the geometry. Here the geometry is the one available on the internet repository Grabcad. Then the finite element mesh needs to be created by setting up the resolution and distribution. It must be considered that the larger mesh, the most CPU power is needed. This restriction will be commented in the following sections. Once this is finished, we can import the load from fluent -specifying its effect on the desired geometries or even parts of it-, defined a fixed support on the whole root chord section of the wing, and run simulation on the structures for the total deformation, the equivalent stress and the equivalent strain, which are the main structural parameters to understand the state of the wing.

### 3. Simulation Setup

Once we perform the static structural analysis, then we are able to make the modal, the buckling analysis and the transient dynamic analysis.

For the Modal analysis we need a pre-stress environment which came from the static structural analysis. We also transfer the engineering data and the geometry from the static structural analysis to the modal analysis system. After that we chose the number of modes we wanted, and we run the simulation in order to have the natural frequencies of the material and each modes shape.

For the buckling analysis, we transfer the engineering data, the geometry, the mesh and the solution from the static structural analysis to eigenvalue buckling analysis system. If not, it is also possible to run the buckling simulation under an unitary pre-stress state in order to then scale the problem with linear values. However, with the first procedure, the final results will be directly obtained for the operating conditions evaluated.

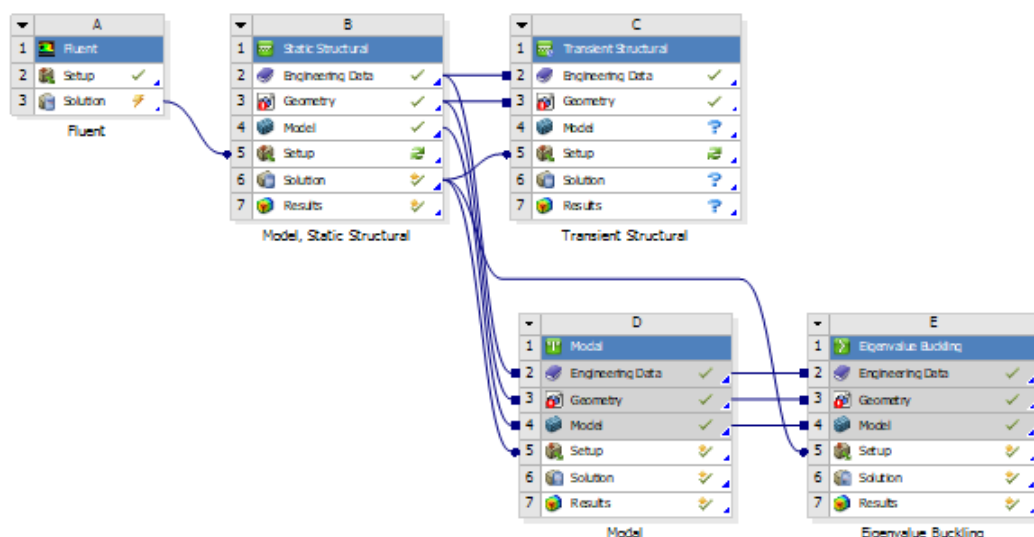


Figure 3.5: ANSYS simulation scheme: inheritance of values for the FSI problem

On the Figure 3.5 we can see the scheme we have used in ANSYS workbench in order to perform the one-way FSI analysis .

### 3.8 ABAQUS Setup (Julio)

ABAQUS software has been one of the selected codes to perform the FEM analysis. As it is widely used in the industry and it also is known by providing strong reliability results, specifically for this study has been used the version 6.14 of the software.

### 3. Simulation Setup

---

To perform the FEM analysis the first thing to do is to import the geometry created, which in this case will be the geometry created in CATIA V5 software described before. Once the geometry is imported, the materials for each part has to be defined. To do it, is needed to go to the properties tab, and create a new material, where the Young modulus, the Poisson coefficient and the density of the material will be introduced. Once the material is defined, a section must be created. The section is needed to define the type of element that will be considered for each part of the geometry. In this case, to simplify the problem and to reduce the computation time, shells will be used as main element. It also important to mention that when a new section is created the thickness of the shell has to be defined, and also the material that will compose that section. After that, is the moment to assign the section to the parts or the regions of the geometry. In this case, a shell section with steel and a 3 mm of thickness has been assigned to the ribs and the spars of the model, and section composed by the aluminum defined before, with 1 mm of thickness has been assigned to the skin.

Once this is done, it is time to mesh all the parts independently, and to do so, it is needed to go to the mesh tab. For creating the mesh for each part first of all, is needed to create the seed through the geometry, which will define the size of the mesh that is going to be created. The next step is to select the mesh element that is going to be used in each part of the geometry, and in order to obtain the best results possible, quads have been selected, as it has been demonstrated widely that in general produce better results than triangles. Moreover, the spars mesh will have a structured shape, however as the ribs and the skin has a complex geometry, their mesh will be unstructured. The mesh generated for both inner structure and for the skin is presented in Figures 3.6 and 3.7, which contains 91,667 elements.

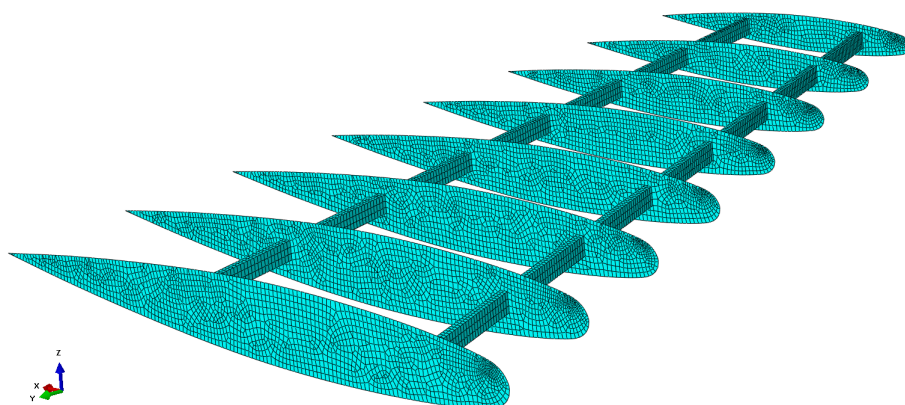


Figure 3.6: Inner structure mesh generated with Abaqus

### 3. Simulation Setup

---

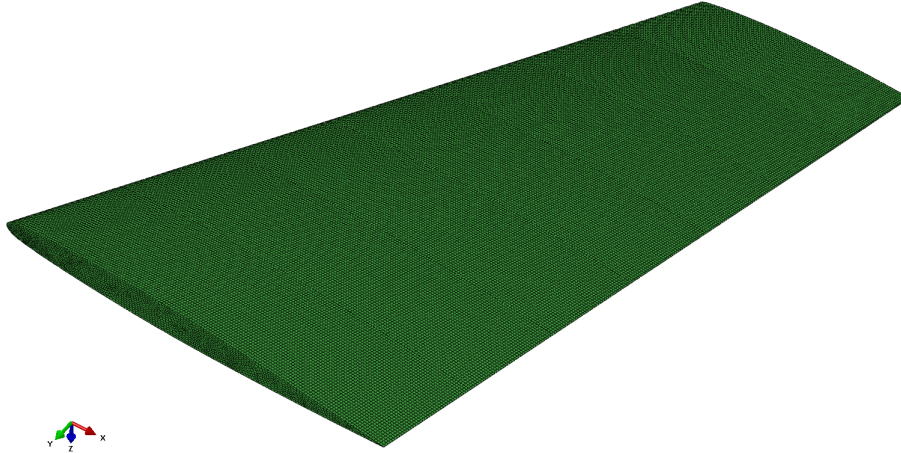


Figure 3.7: Skin mesh generated with Abaqus

The next in the set up of the simulation is to assembly the different parts that compose the geometry, and the interactions between them. In order to simplify the unions between the parts of the wing, it has been decided to consider the whole wing structure as one unique element. To do so, it has been merged the mesh of all the elements in a only one and unique mesh for all the wing, conserving all the individual properties of each element, including each mesh and merging only the boundary nodes. Doing this, the unions are considered perfect, and will not affect the final result.

When the model is assembled, is the moment to insert the boundary conditions and the loads presents on the problem. First of all, is needed to move to the steps tab, where the initial step corresponds to the initial state of the structure, where the BC are defined, and then a step 1 is created by selecting static analysis, that is the moment where the loads are applied. As the structure that is considered is a wing, the boundary conditions that will be defined are a fixation in the zone of the root, which means that this zone is constrained in displacement and rotation in all axis directions. Then in the step 1 the loads are defined, and as it three types of loads approximation will used, it is necessary to explain how is created each one. In the first case, a punctual load is used to approximate the load of the wing. To do so, the nodal force mode is selected and a node on the geometry is selected, as all the force will be applied directly on that point. Afterwards, the components of the force are introduced, and the load is completely defined. In the second case, the load is defined as a uniform load over the upper surface of the wing. To create this load, the pressure type of load is chosen, after that, the upper surface of the wing is selected, and the magnitude of the force that is going to be distributed through the surface is introduced. Finally, the triangular distributed load needs to be input, to do so, it is also selected the

### 3. Simulation Setup

---

pressure type of load, and also the upper surface of the wing. Afterwards, it is needed to introduce a new type of load distribution that is defined by the authors, which corresponds to a triangular distribution of the load, after that the magnitude of it is introduced, and the load is completely defined.

To create the function that define the triangular load distribution considering the dimensions of the wing presented in Figure 3.1, and that the triangular load is going to be done as shown in Figure 3.4, for a load P, the triangular load function is defined as follows.

$$542,7z + P(0.45y - 542,7) = 0 \quad (3.2)$$

Where the  $x$ ,  $y$  and  $z$  are the dimension components with origin on the leading edge of the root. For dimension the load P, reference [4] has been considered, as a similar wing is analysed. In this reference the load comes from wings of real commercial aircraft such as Boeing 787, and has a value of 336,251 N, with a surface of about  $165 m^2$ . As a consequence of this, the calculated load for the Onera M6 wing with a surface of  $0,7362 m^2$ .

$$P = \frac{336,251N \cdot 0,7362m^2}{165m^2} = 1,500.3N \quad (3.3)$$

The description above has referred only to the static analysis that is going to be performed however, modal and buckling analysis is also performed in this study. First of all, to setup the modal analysis, it is necessary to select a different procedure type when the step 1 is created, and select that a non-linear is going to be performed, and then select frequency analysis. After that, the number of eigenvalues that are wanted to obtain in the results is selected, as this is the number of different modes that are going to be obtained, once this is done, the modal analysis is set up.

For the buckling analysis, is also needed to create a non-linear step as before, and then select the buckle analysis. Once this is done, and as well as before the the number of eigenvalues that are wanted to obtain in the results is selected, and afterwards it is also needed to create the load as explained before, which in this case, for making a realistic approximation, the triangular load distribution is applied, and when this is done, the buckling analysis is ready for submit.

The next step to do, when all this set up is done, is to create a "job" to start the simulation. In this job, it is needed to select the type of simulation that is going to be performed,

### **3. Simulation Setup**

---

which in this case is a full simulation, and also the number of CPUs that are going to be used. Once all of this is selected, it is only necessary to "submit" the job and wait until the simulation is complete. Finally, when this is completed, it can be selected the results tab in order to visualize the results obtained, and see the stresses, strains or displacements that the software has achieved, and that are presented in the Results section.

# **Chapter 4**

## **Results**

### **4.1 Materials (Marc)**

Nowadays, current aviation research is based on the optimization of the marginal benefits obtained by reducing the operational cost of the whole performance. As it can be seen in most operation projects and analysis, a significant parameter that seriously affects the journey by limiting the scope, endurance and payload available to be carried is the Maximum Take Off Weight(MTOW), in which the structure of the aircraft is included. Thus, strategies to use lighter materials that are able to resist the aerodynamic forces throughout the whole operation, that do not bend excessively as the lift distribution would not be equal to the one seen until now, and specially that remain strong against fatigue to increase the time between maintenance applied (resulting in more efficiency) and to evade fatal failures are actively pursued.

Composite materials have proved excellent mechanical properties, reduced cost and high suitability to substitute partially or totally the skin of the fuselage of the wings, permitting the introduction of more priceable weight (payload). As it can be seen in relevant literature about composite materials ([55], [11], [12]), some composites present higher ratios of stiffness and strength compared to weight than conventional materials. Actually, current manufacture and latest versions of aircrafts such as Airbus A350, Airbus 320neo and Boeing 737MAX have significantly increased the proportions of these materials up to -according to [56] - a 60 percent of the structural area in comparison with the conventional Al 2024 T3 alloy. Furthermore, nowadays research is constantly analyzing and simulating different polymeric matrices in order to establish the most adequate and efficient for future manufacture. In this document, several composite materials that are used in recent investigations will be simulated. Please see the following table 4.1 in which the mechanical properties of the materials to be analyzed are detailed.

The specifications and theory background of each material has been provided in the Ap-

## 4. Results

---

Table 4.1: Mechanical properties of the materials to be evaluated

Material Properties	Al 2024 T3	Epoxy-Carbon UD	Epoxy E-Glass	Epoxy S-Glass
Ex (GPa)	73.1	121	45	50
Ey(GPa)	73.1	8.6	10	8
Ez(GPa)	73.1	8.6	10	8
Poisson Ratio (xy)	0.33	0.27	0.3	0.3
Poisson Ratio (yz)	0.33	0.4	0.4	0.4
Poisson Ratio (xz)	0.33	0.27	0.3	0.3
Gxy (GPa)	26.6	4.7	5	6
Gyz (GPa)	26.6	3.1	3.846	3.846
Gzx (GPa)	26.6	4.7	5	5
Density (kg/m <sup>3</sup> )	2780	1490	2000	2000
Tensile Strength (MPa)	483	3500	3445	4890

pendix, where the Epoxy Carbon UD, Epoxy S-Glass and Epoxy E-Glass composites are completely documented.

## 4.2 Coarse Mesh. Validation and Verification of the Results (Marc)

### 4.2.1 Flow Problem

The first step to be made is the solution of the flow problem in order to withdraw the pressure distribution over the wing to the structural analysis. The whole fluid domain is defined with 4 regions: far-field, symmetry, interior fluid and wall. Logically, the last two will be the more significant for our FSI simulation and therefore should be refined for the evaluation of accurate solutions. The mesh modelling this domain is composed by a coarse grid by the elements shown in 4.2.

Table 4.2: Configuration of the coarse mesh for the flow domain

Domain	Number of faces
Far-field	9216
Interior	843216
Wall	4608

Now, the only step remaining to conduct is to solve the flow problem for each turbulence model (Spalart-Allmaras, Standard k- $\epsilon$ , Realizable k- $\epsilon$ , Standard k- $\omega$ , and SST k- $\omega$ ).

## 4. Results

---

The methodology has been already explained in the section of ANSYS-Fluent setup, then should the reader revisit it. The maximum number of iteration has been set to 1000 and also the residuals convergence criteria is defined as  $10^{-5}$  for all the flow parameters to serve as a relatively accurate threshold. As it has been said, this threshold will not be reached at any simulation due to the complexity of the flow, however, the stabilization of the residuals around a determined value is noted.

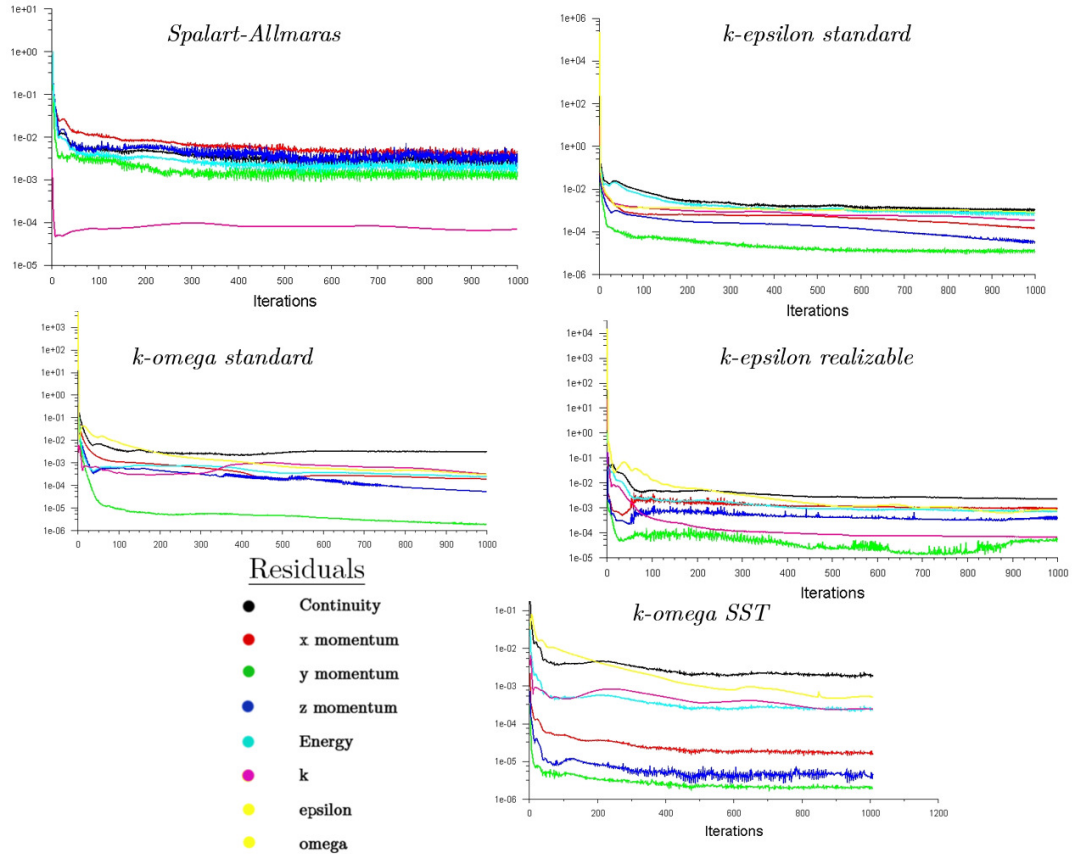


Figure 4.1: Residuals of the turbulence models

As it can be seen, the residuals get stabilized under a particular value ( $10^{-3}$ ), however the rate of stabilization is not the same. The program Fluent did not use the same y-axis for representing the plots (as a consequence of different first-steps values of some parameters) then the scale is not the same and it must be considered when analyzing the previous image. Figure 4.1 reveals that the convergence of the solution does not take place at the same rate. Spalart-Allmaras shows the best convergence, results can be withdrawn rapidly. Then, the k-epsilon models show better convergence than the k-omega models, fact that was already explained in the Theory Fundamentals section. Overall, the graphics provide reasonable and expected results and the accuracy is enough to consider moving

## 4. Results

---

on to evaluate the results.

Although the pressure distribution (as it can be seen in 4.2) is the main parameter needed to conduct the posterior structural FEA analysis, a validation of the flow problem is required in order to evaluate the accuracy of our numerical approach and to recognize which of all the turbulent models suppose a better description of the physical problem. Due to

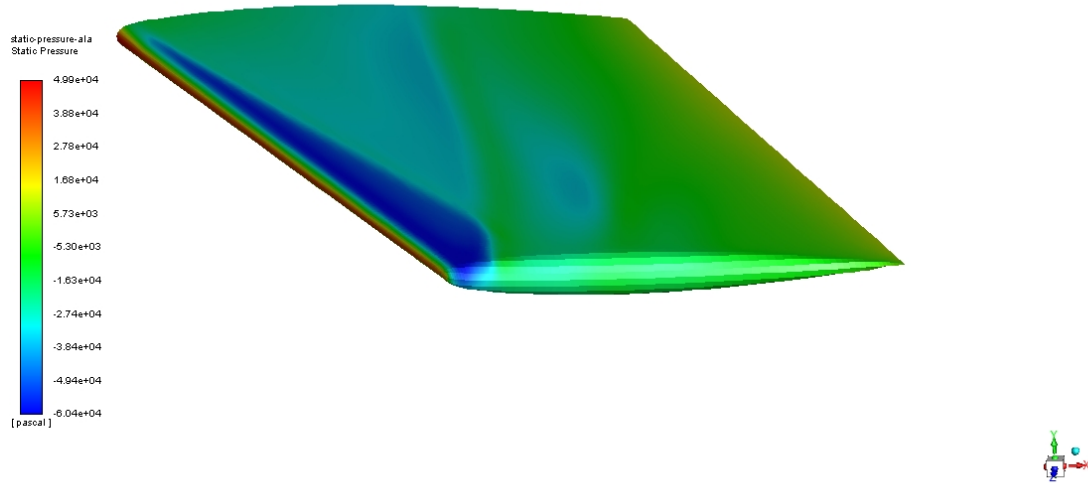


Figure 4.2: Static Pressure Distribution along the wing

the wing characteristics, it cannot be considered as infinite and actually the Aspect Ratio entails a huge difference of geometry between the root and the wingtip. This is why a huge influence of the wingtip vortical structures will be perceived along the wing and will diminish as the root is faced. This is why, it is wise to evaluate the results in three different sections ("airfoils"): one in the wingtip, one in the root and one in half of the wing. Besides, the flow variables across them will be more easily evaluated with special attention of the prediction of non-linear waves.

## 4. Results

---

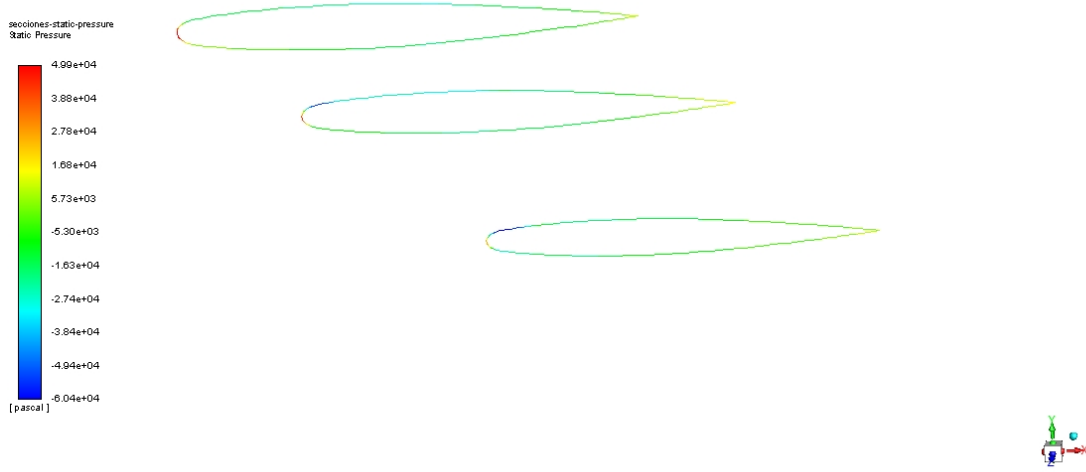


Figure 4.3: Static Pressure Distribution for the 3 selected sections

As Figure 4.3 reveals, the pressure contour of the wall is not even similar in all the "airfoil" sections. This issue is a direct consequence of the wingtip vortical structure explained and greatly captured by the k-omega SST method, although the Spalart-Allmaras turbulence model also provided a reasonable prediction of this effect. Its influence and variation is notorious depending on the wing coordinate we are evaluating.

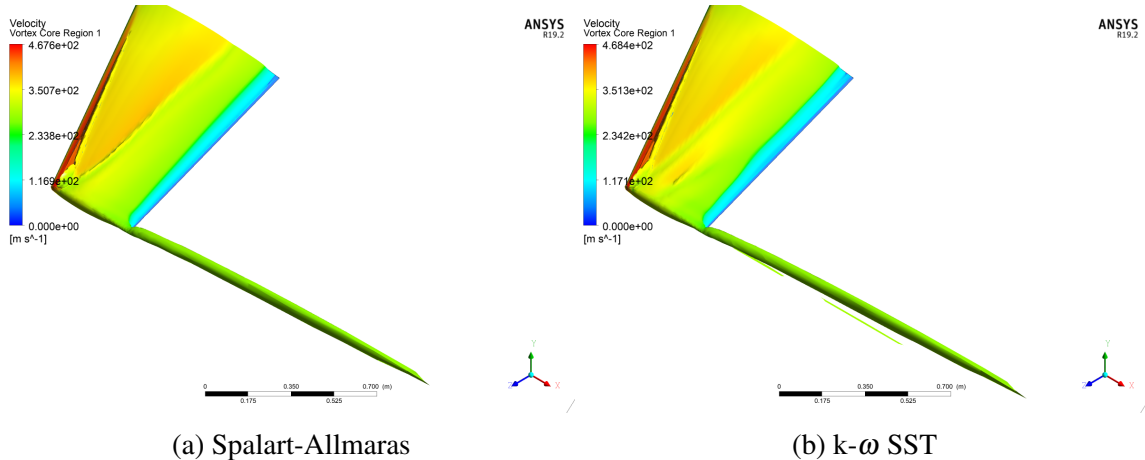


Figure 4.4: Q criterion of value  $197565\text{ s}^{-2}$  to represent the wingtip vorticity for the SST and Spalart-Allmaras turbulence models

In order to validate our results, the experimental values obtained by [1] will serve as a benchmark reference to evaluate the accuracy of our turbulence models considering the approach made.

## 4. Results

---

For this case, [1] did not provide results for a middle section of the wing ( $Z=50\%$ ) but it did for  $Z=60\%$ , hence a new section in the same location will be created in each turbulence model and contrasted. It is also interesting to compute the  $c_p$  at the wingtip where the vortical structure shows the biggest influence.

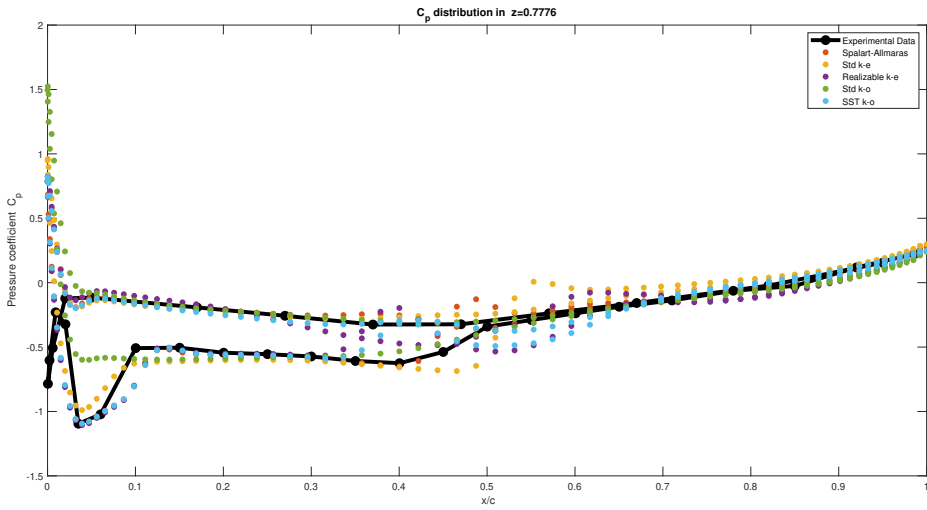


Figure 4.5: Validation of the airfoil in  $z= 60 \%$  of the wing with experimental values from [1]

As it can be seen, quite all of the turbulence models present some inconsistencies and attention must be paid on to withdraw the most accurate method. The pressure coefficient envelope of k-epsilon models slightly cross the wing's surfaces at some point and this effect should not take place. Considering the fact that k-epsilon shines for the mean flow but struggles at near-wall or boundary treatment, in this sense those artifacts could be expected. Nevertheless, if the bottom front is analyzed, the standard k-omega model reveals a really inaccurate performance and a significant error is present if it is compared to the experimental results. This is why, and as it can be seen, the Spalart-Allmaras and the k-omega SST models are subsequently the closest models to the experimental physical problem and we should expect them to state as the most reliable to compute the pressure in the wall. Each of the both have advantages and cons that will gain relevance according to the simulation aimed. This insight will be later detailed in the conclusions section.

More properties of the simulation should be evidently reviewed in order to devise the most accurate turbulence model to compute the pressure distribution along the wing. In the transonic environment, special phenomena such as non-linear waves, specially shocks, take place and represent a huge impact in the flow behaviour and its magnitudes. Given the knowledge on how they act, we will be able to analyze which of the turbulence model

## 4. Results

---

simulations will share more common points with the expected results. Therefore, the Mach value along the medium section ( $Z=50\%$ ) will be displayed in Figure 4.6

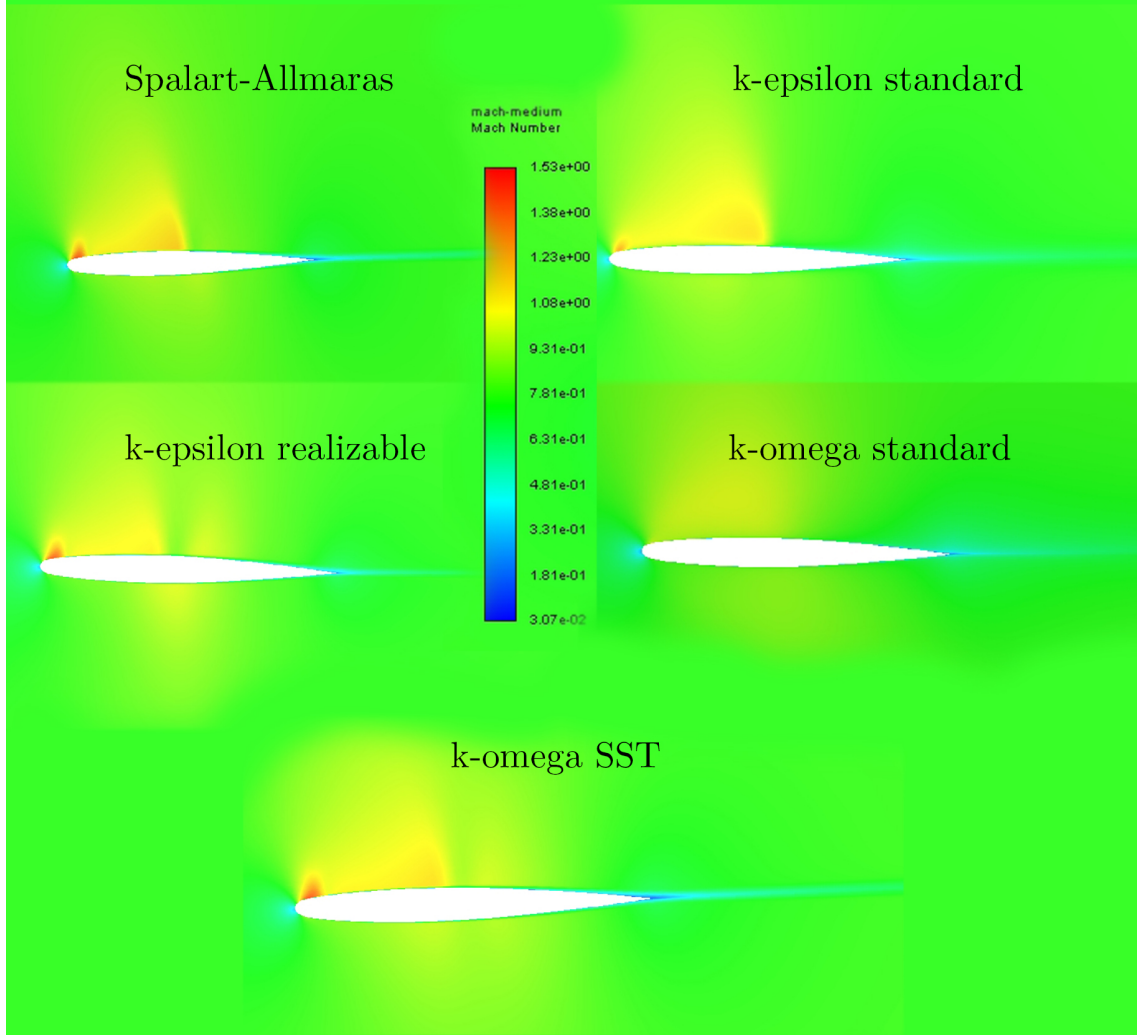


Figure 4.6: Mach Contours in medium section,  $Z=50\%$

The problem of shocks under a discretized domain redounds in the needed solution for n Riemann Problems per dimension, which is nicely solved by the Godunov-Type ROE-FDS Flux Riemann Solver. The Mach distribution reveals different traits which were not easily noticed in Figure 4.5, where Spalart-Allmaras and  $k-\omega$  SST models stood as the most beneficial. Here, in this case, the Spalart-Allmaras shows a slight overprediction of the expansion zone just past the shock wave where the supersonic region is embedded, incurring in another strong supersonic region. Actually, the real expansion does take place but not with such intensity. This problem is similarly sighted in the k-epsilon model. In the other hand, the k-omega standard model does not capture in any case the supersonic

## **4. Results**

---

region just after the shock wave and therefore the flow -according to it- is not transonic, this is why here the worst performance is sighted. Therefore, the models that greatly captured the flow behaviour and the effect of the shock wave are k-omega SST and k-epsilon realizable, whose results look almost identical.

A thorough analysis could be done regarding each of the flow variables, yet this it would imply a lot of time consumption and it is not the main aim of this research. Three turbulence models so far show great suitability for representing the most accurate solution: k-omega SST in most of the plots and then k-epsilon realizable and Spalart-Allmaras show different strengths depending on what is evaluated.

The final and probably most important plot of the flow problem to be analysed -since it will be the input for the structural problem- is the static pressure distribution along the wall (wing). It is attached in Figure 4.7

## 4. Results

---

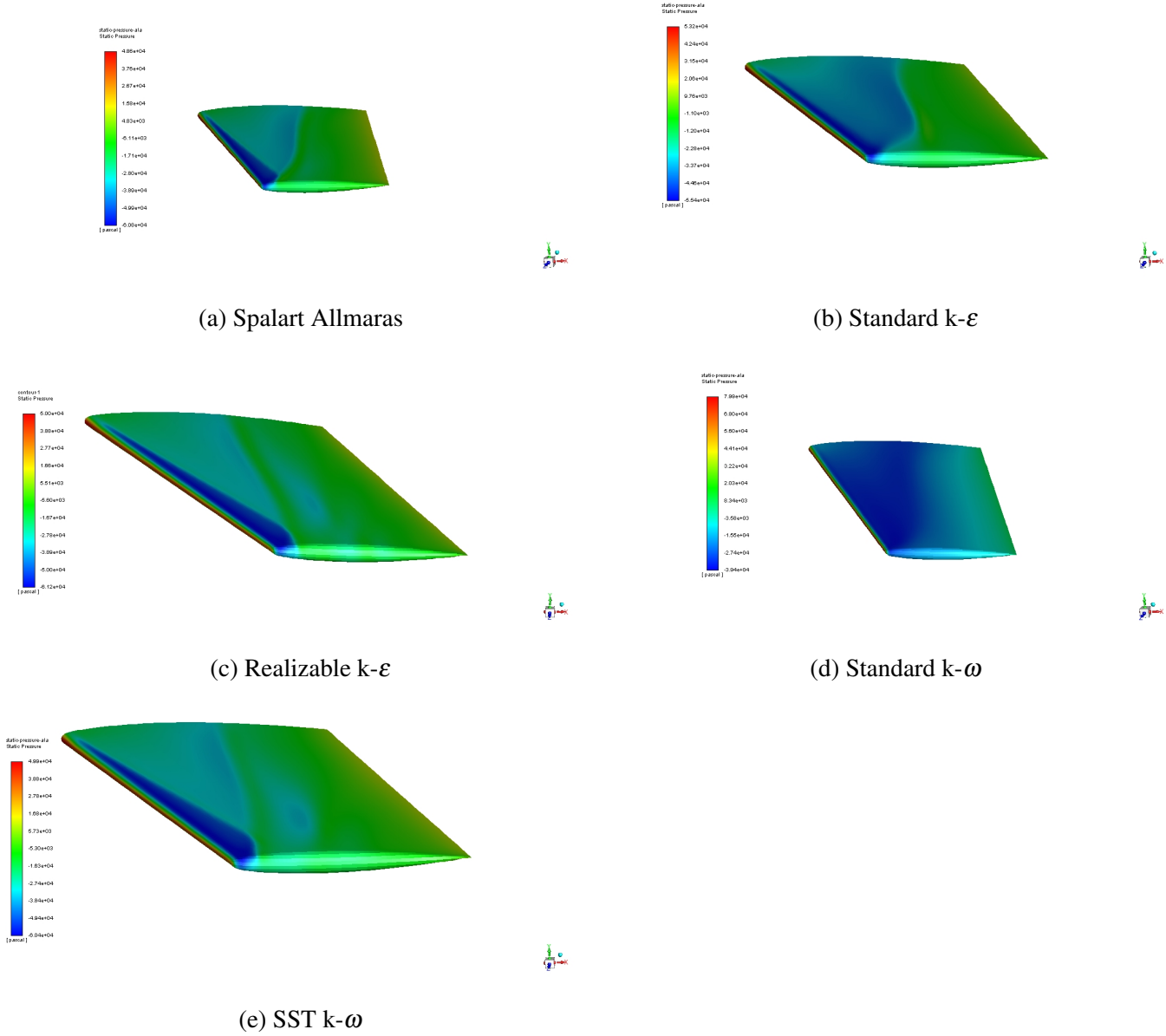


Figure 4.7: Static pressure distribution along the ONERA M6 wing

This Figure shows an overall correct behaviour of the pressure distribution that the flow creates in the ONERA M6 wing, except for the  $k-\omega$  turbulence model, whose magnitude is approximately the double ( $8 \cdot 10^4$  Pa) of the other turbulence models ( $5 \cdot 10^4$  Pa). In this case, the most accurate results are sighted in the  $k-\omega$  turbulence model but also in the realizable  $k-\epsilon$  where the plot is practically equal. Especial attention must be driven into the Spalart-Allmaras model where the results remain really accurate but its convergence rate has no rival: withdraws good result within a short amount of time. This case is a

## 4. Results

---

certain result of the fact that the Spalart-Allmaras model was fully developed by NASA and completely oriented to the aerospace flow environment, hence its efficiency when aerodynamic flows are numerically treated.

Once results are validated with literature source and experimental data from [1], and graphically reviewed that the best approach accounts for  $k-\omega$  SST,  $k-\epsilon$  and if quick results are aimed by Spalart-Allmaras, these pressure distributions will be attached to the setup of the structural problem as a imported distributed load along the structural wing geometry.

### 4.2.2 Structural Problem

The ONERA M6 Wing is known to be a widely used CFD benchmark geometry for testing the accuracy of algorithms and numerical schemes; usually dealing with transonic environments, hence a huge amount of publications can be used to compare and validate our own results. However, almost no literature has been reported of the structural analysis for this wing, probably due to the fact that its geometry parameters do not make it an efficient wing for either civil and military aircrafts. In this sense, there's no interest in the structural analysis.

However, aviation manufacturers do have an special interest in FSI simulations as they represent the most accurate approach to the physical real problem. In distinctively adverse and complex flows, the analytical Newtonian and aerodynamic methodologies based in weak assumptions may not be enough to achieving the high standards of safety and accuracy process, even though they have been normally used during the last century. However, the advantages of the FSI method is gaining prominence due to its high ability to asses a real problem. This is why, we have been able to find some literature of this insight and can serve as an initial comparison.

The results of the structural analysis are going to be therefore compared to similar geometries and the influence of the turbulence models will be statistically dealt in order to be able to rely on the results.

#### 4.2.2.1 Static Analysis

The static analysis will be mainly held by the evaluation of three important parameters that can describe most of the static situation: total deformation, equivalent stress (calculated with von Mises formulation) and equivalent elastic strain.

The mesh of the structural problem is generated independently from Fluent, using a CAD available from the internet repository Grabcad. Initially, the mesh is coarse as it can be seen in the following image.

## 4. Results

---

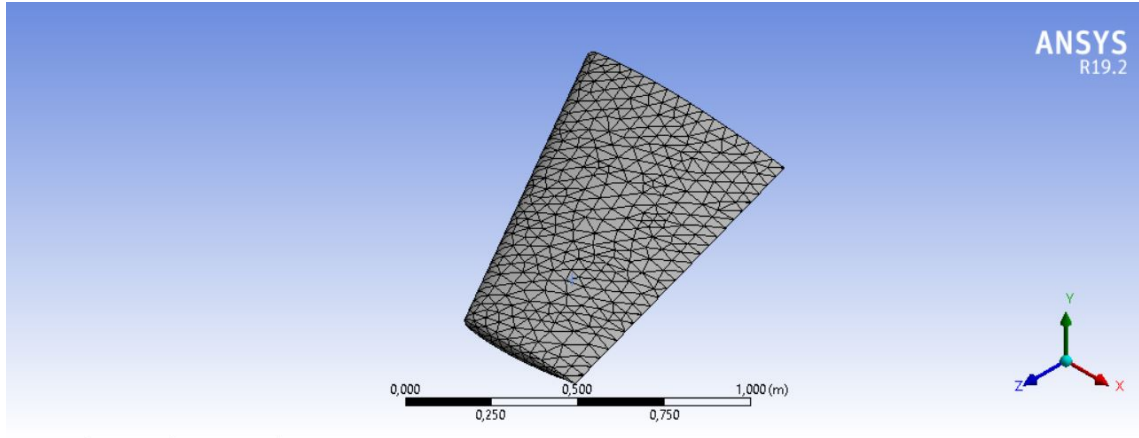


Figure 4.8: Coarse Mesh for the Structural Analysis

The CFD results from Fluent are then imported to the structural static analysis (Figure 4.9) in the form of setup loads in initial conditions. The load is evidently distributed along the upper and lower surfaces of the wing.

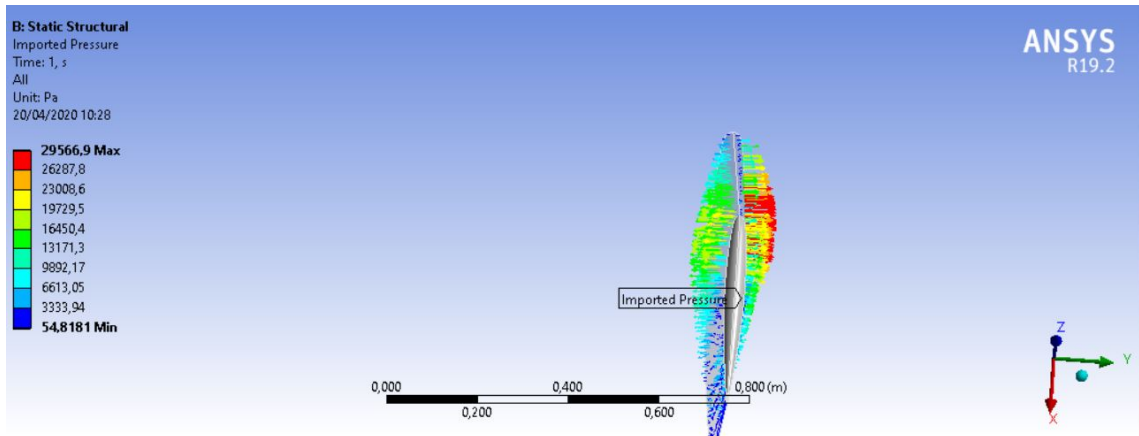


Figure 4.9: Imported Pressure from the CFD

The fact that the two surfaces of pressure are considered is quite new regarding the fact that most FSI literature of wings only use the imported pressure for the upper surface or import the CFD results as a nodal force applied to the center of pressures (see ([2], [4])). However, in this sense, as the whole geometry is fully immersed in the flow, the approach taken in this study might suppose a greater approach to the real physical problem.

The order of magnitudes are consistent with the imported pressure from [2], although as it has been mentioned they only consider the upper wing surface. Their simulation is made through a hybrid method RANS-LES studying the turbulent transonic flow over the wing geometry AGARD 445.6 for the AoA=3.06 °. As it can be seen neither the flow

## 4. Results

---

case nor the wing geometry are the same yet they share some common points that will be interesting to comment. The imported pressure plot is available in where they ran the k-omega SST and Spalart-Allmaras turbulence models due to their strength to correctly capture the flow in this aerospace environment.

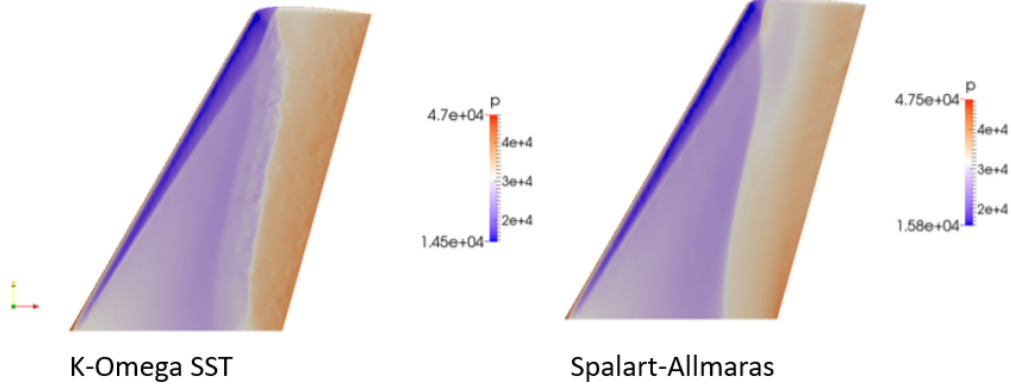


Figure 4.10: Pressure distribution along the AGARD 445.6 wing from [2]

The minor differences seen between their plot and ours are certainly caused by the different geometry, AoA and that their simulation approach (Hybrid) is better than our RANS as LES is able to provide more detail of the flow properties.

Now, the simulation is executed and results for the three static parameters (total deformation, equivalent stress and equivalent elastic strain) are obtained.

The total deformation plot from Figure 4.11 reveals an overall similar behaviour of the structure under the action of the imported loads. The values oscillate between  $3 \cdot 10^{-5}$ , - and  $4 \cdot 10^{-4}$  for the Spalart-Allmaras - m which is, at any case, a really small value of total deformation. For the transonic operation, it is considered to be safe with a wide margin, this deflection in a transient flow study would not provoke any significant perturbation of the t+1 flow. Besides, it must be taken into account that this CAD geometry does not include the action of the structural elements such as ribs, spars and longerons which provide a stiff basis and structural reinforcement for the wing skin that is, at most, 1 mm thick.

## 4. Results

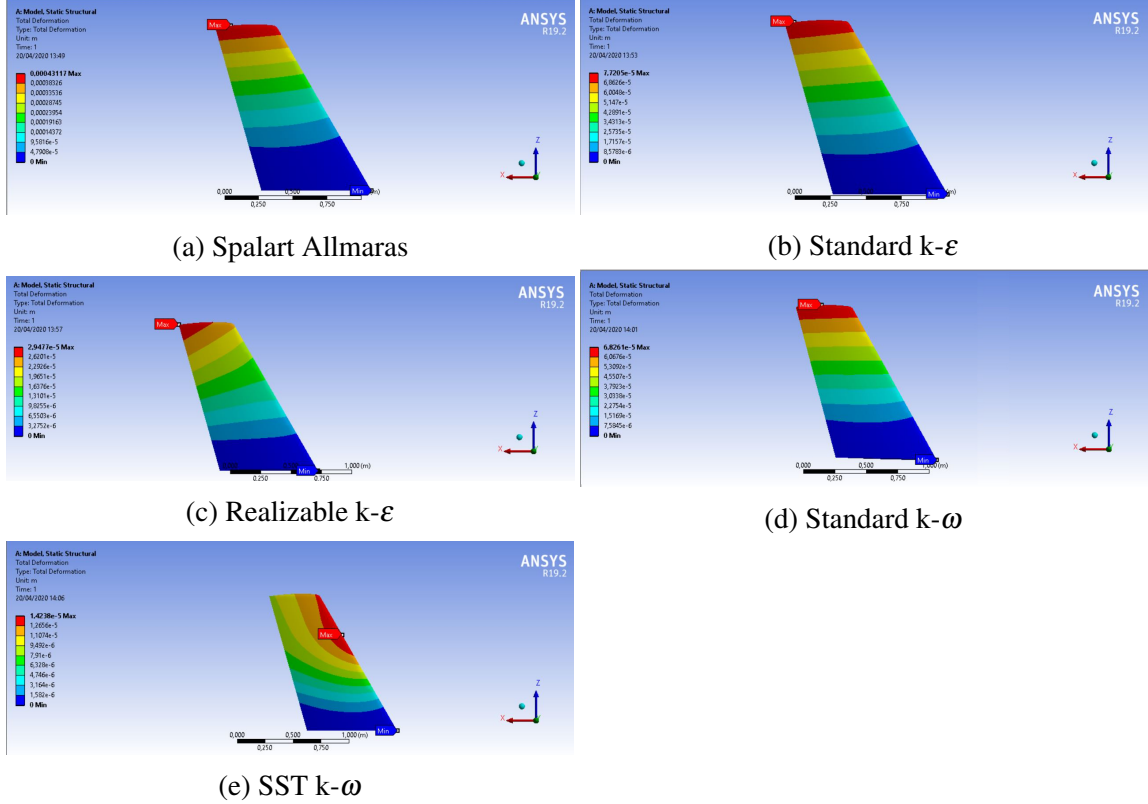


Figure 4.11: Total Deformation of the ONERA M6 Coarse mesh for Al 2024 T3

Results for this plot behave similarly to the FSI simulations of [57] and [58] where the subsonic flow ( $M=0.4$ ) has been studied over the geometries of wings formed by the airfoil NACA 23-012 and NACA2412 respectively. The distribution of total deformation, stress and elastic strain is almost identical although their values of deformation are a little bit higher - around  $10^{-2}$  m- which are a little bit high for operations under this regime. The difference in values is mainly caused by the different geometry and also the different flow operation and AoA, but specially due to the fact that they do not consider the effect of the lower surface which contributes in the opposite direction and softens the whole pressure effect.

Whilst [57] did not define an AoA and used the  $k-\epsilon$  standard turbulence model to simulate the fluid problem, [58] rather chose the  $k-\omega$  SST under the effects of  $AoA = 5$ . Both have used Aluminium alloys such as our simulation, and even though [57] did not specify the exact composition, [58] used the widely-seen 7075-T6 aluminium alloy.

From our plots, the only one that does not match with their results but not even with the general tone of the turbulence models is the  $k-\omega$  SST total deformation. The distribution is not accurate and sharp. This bad performance could be a consequence of several issues to

## 4. Results

consider: over-prediction of the shear stress, special sensitivity to the inlet boundary and initial conditions and the fact that the mesh is too coarse to achieve good static prediction is a strong possibility as well. This problem will be also seen -despite not so evident- in the stress and strain plots from Figures 4.12 and 4.13.

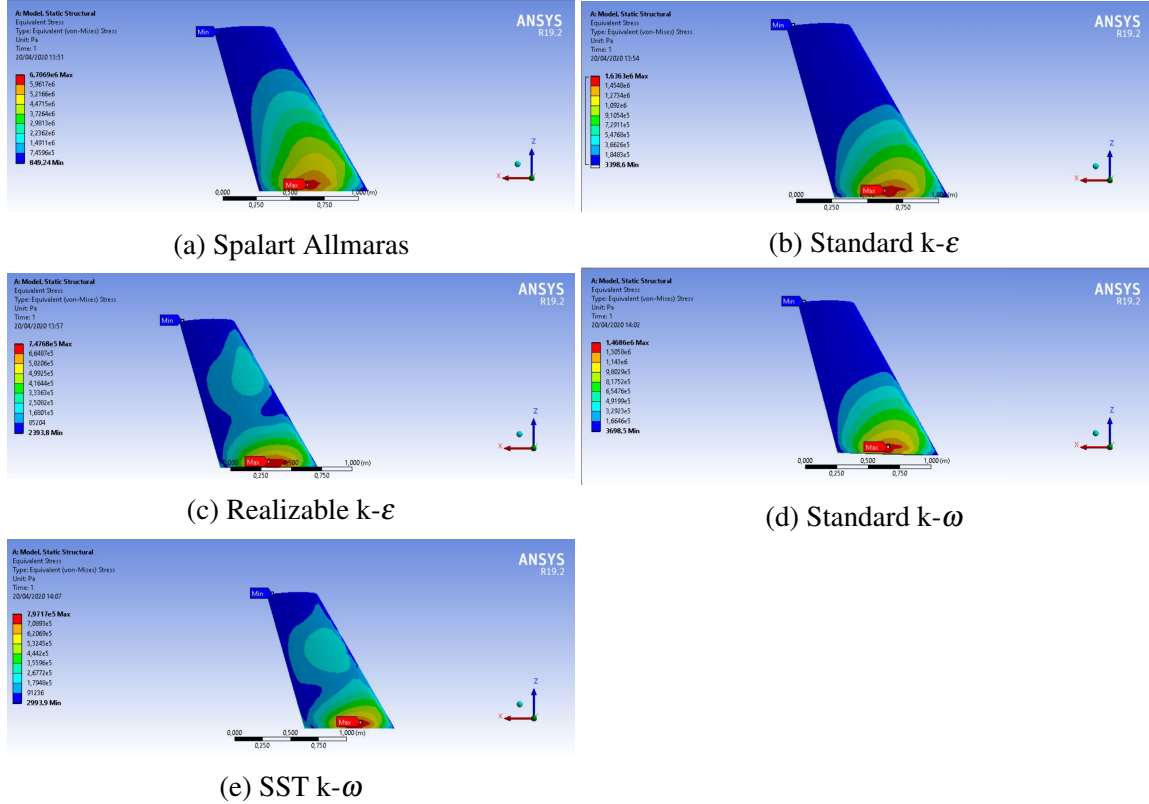


Figure 4.12: Equivalent stress of the ONERA M6 Coarse mesh for Al 2024 T3

The Equivalent Stress and Elastic Strain plots, which are given under von-Mises criteria, do match with the results from [57] and [58]. For equivalent stress, the results have been of approximately  $1\text{e}07$ ,  $1\text{e}08$  accordingly, (Pa) whilst our simulation provided  $1\text{e}06$ . Here we experience again the effects of the bottom surface which they did not consider in their study, apart from the different geometry and flow conditions. The SST plots do not provide the best results such as it happened with the total deformation although here it is not that evident. This issue will be patiently investigated in the following lines.

## 4. Results

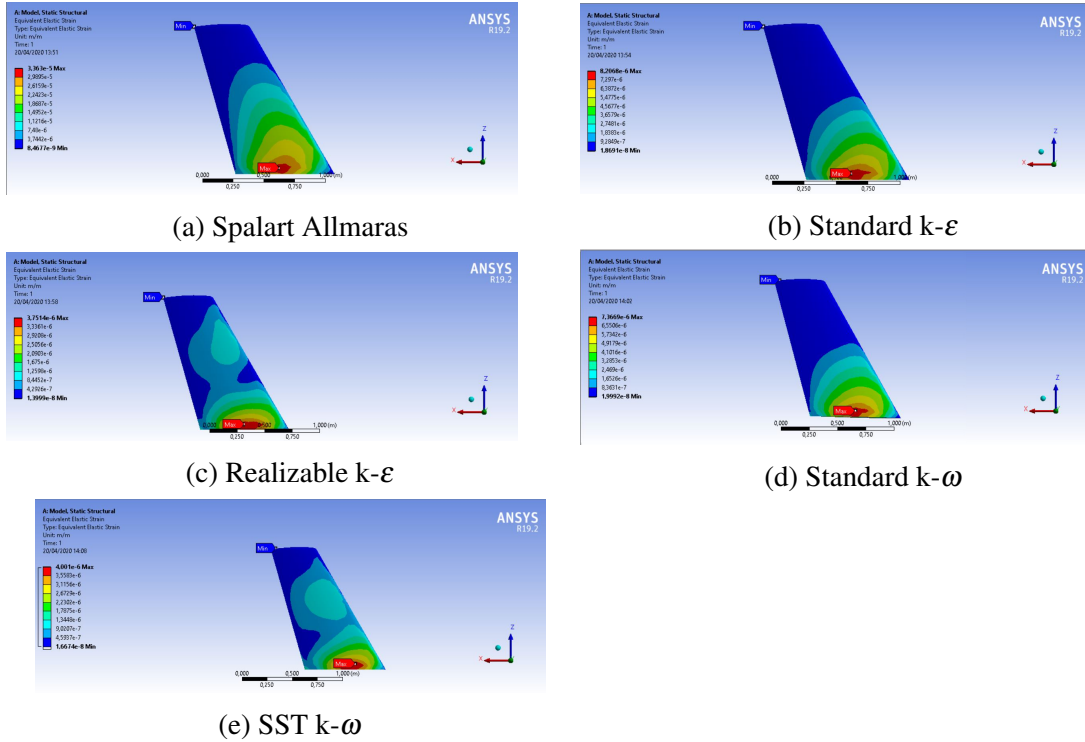


Figure 4.13: Equivalent Elastic Strain of the ONERA M6 Coarse mesh for Al 2024 T3

As the most easy possibility to test and solve from the SST sighted issues is the resolution of the grid, a refinement of (x5) to the whole structural domain will be applied. The simulations have been run on a last-generation computer which is limited by 8GB of RAM, this is why ANSYS software did not allow us to simulate for stronger refinements. Now, the mesh -as Figure 4.16 demonstrates- is significantly better and will describe the structural behaviour more accurately.

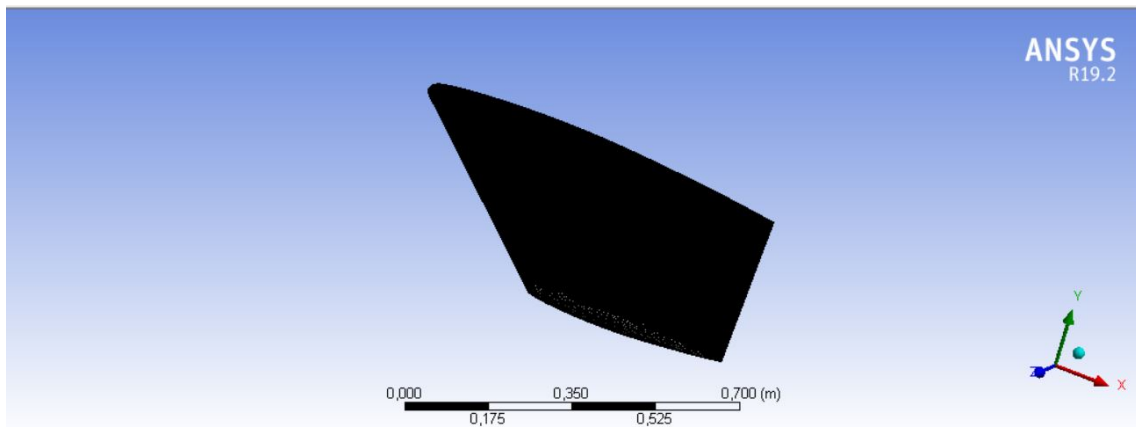


Figure 4.14: Refinement of factor 5 to the whole structural domain (skin)

## 4. Results

When now the SST Results are imported as pressure distribution and the simulation is run (Figure 4.15), excellent results are obtained. They match with the all other turbulence but they even provide a better insight: the equivalent stress and elastic strain in the real physical problem is narrower than the other turbulence models and those regions are located next to the fixed wing root.

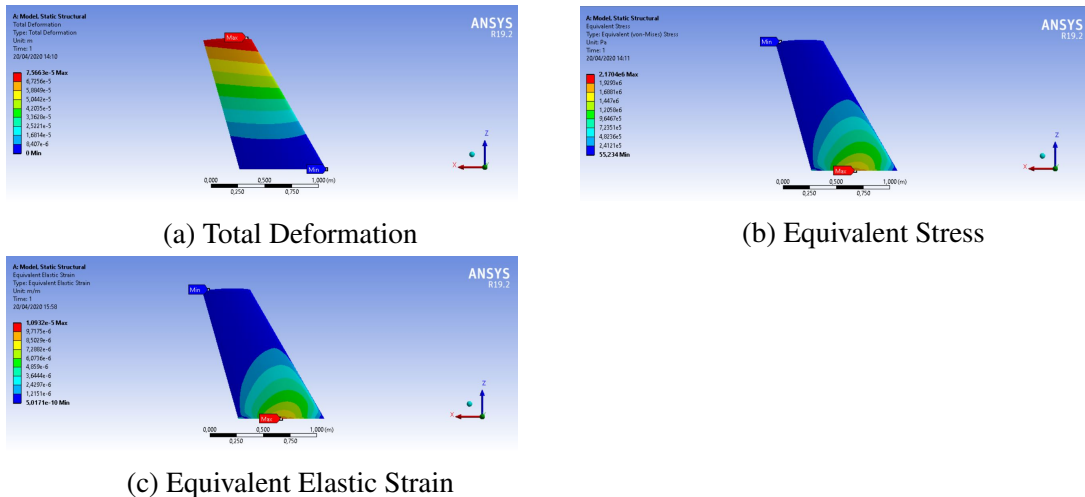


Figure 4.15: Static Results for the SST  $k-\omega$  FSI interaction with fine mesh, Al 2024 T3 alloy

All the static structural results for the "coarse mesh" are gathered and summarized in the following table.

As it has been said, there is no literature available to validate the structural geometry of the ONERA M6 wing, specially as FSI and given the same flow conditions. This is why the validation has been performed throughout graphical comparison with other similar cases and geometries where the general properties and similarities that should be common have been satisfactorily evaluated. However, the general properties must be also shared between the results of the different turbulence models for the own simulation, as they can be statistically and numerically studied. More detail can be obtained within this methodology. This is why the study of norms of deviations between the different turbulent models has been done in using the total deformation, which may be the most important parameter in the whole static structural analysis. For the process, a solid model - for instance,  $k-\omega$  SST or Spalart-Allmaras- is considered as a reference in order to calculate the variances from it that present all the other models.

## 4. Results

---

Deviations from SST				
		Norm 1	Norm 2	Norm 3
<u>Spalart-Allmaras</u>		1.31E-04	3.40298E-08	0.000421296
<u>k-epsilon standard</u>		2.03722E-05	6.09313E-10	6.80986E-05
<u>k-epsilon realizable</u>		3.60124E-06	3.72859E-11	2.04346E-05
<u>k-omega standard</u>		1.73E-05	6.09313E-10	5.86666E-05

Deviations from Spalart Allmaras				
		Norm 1	Norm 2	Norm 3
<u>SST</u>		1.31E-04	3.40298E-08	0.000421296
<u>k-epsilon standard</u>		0.000110564	2.55355E-08	0.000354042
<u>k-epsilon realizable</u>		0.00012748	3.1966E-08	0.000403397
<u>k-omega standard</u>		0.00011367	2.55355E-08	0.00036303

Figure 4.16: Norms of the deviations between the turbulence models for the Total Defor-mation

It is relevant to note that here we are talking about deviations and not errors as there's no reference data (either analytic or experimental) to serve. Once the methodology and algorithm is validated in the coarse mesh, the influence of the different turbulence models and materials (conventional aircraft aluminium alloy and interesting composites) will be studied in the following section.

### 4.3 Grid Convergence Study (Léa, Erwan, Marc)

Setting the time and space steps are very important to correctly solve numerical models which generate errors like the truncation or the round-off. Usually, the error drops when the discretization is made with smaller steps. To examine that is what we know as the grid convergence study. The solution will converge when the errors will reach a user-defined value [59]. In Ansys-Fluent, the default value is set to 10-3 for most equations and 10-6 for the energy equation because they suit for many problems. However, these values are not universal and so, it can be relevant to check coefficients such as heat transfer or drag [60].

The need of performing a grid convergence study comes from companies to be more cost-effective. It was shown that increasing the number of cells in the mesh also increased the accuracy of the solution until a certain point, where no significant improvement could be found. One difficulty in this study is that when we refine the mesh, for example times

## 4. Results

---

2, the number of nodes grows by 8 times, which leads to complex meshes notably for 3D structures. Often, this study can't be done properly because of two reasons: the first one is that the mesh may be too coarse and so gives nonphysical results. Therefore, it's not possible to coarsen the mesh. The second reason is because the mesh is too fine. A computer has limited resources and if the mesh reaches it, it won't be possible to refine it [61].

The Grid Convergence study, in Computational Fluid Dynamics, relies on a procedure proposed and detailed by Roache in [62]. The idea is to evaluate the convergence of the error regarding the comparison of ratios along an isosurface, which are then supported by the appliance of Safety factors. In the end, what should be devised is the approximation of the points evaluated to the convergence asymptote.

Another procedure which is strongly related with the Roache's procedure is the Richardson Extrapolation, which has been greatly explained at [63]. His idea is to evaluate (extrapolate) the function in a determined value through the approximation of the values of the function in near points separated by the distance  $h$ , and then evaluate it when  $h \rightarrow 0$ . In this sense, the term of error  $O(n)$  is reduced and the approximation is more accurate. With this methodology, it can be evaluated how the difference between the values of the same point from different meshes (one coarse and one finer) leads to error convergence or not.

In the end, the refinement has been applied in the structural mesh from ANSYS with a refinement factor of 5. Therefore, it is not purely CFD ambit. In the process of conducting the Grid Convergence Study, we found out that ANSYS is not able to export the point deformation in an isosurface as it is usually done in fluent. It only withdraws the column with "nodes label" and "values" of the structural magnitude analysed. This is why, it cannot be compared between coarse and fine meshes: the nodes are not equal and either identified.

Another option could be running the convergence control of ANSYS, but it is incompatible with imported loads. As ours come from fluent and are the input of the FSI, they cannot be neglected, thence this approach is not considered.

Finally, there are only two options available: running the GCI for points selected manually, even consider total magnitudes as a result of an integrative variable (such as it is usually done with  $C_L$  and  $C_D$ ) or to use images to validate graphically the convergence study. A set of 6 points along the upper surface will be evaluated through the total deformation magnitude in both coarse and fine meshes. The points chosen are certainly the ones shown in the following image, Figure 4.17.

## 4. Results

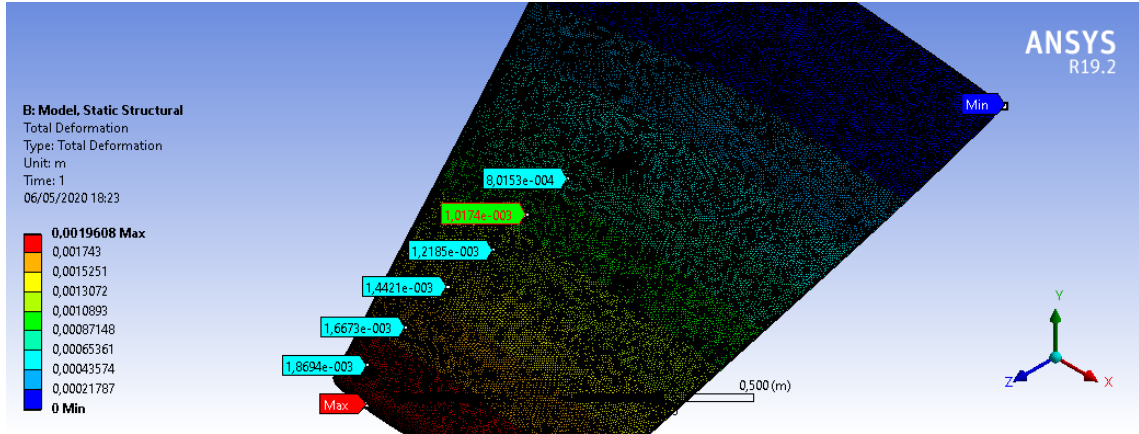


Figure 4.17: Chosen points to conduct the Grid Convergence Study, Fine Mesh

These same (X,Y,Z) points have been chosen in the Coarse Mesh and the values of the total deformation of them is revealed in Table 4.3, with the calculation of normalized deviation, Richardson Extrapolation and the Grid Convergence Index. Additionally, the overall and dimensionally independent magnitudes of maximum and average total deformation have been also included in the procedure.

Nodes	Coarse	Fine	Normalized Error	RE	GCI
1	0.001899542	0.0018694	0.139292269	0.001657623	0.725480567
2	0.0016449	0.0016673	0.14062825	0.00143365	0.732438805
3	0.0014077	0.0014421	0.155272876	0.001210617	0.808712898
4	0.00116299	0.0012185	0.143100059	0.001011334	0.745312807
5	0.00096961	0.0010174	0.209698951	0.000794527	1.092182035
6	0.0007243	0.00080153	0.630609955	0.002012321	3.28442685
Maximum	0.0019408	0.0019608	1.713950106	0.00066405	8.92682347
Average	0.00070169	0.00071512	0.018780065	-2.92371E-05	0.097812838

Table 4.3: Grid Convergence Study

Table 4.3 reveals the values of the Richardson Extrapolation and the Grid Convergence Index proposed by [62]. As it can be seen, the excellent values from the GCI show the approach of the error convergence to the asymptote (GCI close to the unitary magnitude). The refinement has contributed to significantly improve the results but was not excessive. Besides, this process was easily corroborated by analyzing the results from the SST coarse mesh (Figure 4.11e) and the fine (Figure 4.15a), where in the first they the mesh is not enough to capture the total deformation distribution along the wing but in the second it does with excellent performance.

## 4. Results

---

### 4.4 Only Skin CAD

#### 4.4.1 Static Analysis (Léa, Erwan)

In this section, we show the total deformation, the equivalent (von-Mises) stress and the equivalent elastic strain for several materials, the Al 2024-T3 (table 4.4), the Epoxy carbon UD (table 4.5) and the Epoxy S-Glass (table 4.6), which are commonly used for the aircraft design .

The first thing we can notice, is that for each material, the results for the total deformation, the equivalent stress and the equivalent strain strongly depend on the turbulence model used. Indeed, the imported loads from fluent correspond to the applied loads in the static analysis of the wing, .

Firstly, we will compare the turbulence models. For the aluminium 2024 T3 (table 4.4) , the Standard k- $\varepsilon$  turbulence model gives the highest total deformation, equivalent stress and equivalent strain. Contrary to the Standard k- $\varepsilon$  turbulence model, the Standard k- $\omega$  gives the lowest equivalent stress and equivalent strain and the the SST k- $\omega$  gives the lowest total deformation. With the Epoxy-Carbon UD (table 4.5), and the Epoxy S-Glass (table 4.6), we notice the same than with the aluminium alloy apart from the fact that now the lowest total deformation is given by the standard k- $\omega$  model.

Table 4.4: Static structural results for the Aluminium 2024 T3

	Spalart-Allmaras	Standard k- $\varepsilon$	Realizable k- $\varepsilon$	Standard k- $\omega$	SST k- $\omega$
Total deformation(mm)	0.30315	0.4526	0.34333	0.23287	0.07566
Stress(MPa)	3.1834	3.7625	3.3833	2.3642	2.1704
Strain	4.4837e-5	5.2994e-5	4.7652e-5	3.3299e-5	1.0932e-5

Table 4.5: Static structural results for the Epoxy-Carbon UD

	Spalart-Allmaras	Standard k- $\varepsilon$	Realizable k- $\varepsilon$	Standard k- $\omega$	SST k- $\omega$
Total deformation(mm)	2.6408	3.9066	2.9893	2.0192	2.2814
Stress(MPa)	2.7315	3.297	2.9231	2.028	2.841
Strain	4.2856e-4	5.1709e-4	4.5857e-4		4.5171e-4

Table 4.6: Static structural results for the Epoxy S-Glass

	Spalart-Allmaras	Standard k- $\varepsilon$	Realizable k- $\varepsilon$	Standard k- $\omega$	SST k- $\omega$
Total deformation(mm)	2.2737	3.388	2.579	1.7364	1.9408
Stress(MPa)	2.7449	3.3211	2.9429	2.0407	2.4929
Strain	3.6654e-4	4.4264e-4	3.923e-4	2.7213e-4	3.3237e-4

## 4. Results

---

As we said previously, the standard  $k-\omega$  model did not show a good pressure distribution along the wing because this turbulence model is very sensitive to the mesh resolution near the wall, while the SST-  $k-\omega$  and the realizable  $k-\varepsilon$  did. If we compare those two models and the Spalart-allmaras (which gave good results in the validation process), we see the worst case scenario for each material in the table 4.7, which is given by the realizable  $k-\varepsilon$ .

Table 4.7: Worst case scenario for the static structural

	Al 2024-T3	Epoxy-Carbon UD	Epoxy S-Glass
Total deformation(mm)	0.34333	2.9893	2.579
Stress(MPa)	3.3833	2.9893	2.579
Strain	4.7652e-5	4.5857e-4	3.923e-4

Now if we compare the different the materials, we can see that whatever turbulence model is used, the Aluminium 2024 T3 gives the lowest total deformation. The Aluminium gives also the highest equivalent stress for each turbulence model apart from the SST  $k-\omega$ . The value of the equivalent stress are very similar for the Epoxy-Carbon UD and the Epoxy S-Glass. In addition to this, the Aluminium gives the lowest value for the equivalent strain for each turbulence model apart from the SST  $k-\omega$ . These results almost correspond with the results that Salu Kumar Das and Sandipan Roy (Das, S K and Roy, S, 2018) have in their study. They also found that the Aluminium alloy gave the lowest total deformation and the highest equivalent stress. However, the aluminium alloys gave the lowest equivalent strain value whereas we found the contrary. In the end, we can see that the composite materials like the Epoxy-Carbon UD and the Epoxy S-glass, as we can expects for a more elastic material than the aluminium alloys, they have a higher value for the total deformation and for the equivalent stress. And also a lower value for the equivalent strain than the aluminium alloys. This fact is not relevant if we consider the values per weight, giving a more favorable ratio than the conventional aluminium alloy, and its not-normalized values demonstrate the adequacy of using the composite materials for resisting the operation, which is indeed what we expected from this study.

### 4.4.2 Modal Analysis (Léa, Erwan)

The modal analysis determines the natural frequency structural parts and its mode shape. We choose to have get the first mode because the vibration will be smaller than if we take the modes with high frequency. Here, the different turbulence model do not involve much change in the results because the modal analysis does not need the distributed load provided by these models. On the table 4.8, we can see the natural frequencies obtained for the first six modes. As the number of modes increases, it's clear that so does it the

## 4. Results

---

natural frequency. If we compare the Aluminium alloy, the Epoxy carbon UD and Epoxy S-Glass, it seems that the Al 2024-T3 has a higher natural frequency than the other materials. However, in their study, Salu Kumar Das and Sandipan Roy (Das, S K and Roy, S, 2018), found different results. They showed that the Epoxy carbon UD had higher natural frequency.

Table 4.8: Natural frequency (Hz) of the wing for each turbulence model assessed and wing material

Spalart-Allmaras			Standard k- $\varepsilon$			Realizable k- $\varepsilon$			
Modes	Al 2024 T3	Epoxy Carbon UD	Epoxy S-Glass	Al 2024 T3	Epoxy Carbon UD	Epoxy S-Glass	Al 2024 T3	Epoxy Carbon UD	Epoxy S-Glass
1	39.854	19.123	17.631	39.855	19.124	17.231	39.854	19.124	17.631
2	171.88	83.9	77.255	171.88	83.899	77.255	171.88	83.9	77.255
3	207.03	133.22	120.46	207.03	133.22	120.46	207.03	133.22	120.46
4	336.7	166.42	153.3	336.7	166.42	153.3	336.7	166.42	153.3
5	410.48	206.59	190	410.48	206.59	190	410.48	206.59	190
6	468.81	297.1	269.58	468.81	297.1	269.58	468.81	297.1	269.58

Standard k- $\omega$			Shear Stress Transport k- $\omega$			
Modes	Al 2024 T3	Epoxy Carbon UD	Epoxy S-Glass	Al 2024 T3	Epoxy Carbon UD	Epoxy S-Glass
1	39.854	19.124	17.631	40.003	19.122	17.631
2	171.88	83.899	77.255	172.67	83.89	77.255
3	207.03	133.22	120.46	208.09	133.21	120.46
4	336.7	166.42	153.3	336.42	166.41	153.3
5	410.48	206.59	190.00	413.41	206.56	190.00
6	468.81	297.09	269.57	471.59	297.06	269.57

The mode shapes represent the response of the structure to the natural frequencies. This is very useful to describe a wing [64]. On the table 4.9 are shown all the results we simulated. We see that the biggest amplitude of vibration is 688.22 mm using the Standard  $k - \varepsilon$  for the mode 5. This is given by the Epoxy-UD. Also, this material always gives higher amplitudes of vibration compared to the two other materials. Comparing the Aluminium alloy and the Epoxy S-Glass, the AL 2024-T3 has lower results except for the modes 2 and 5.

Table 4.9: Maximum amplitude of vibration (mm) for each mode shapes for each turbulence model assessed and wing material

Spalart-Allmaras			Standard k- $\varepsilon$			Realizable k- $\varepsilon$			
Modes	Al 2024 T3	Epoxy Carbon UD	Epoxy S-Glass	Al 2024 T3	Epoxy Carbon UD	Epoxy S-Glass	Al 2024 T3	Epoxy Carbon UD	Epoxy S-Glass
1	304.51	400.21	347.82	304.51	400.2	347.82	304.51	400.21	347.82
2	490.93	551.77	487.58	490.94	551.78	487.59	490.93	551.77	487.58
3	415.2	505.53	435.97	415.2	505.53	435.97	415.2	505.53	435.97
4	286.71	397.4	342.42	286.71	397.4	342.42	286.71	397.4	342.42
5	725.08	688.22	614.31	725.08	688.22	614.32	725.08	688.22	614.32
6	497.95	599.73	520.64	497.95	599.73	520.64	497.95	599.73	520.64

## 4. Results

---

Modes	Standard $k-\omega$			Shear Stress Transport $k-\omega$		
	Al 2024 T3	Epoxy Carbon UD	Epoxy S-Glass	Al 2024 T3	Epoxy Carbon UD	Epoxy S-Glass
1	304.51	400.2	347.81	305.12	400.19	347.82
2	490.92	551.72	487.54	491.69	551.71	487.58
3	415.19	505.52	435.97	416.34	505.5	435.97
4	286.71	397.4	342.42	287.12	397.39	342.42
5	725.08	688.17	614.27	730.72	688.1	614.31
6	497.95	599.72	520.64	495.8	600.29	520.64

The following figure 4.18 shows the amplitude of vibration of the Onera M6 wing for the first three modes. This figures are simulated with the SSt- $k - \omega$ , but, as we said it previously, the turbulence model does not influence the results. For the first mode (figure 4.18a), we see that the deformation is more important at the wing tip and it decreases along the wing. We notice bending. In the mode 2 (figure 4.18b), twisting begins to be visible but the bending still dominates. For the mode 3 (figure 4.18c), the deformation concentrates on the trailing edge and around the corner of the leading edge and the wing root. With an increased number of nodes, we see more twisting in the wing (figures 4.18d, 4.18e, 4.18f) .

## 4. Results

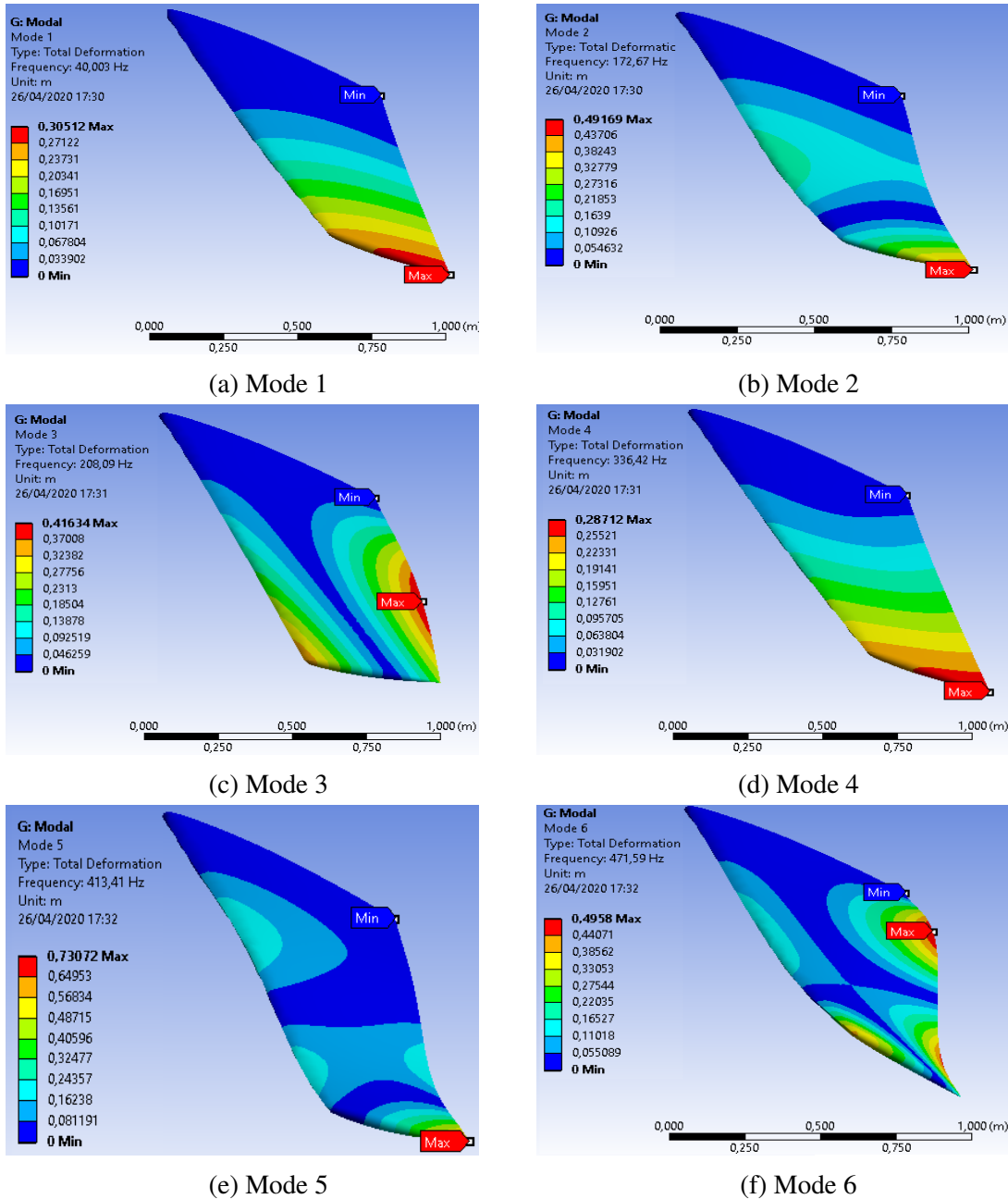


Figure 4.18: First six modes for the SST  $k - \omega$  with the Al 2024-T3

### 4.4.3 Buckling Analysis (Marc)

The Eigenvalue Buckling Analysis -also known as Linear Analysis- aims for establishing a parametric study of the stability of the response of the structure over different loads and equally tries to establish at which point the deformations will cause the structural collapse of the geometry. At this point, the load will be known as critical load and can be

## 4. Results

---

calculated with the expression 2.14.

It must be said that most definitions seen in literature such as [7] state that what is analyzed is the response of the structure to compressing forces. This definition is clearly incomplete as the shear component is significant enough to contribute to the buckling effect and must be also considered. This is why, the situation to be analyzed is equally the pressure distribution in the surface structure caused by the flow. However, experience has demonstrated that shear may compromise the stability analysis of shell or plate elements hence it is important to quantify and appraise its contribution in order to know if it should be involved for those elements.

The linear buckling, according to the PDE Euler equation derived from the motion expression from 2.6,

$$[K] + \lambda_i[S][\Psi_i] = 0, \quad (4.1)$$

may not be enough to describe the real stability analysis of the structure where 2nd or higher order terms (of deformations) are not considered. Neither effects such as material imperfections, or even the relevant effect of the yielding cannot be modelled with this approach. Hence the creation of non-linear buckling science to account for these facets that may be important for real structures under complex operating conditions. However, most of times the linear approach is used as the performance to describe the overall effects is fairly good. Here, therefore the Eigenvalue Buckling of the different turbulence models with different materials of the skin of the ONERA M6 wing will be reviewed.

The setup of the simulation has been done in 6 modes where different possible loads can incur in the buckling of the structure. For each mode, a load factor and the total deformation plot has been provided by the ANSYS software. The load factor indicates the ratio between calculated critical load and the current load, therefore if it is bigger than 1 the structure will not buckle. This is why, sometimes it is known as safety factor. Depending on the mode and the forces of it it can be positive or negative due to the sign criteria, this is why we should only consider the magnitude or absolute value of it.

In other words, the magnitude of the load factor says " how many times the load present in the ideal model should be increased in order to fail due to elastic stability". Therefore, plastic behaviour is neither considered.

Table 4.10: Buckling Load Factor for each turbulence model assessed and wing material

Modes	Spalart-Allmaras			Standard k-ε			Realizable k-ε		
	Al 2024 T3	Epoxy Carbon UD	Epoxy S-Glass	Al 2024 T3	Epoxy Carbon UD	Epoxy S-Glass	Al 2024 T3	Epoxy Carbon UD	
1	-4916.1	-1111.6	-1215	-4797.8	-1089.7	-1191	-4842.4	-1095.9	-1197.9
2	-4703.5	-1085.5	-1185.3	-4583.7	-1064.9	-1162.6	-4632.1	-1070.4	-1168.
3	-3946.9	-949.28	-1059.5	-3868.5	-914.4	-1021	-3890.8	-933.35	-1041.9
4	-3742.6	-582.42	-643.99	-3670.6	-560.39	-619.48	-3689.9	-572.74	-633.3
5	-3250.4	749.65	845.04	-3120.5	717.67	808.59	-3194.9	736.86	830.57
6	4319.2	1182.4	1327.3	4125.5	1134.3	1273.7	4244.1	1162.7	1305.3

## 4. Results

---

Modes	Standard k- $\omega$			Shear Stress Transport k- $\omega$		
	Al 2024 T3	Epoxy Carbon UD	Epoxy S-Glass	Al 2024 T3	Epoxy Carbon UD	Epoxy S-Glass
1	-5876.4	-1342	-1466.4	-6794.2	-1123.2	-1227.6
2	-5613.9	-1310.9	-1430.8	-6681.3	-1096.7	-1197.4
3	-4758.5	-1117.4	-1247.7	-5017.3	-960.15	-1071.6
4	-4517.9	-671.39	-741.62	-3310.2	-587.76	-649.82
5	-3726.4	852.07	959.11	4423.2	757.23	853.48
6	4861.9	1383	1552	7262.6	1196.8	1343.2

As it can be seen in 4.10, all the values are of the order of  $10^3$ . This number is really positive as it is huge enough so that it can be assured that the structure will never buckle. When considering the materials, the biggest values account for the Aluminium Alloy 2024 T3 and are approximately 4 times the values of the Composite Materials (Epoxy Carbon UD, Epoxy S-Glass). Between these two, the most favorable load factors are seen in the Epoxy S-Glass by roughly a 10% of difference. However, all three materials provide results large enough to not care for linear buckling.

The differences between the turbulence models are not huge, the response of the structure behaves equally. The biggest deviation is presented between the k- $\omega$  SST and the k- $\epsilon$  standard turbulence models in the 6th Mode ( LF= 7262.6 and 4244.1), which are respectively the best and the worst models of the evaluated for the FSI simulation.

The total deformation of each mode is equally provided by the ANSYS software. It is important to mention that, although the plots withdrawn show deformation of 1 meter as maximum value for each Load Factor and mode, this information is not literal. The plot is actually normalized with the maximum value, and then when it is present it has a unitary value, so that all of them are referred to it. With this procedure, it is more easy and visual to interpret and manage the information instead of dealing with infinite and other huge values. Then, a linear scale can be applied to all of the values in order to consider any deformation or load. Once given this clarification, let's take a look at the results of the Total Deformation for each Buckling Mode in the Materials of Al 2024 T3 and Epoxy S-Glass, using the k- $\omega$  SST turbulence model.

## 4. Results

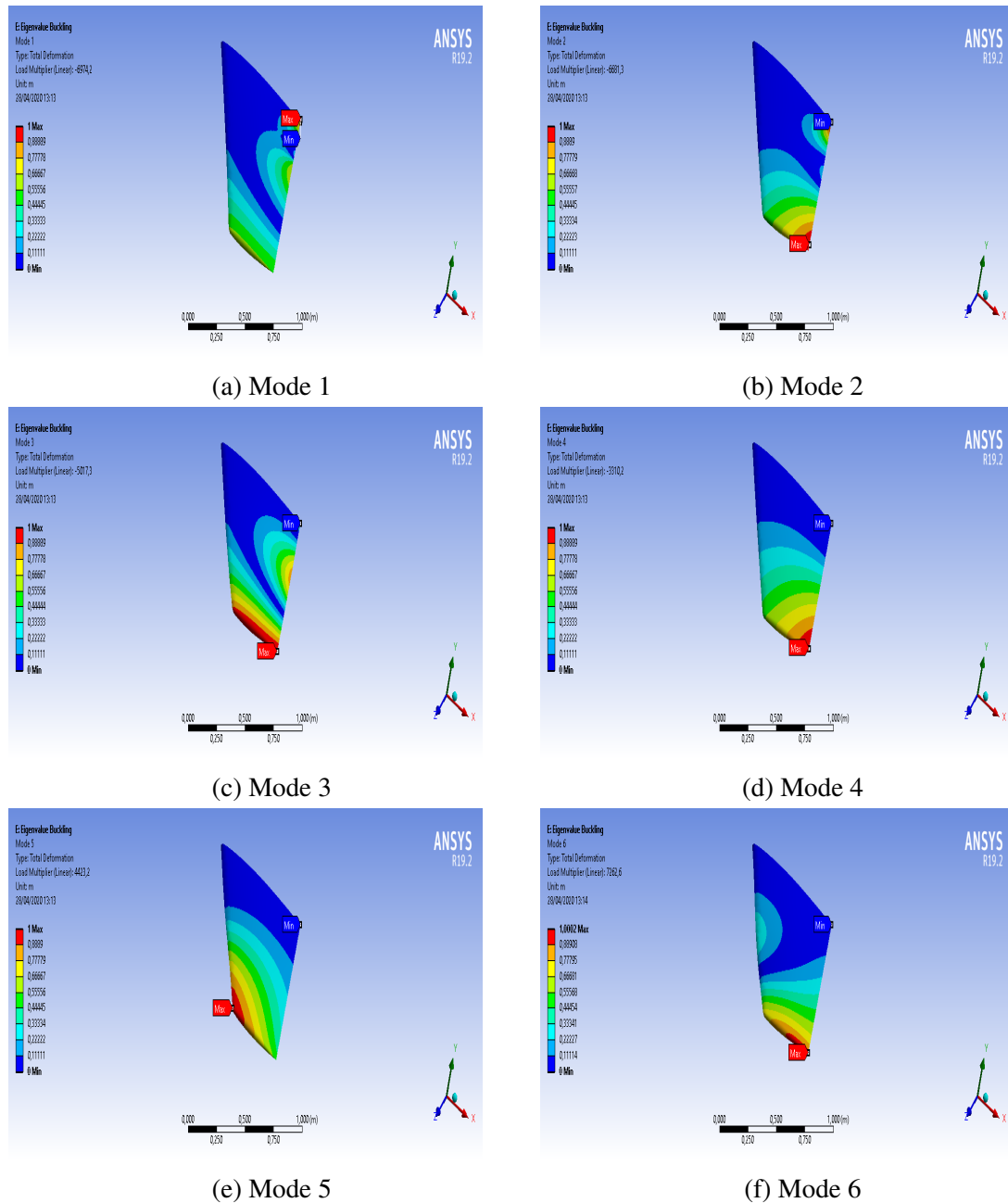


Figure 4.19: Buckling Modes: Total Deformation plot for the SST  $k - \omega$ , Al 2024-T3

## 4. Results

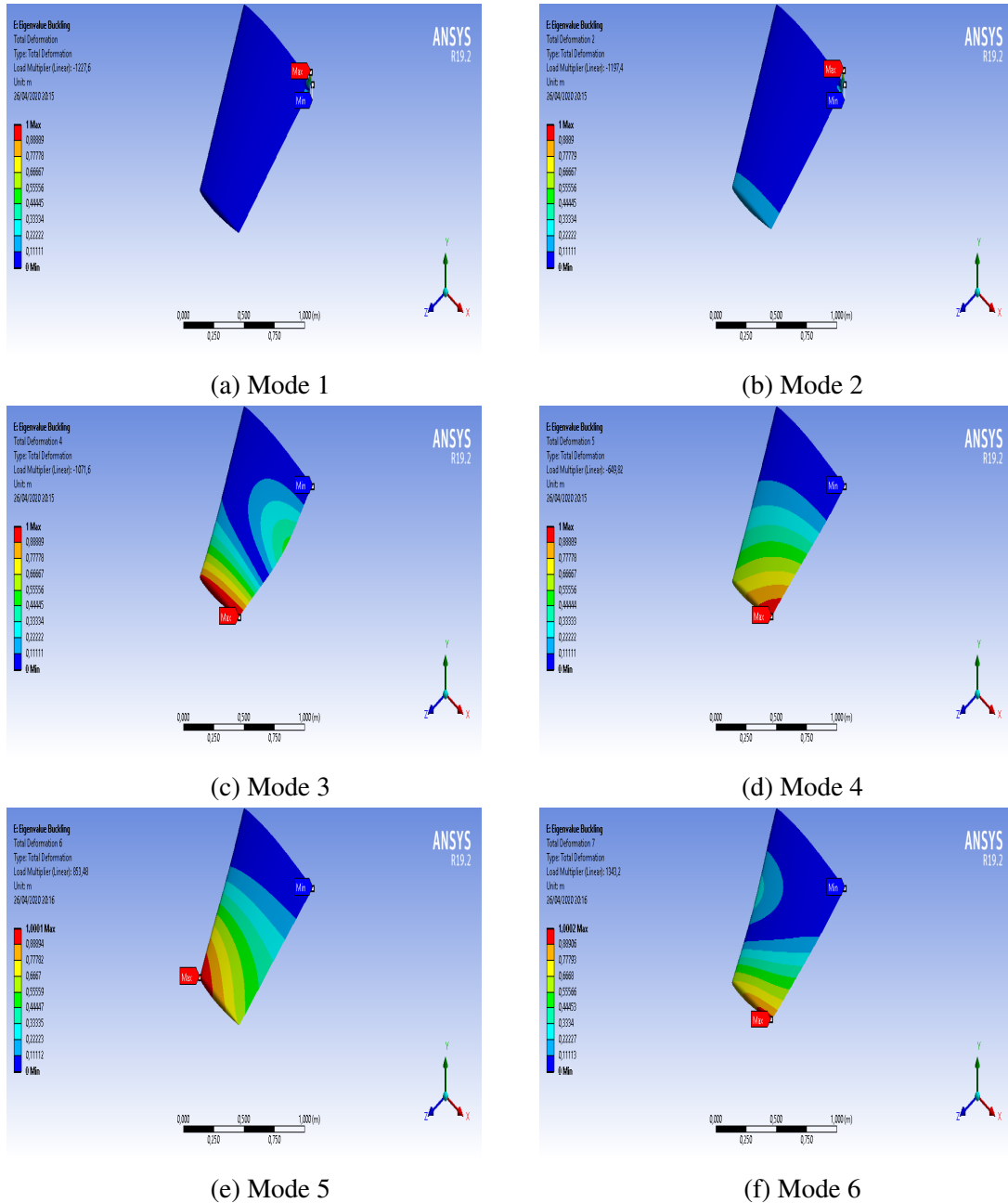


Figure 4.20: Buckling Modes: Total Deformation plot for the SST  $k - \omega$ , Epoxy S-Glass

Both Figures the overall effect of the mode is similar for both materials. What is clearly perceived is that the deformation of the modes is more transmissible in the Al 2024 T3 alloy instead of the Epoxy S-Glass. This can be explained if the elastic properties of the materials are compared, as the composite material reaches sooner the plastic behaviour. Besides, the load factor applied is at least 4 times bigger than in the Epoxy S-Glass and

## 4. Results

---

evidently contributes to this appreciation.

Moreover, the plasticity behaviour cannot be considered with the Linear Eigenvalue (or Euler) Buckling as a result of the non-linearity of the material needed. This effect must be considered as the real structural stability is limited to the minor value of plasticity failure or linear buckling failure. Plasticity acquires importance when stock elements are evaluated, where linear buckling predominates in thin and large elements. For medium-shaped elements, it is a compromise solution between both linear and non-linear effects.

### 4.4.4 Transient Dynamic Analysis (Tharindu)

In this section it will be shown the results of the transient dynamic analysis on the Onera wing M6 without the structural components. Through this analysis it was possible to determine the time varying displacement (total deformation), stresses and strain. This analysis was conducted by coupling with turbulence models such as  $k-\epsilon$  Realizable, standard  $k-\epsilon$ ,  $k-\epsilon$  RNG, Spalart-Allmaras and the standard  $k-\omega$ , SST  $k-\omega$ .

The table 4.11 below shows the maximum displacement occurred during the analysis coupled with all the turbulence models mentioned above, studied on the 4 materials chosen from material selection.

Table 4.11: Transient analysis maximum total deformation

	$k-\epsilon$ real	$k\epsilon$ RNG	$k-\epsilon$ stand	Spalart	SST $k-\omega$	Stand $k-\omega$
AL 2024 T3	0.0003177	0.00031725	0.00039993	0.000277	0.00024178	0.00021076
Carbon Epoxy UD	0.0028837	0.002875	0.0035902	0.0025238	0.0022058	0.0019109
Epoxy S-glass	0.0024853	0.0024772	0.0031228	0.0021702	0.0018816	0.0014061
Epoxy E-glass	0.0024614	0.0024541	0.0030841	0.0021525	0.0018934	0.0016312

From the table 4.11 it was possible to notice that the highest displacements have been occurred on the carbon epoxy UD material under  $k-\epsilon$  standard model while the lowest has been determined to be  $k-\omega$  model 0.0021076m. However, it was possible to notice that even if the turbulence models were different that the lowest displacement has resulted is with Aluminium

.  
The table 4.12 shows the transient dynamic analysis conducted to study the time varying stresses.

## 4. Results

---

Table 4.12: Transient analysis maximum stress

	k- $\varepsilon$ real	k- $\varepsilon$ RNG	k- $\varepsilon$ stand	spalart	SST k- $\omega$	Stand k- $\omega$
AL 2024 T3	2605800	2576900	2534900	2434100	2242100	1796300
Carbon EpoxyUD	2526900	2269200	2250900	2136000	1962600	1574900
Epoxy S-glass	2281600	2253000	2235000	2120600	1948300	1563400
Epoxy E-glass	2564800	2288600	2259500	2156200	1983300	1753200

The table 4.12 shows the maximum stress level reached in the time step 0.5 seconds. It was possible to notice that the highest stress has been calculated on Aluminium under realizable k- $\varepsilon$  model and the lowest has again occurred under standard K- $\omega$  model, but this time on the Epoxy S-glass material. In the above table the least stress occurred material on different turbulence models is the Epoxy S-glass material

The table 4.13 shows the varying maximum strain occurred during the transient dynamic analysis

Table 4.13: Transient analysis maximum strain

	k- $\varepsilon$	k- $\varepsilon$ RNG	k- $\varepsilon$ stand	Spalart	SST k- $\omega$	Stand k- $\omega$
Al 2024 T3	0.000037821	0.000037406	0.000036872	0.000035209	0.000032401	0.000025981
Epoxy Carbon UD	0.00039558	0.00039087	0.00039439	0.000366	0.00033499	0.00027034
S-glass	0.00034164	0.00033757	0.00034128	0.00028614	0.00028901	0.00022932
E-glass	0.00033523	0.00033132	0.00033311	0.00031048	0.00028445	0.00023326

The table above shows the maximum strain happened during 0.4s time step. It shows that the highest strain has occurred on the Carbon Epoxy UD material under realizable k- $\varepsilon$  model. While the lowest strain recorded on the table is Aluminium under standard k- $\omega$ . It was also possible to notice that the material with lowest strain in this study was S glass, with every turbulence model.

From the results of the analysis it was possible to determine that there are two materials that offer good results which are Aluminium and S glass

For a better selection between the two materials Aluminium 2024 T3 and Epoxy S glass, the author chose to study the results with graphs using k- $\varepsilon$  realizable model. This turbulence model was chosen as it produced the highest total deformation and strain for Aluminium and the highest stress for the Epoxy S-glass compared to the other models

## 4. Results

---

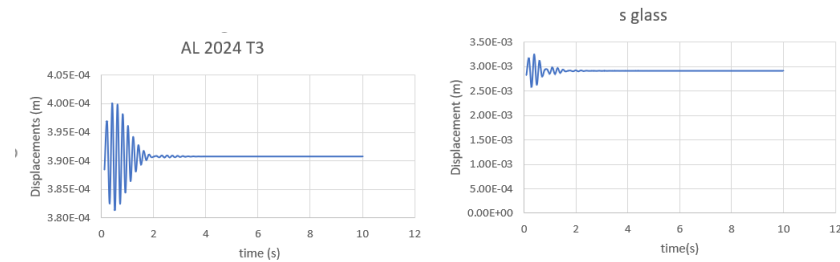


Figure 4.21: AL 2024 T3 (left) and S-glass (Right) produced Total deformation of Transient analysis

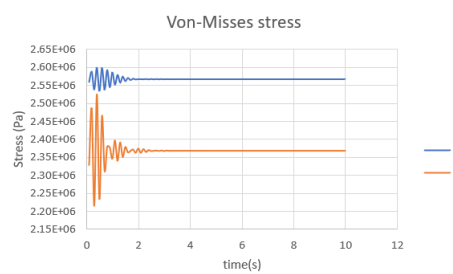


Figure 4.22: AL 2024 T3 and S-glass produced by von-Mises stress of Transient analysis

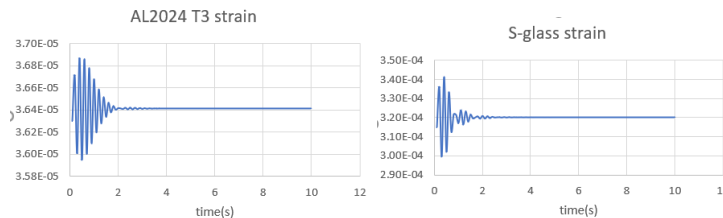


Figure 4.23: AL 2024 T3 (left) and S-glass (Right) produced von-Mises strain of Transient analysis

From the graphs in figure 4.21 it is possible to notice the total deformation , with S glass the time varying displacement stops soon after the time step of 2 seconds while Aluminium even if the displacements are lower than the S glass it keeps continuing even after the time step of 3 seconds.

From the stress graphs in figure 4.22 it was possible to notice that the variation stress of Aluminium gets stabilize at the time step of 2 seconds while the S glasses stress variations keep continuing even after 2 seconds. The variation intensity is in a range of 0.3 MPa for S glass while the Aluminium has a range of 0.05 MPa

In the strain graphs in figure 4.23 both continue the variation a small amount of time further even after the time step of 2 seconds till it get stabilized. In the strain graph the

## 4. Results

variation of the Aluminium decreases gradually while the S glasses variation has a sudden decrement. Another feature to be noticed is that the strain occurring in Aluminium is much lower than the strain occurred with S glass.

### 4.5 Loading analysis (Tharindu)

In this section a static analysis is completed on the Onera M6 wing without the structural elements and it presents the deformation and the von-Mises stresses on the 4 materials studied in the material selection section. This study was also conducted to compare the results obtained from the analysis with structural elements.

The study was conducted by 3 types of loads:

- Punctual load at the centre of pressure
- Distributed load, over the upper surface area of the wing
- Triangular distributed load, over the upper surface of the wing

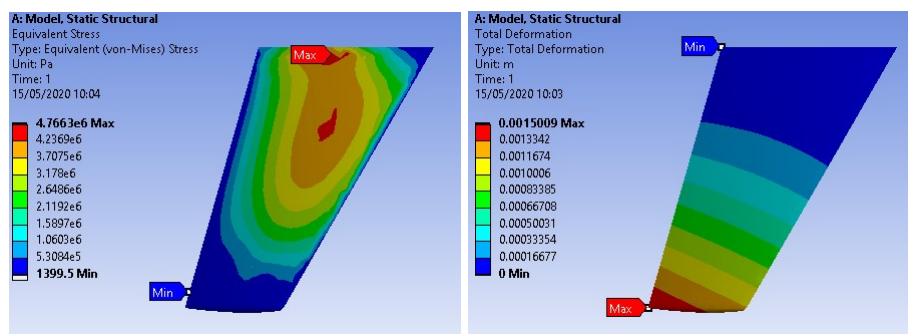


Figure 4.24: von Mises Stress (Left) and displacements (Right) produced by punctual load load AL 2024 T3

As it is possible to see the displacements are more concentrated on the tip of the wing, while the stress is spread mainly over centre of the wing.

## 4. Results

---

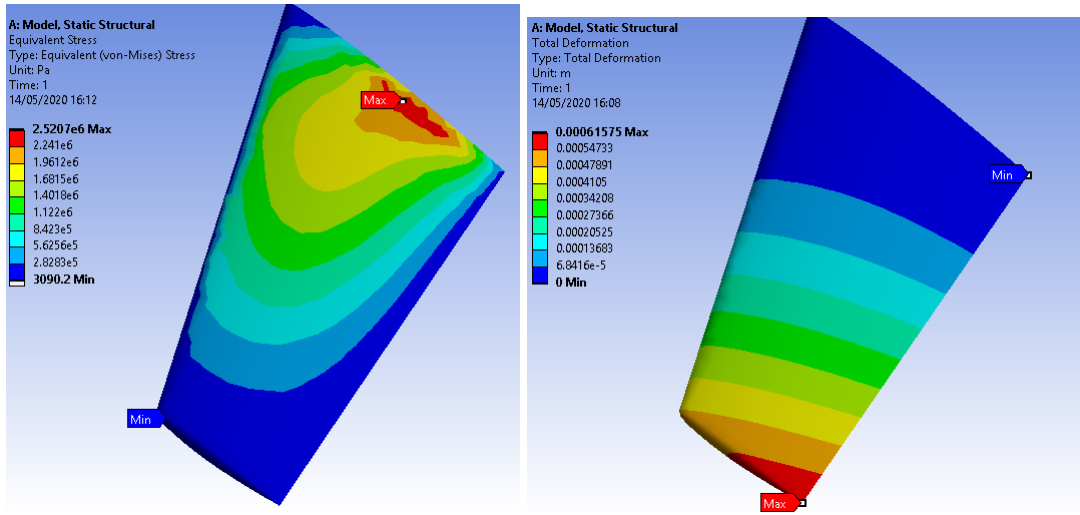


Figure 4.25: von Mises Stress (Left) and displacements (Right) produced by distributed load AL 2024 T3

In the above figure 4.25 the displacement occurred at the wing tip is lower compared to the punctual load and it is possible also to notice that even though the stresses are spread all over the wing surface, the highest stress area is at the wing root

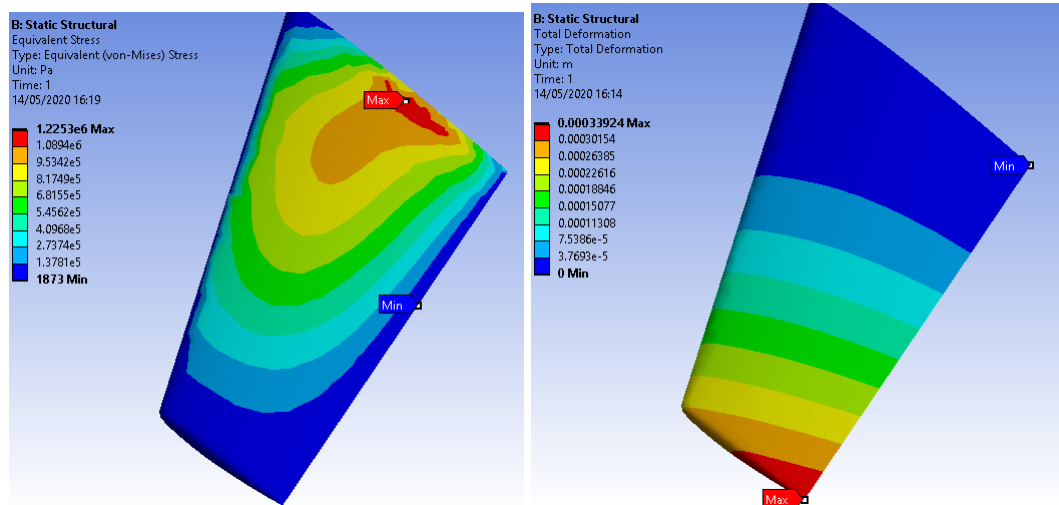


Figure 4.26: von Mises Stress (Left) and displacements (Right) produced by triangular load AL 2024 T3

From the triangular load analysis, it was possible to notice that the deformation has been reduced compared to punctual and distributed load at the tips and it has been same with the stresses too.

## 4. Results

---

Table 4.14: AL 2024 T3 results on Punctual, Distributed, Triangular loads

	Punctual	Distributed	Triangular
Deformation (mm)	1.5	0.62	0.33
Stress (MPa)	4.77	2.52	1.23

In the table 4.14 the types of loads have been compared with results obtained. However from the pictures above mentioned it was possible to notice that the stressed zones displacement zones doesn't differ very much, even if the distributed loads and triangular loads are different. The reason why the zones doesn't differ is because of the missing structural elements.

However through this analysis it not possible to choose what type of load analysis is better between distributed and triangular analysis, due to the fact that the effected displacement and stressed zones aren't different, even if the displacement values occurring in that area are very similar to the analysis conducted on the Onera wing M6 with structural elements.

In order to compare the results with the CAD with the structural elements the triangular loading method was applied on other materials in this section.

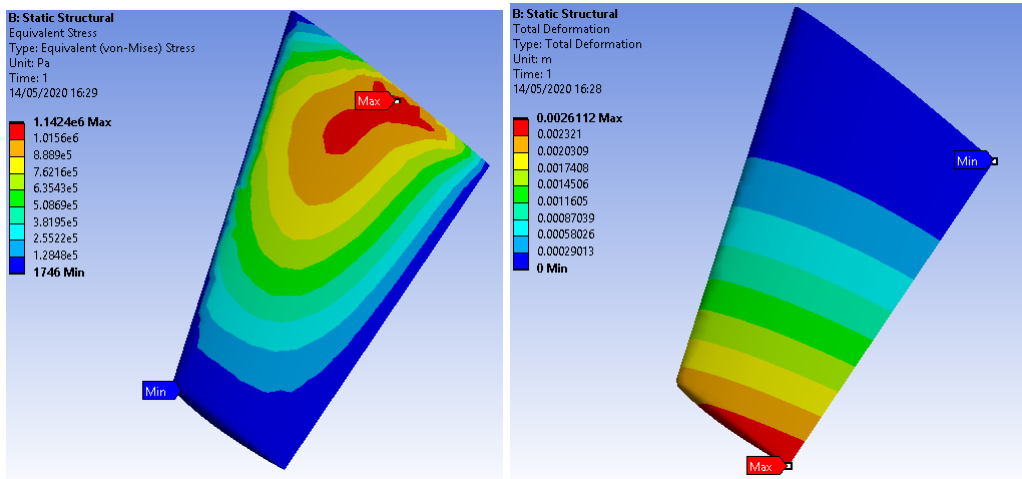


Figure 4.27: von Mises Stress (Left) and displacements (Right) produced by triangular load Carbon Epoxy UD

## 4. Results

---

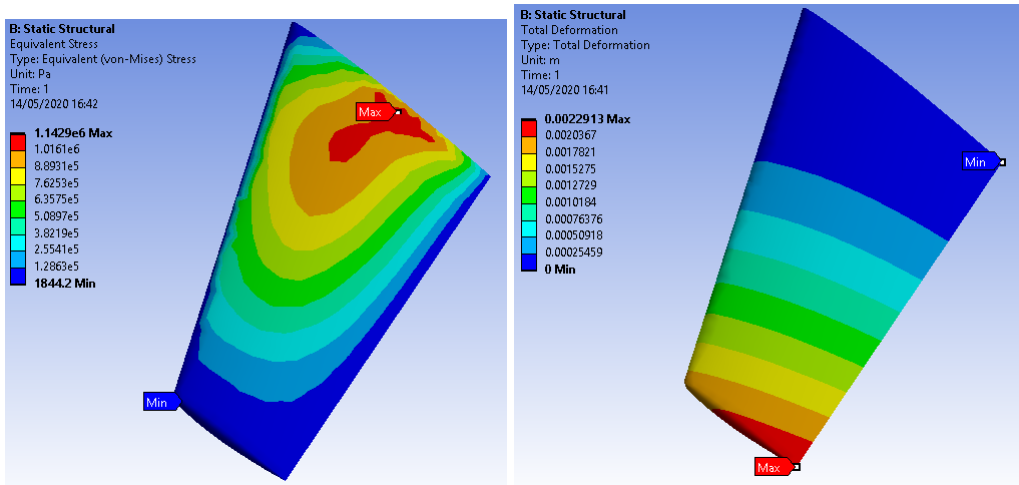


Figure 4.28: von Mises Stress (Left) and displacements (Right) produced by triangular load Epoxy E-glass

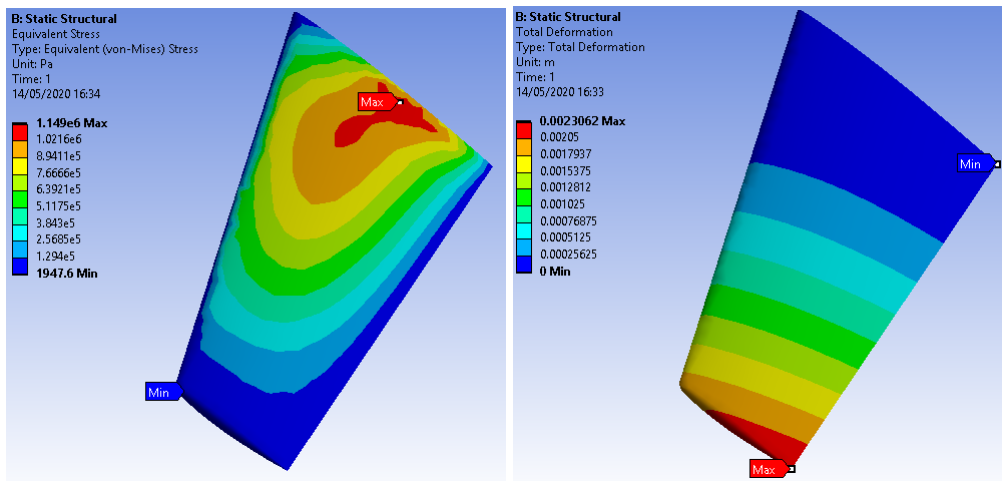


Figure 4.29: von Mises Stress (Left) and displacements (Right) produced by triangular load Epoxy S-glass

As it was mentioned before the zones where the stresses are concentrated are the same. The stress intensities and the displacements vary as the materials are changed. However, it is possible to see the displacements in Carbon Epoxy UD, Epoxy S-glass, Epoxy E-glass are higher compared to Aluminium even if they suffer more from higher stresses. The table below show the results obtained:

## 4. Results

---

Table 4.15: Triangular loading on 4 different materials

	AL 2024 T3	Carbon Epoxy UD	Epoxy E-glass	Epoxy S-glass
Deformation (mm)	0.33	2.66	2.29	2.23
Stress (MPa)	1.2253	1.15124	1.1429	1.149

Comparing the results with table 4.15 to the results obtained from the load analysis studied on the CAD design the with the structural elements. The displacements in the above table (4.15) differ only by 1 mm while stress intensities are very low compared to the Onera wing design with structural element (referring to table 4.17).

## 4.6 Self-designed CAD (Julio)

In the present section the results of structural analysis performed with Abaqus software to the Onera M6 model are shown. This results are specially important due are the first in this study that, includes inner structural elements such ribs and spars, which have been design and dimensioned by the authors. Moreover, all the analysis have been performed considering the materials defined before for the skin of the wing, due the internal elements of the structure are constructed in steel, with the following properties.

### 4.6.1 Static Analysis (Julio)

This sections presents the deformations and von-Mises stresses obtained from the static analysis performed to the own modeled Onera M6 wing, for the materials defined in this study, Al 2024-T3, Epoxy carbon UD, Epoxy E-Glass and Epoxy S-Glass.

#### 4.6.1.1 Aluminium 2024 T3

The first case of study is going to be performed with Aluminium material, specifically with the alloy AL 2024 T3 which is widely used in the aerospace industry. In order to perform the simulation, it must be considered how to apply the load on the wing, and without the possibility of extracting the fluid loads due the complexity of the process, three possibilities have been presented. The first one, which is the simplest, is to simulate the wing load by reducing it into a force vector applied in the wing center of pressure. Another way of simulating the wing load, in a more realistic way, is by distributing the total load over the surface of the wing. The problem of this methodology is that in big part of the surface of the wing the load is overestimated. Finally, the last approximation that has been applied in order to apply the load the more realistic as possible, is by using the triangular load distribution explained before in this study.

## 4. Results

---

The first result presented in Figure 4.30 shows the von-Mises stresses and the displacements suffered by the Onera M6 wing with the punctual load approximation.

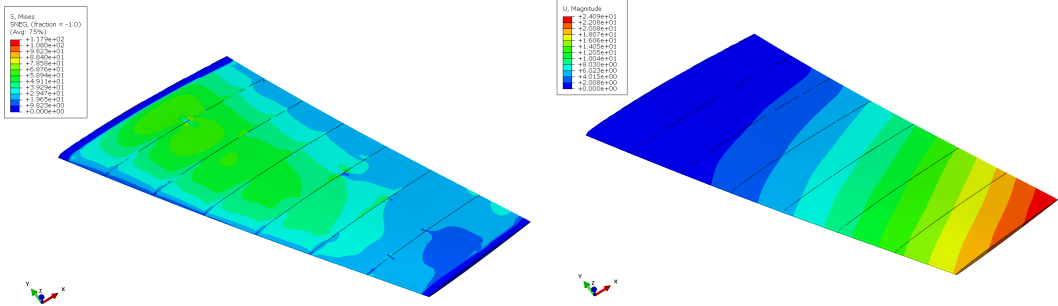


Figure 4.30: von Mises Stress (Left) and displacements (Right) produced by punctual load for Al 2024 T3

As can be seen in figure 4.30 the displacements with this approximations affects specially to the trailing edge, which of course is the weakness part of the wing, and it should not bear that deformation. However, it is good at first approximation of what happens to the wing in flight, and how its behaviour is. The same happens with the stress, as the total force is applied in just one point, the region where it is, is over stressed, but as said, those results are good as first approximation.

In Figure 4.31 the results for stress and displacements of the second load approach are presented.

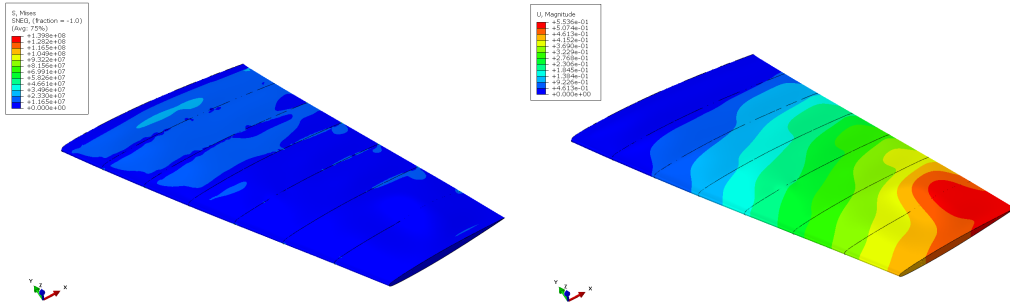


Figure 4.31: von Mises Stress (Left) and displacements (Right) produced by Uniform load for Al 2024 T3

In Figure 4.31 the load is applied uniformly along all the upper surface of the wing, making the load more similar to the real one. As can be seen, the stresses in this case are more spread in all the surface of the wing, making that the wing suffers in general lower stresses. However, in terms of displacements, even they are more similar to the real ones,

## 4. Results

---

in the trailing edge of the wing still the forces are overestimated producing big displacements on this region. As a consequence of this, and in order to produce the more realistic conditions, the next step is to simulate the load with triangular distribution along the upper surface of the wing.

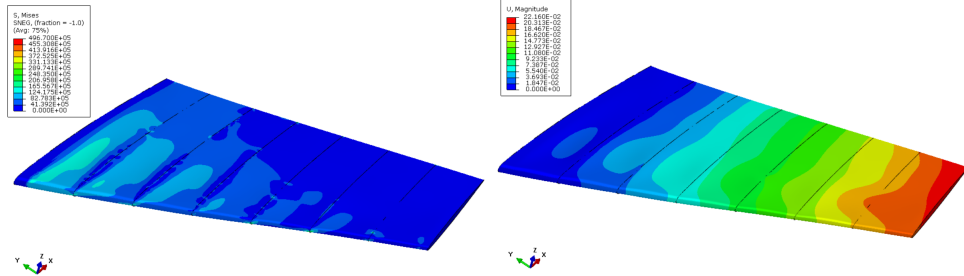


Figure 4.32: von Mises Stress (Left) and displacements (Right) produced by triangular load for Al 2024 T3

From Figure 4.32 the stress suffered by the wing with triangular distribution, is triangular, as obvious. Presents high stresses at the root and near the leading edge, and low stresses at the wingtip but all concentrated at leading edge. The same happens with the displacements results, the major zones affected correspond of course to the wingtip, but not as before as it is more distributed, and follows the lift behaviour, which makes that the principal zone affected is approximately the center of pressure of the wing. This results are the more near to reality, and present a similar behaviour to the reference [4], in terms of stresses and displacements. As the wing is different, but with similar loads, both present very similar behaviour, it can be considered that the results of this study are valid and correct.

Table 4.16: Static analysis results comparison with different load approximations

	Punctual Load	Uniform load	Triangular load
Max Deformation (mm)	24,09	5,54E-1	2,21E-1
Max Stress (MPa)	117,9	139,8	49,67

In Table 4.16, a comparison between the different load approximations has been made. One most more remarkable things that can be extracted from the table is that, the maximum deformation decreases when the load approaches to the real one, which makes sense, because the punctual load, and uniform distributed load, are more conservative approaches than the triangular one. As a consequence, it produces major displacements and also major stresses to the wing. It is also noticeable that, the uniform distributed load,

## 4. Results

produces a higher maximum stress than the punctual load. This is a consequence of applying the same load to all the surface of the wing, instead of applying it into only one point.

The conclusion of the cases studied in this section, is that the triangular distributed load is the one that simulates better the real behaviour of the wing, and subsequently, this load methodology will be used to test several materials, and see the behaviour of each one.

### 4.6.1.2 Epoxy-Carbon unidirectional (UD)

In this section the static structural analysis is performed with Epoxy-Carbon UD, a composite material that is one of the new standards in the industry. This material will obviously be used only for the skin of the model, due the inner structure will remain in steel. In Figure 4.33 the results for von-Mises stresses and displacements can be observed.

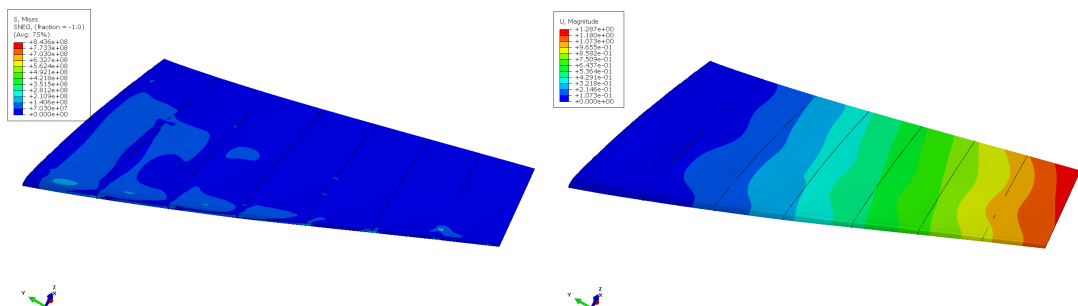


Figure 4.33: von Mises Stress (Left) and displacements (Right) produced by triangular load for Epoxy-Carbon UD

The first remarkable thing that can be seen is that the displacements with this material are wide large than the observed with the aluminium alloy. This was expected as the carbon fiber is in general more elastic than aluminium and can suffer major displacements and major stresses without crashing. And this case, is a good example of it, as with the same load as before, the stresses and the displacements have increased significantly. However, the pattern where the stresses are suffered, as well as the displacements, remain similar to the ones observed with the aluminum alloy.

### 4.6.1.3 Epoxy E-Glass

The Epoxy E-Glass is a composite material that can be used as an alternative to the carbon fiber seen on the section above, even it is not widely used as the carbon fiber, it is also

## 4. Results

---

interesting to see its behaviour. The results obtained for Epoxy E-Glass are presented in Figure 4.34.

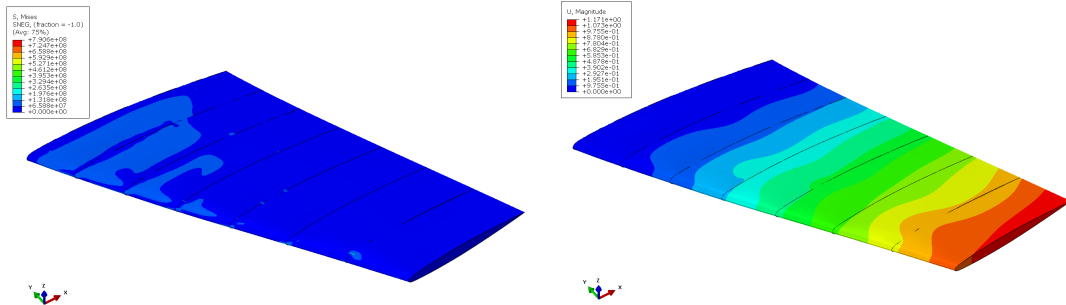


Figure 4.34: von Mises Stress (Left) and displacements (Right) produced by triangular load for Epoxy E-Glass

As it can be observed from the results, the maximum displacement in this case, as well as the maximum stress have decreased from the ones observed on the carbon fiber results. This was expected, as in general the glass fiber has lower elastic properties than the carbon fiber. However, it still permits higher displacements than the aluminium alloy, and it is a real alternative to it. In terms of the stress and displacement patterns, they remain similar to the ones observed in the aluminium simulation, which tells that the load is still similar to the lift distribution.

### 4.6.1.4 Epoxy S-Glass

The Epoxy S-Glass is composite material, similar to the one studied in the section above, but with more similar properties to the carbon fiber. As a consequence, this one is also presented as an alternative of the commonly used carbon fiber. The results obtained with this material for the stress and displacements are shown in Figure 4.35.

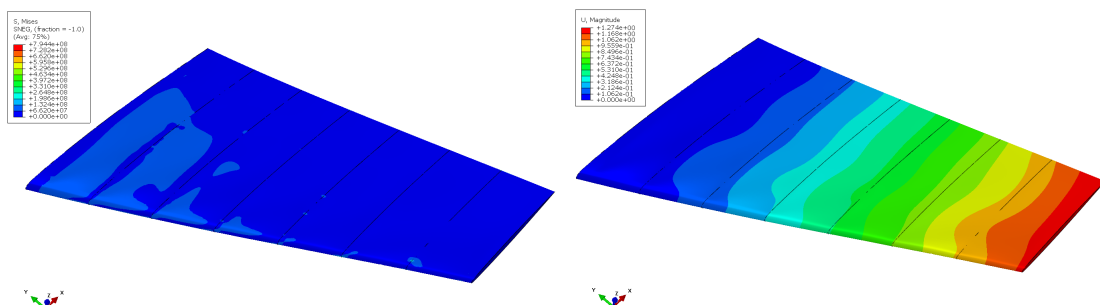


Figure 4.35: von Mises Stress (Left) and displacements (Right) produced by triangular load for Epoxy S-Glass

## 4. Results

---

The first thing that is remarkable from the results is that this material allows higher displacements than the E-Glass fiber presented before. Moreover, the displacements results, present a similar behaviour to the ones seen on the carbon fiber results, and it is also interesting to observe that the stresses are more similar to the ones obtained with Epoxy E-Glass. Thus, this material present the benefit of the ones presented before and allows significant displacements with contained stresses.

In the Table 4.17 all the results obtained for the all the materials in the static analysis, has been summarized.

Table 4.17: Static analysis results comparison with each material for triangular loads

	Al 2024 T3	Carbon UD	E-Glass	S-Glass
Max Deformation (mm)	2,21E-1	1,29	1,17	1,27
Max Stress (MPa)	49,67	843,6	790,6	794,4

On Table 4.17 the results that have been commented before can be seen , and it is easier to see all the conclusion that have been achieved, such as that the composites materials present a major displacements, but also suffers major stresses, as they are more elastic materials. Another deduction is the fact that Epoxy S-Glass, even presenting similar mechanical properties to the other glass fiber, shows more similar displacements to the carbon fiber, but with lower stresses.

It can be also concluded from this analysis that with this results, it easy to understand why the industry is moving towards the composites materials, and using in a lower ratio the aluminium alloys.

### 4.6.2 Modal Analysis (Julio)

In the modal analysis it is studied the natural frequency of the structure and the effect that it produces to it. The most important feature to consider in this case is the lowest natural frequency of the model, because it is the most probable to take place, and this is when it can cause an erratic behaviour of the structure incurring into the crash of the structure.

In order to validate the results that are presented in this section the results provided by (El Maani et al., 2016) [32] in which a modal analysis was performed to an only skin Onera M6 wing, will be useful as a reference data. On Table 4.18 the natural frequencies

## 4. Results

---

obtained for the first 5 modes, and all the materials considered in this study are presented.

Table 4.18: Natural frequencies (Hz) of the wing for each material

Modes	Al 2024 T3	Epoxy Carbon UD	Epoxy E-Glass	Epoxy S-Glass
1	29,78	28,015	24,996	24,267
2	51,113	55,392	36,105	36,822
3	76,401	71,088	50,25	51,04
4	85,72	86,548	61,691	63,497
5	100,75	98,656	66,661	65,061

The first thing that can be extracted from Table 4.18 is that the first mode of all materials, specially the aluminium alloy, is near the first mode presented (El Maani et al., 2016) [32], which could indicate that the results are correct. However, as in this case it is considered a model with a inner structure is expected that the results diverge from the reference, as it happens with the followings modes.

If we compare the modes obtained with the aluminium alloy with the ones obtained by the composites materials, it can be observed that in general the aluminium provide higher natural frequencies than the others, even the Epoxy Carbon UD remains very close to it. The shape of the deformation for every mode is very similar between materials, and due this reason, it has been decided to present only the deformation shape of the first 5th modes of the aluminium allow, which can be seen in Figure 4.36.

The first natural frequency mode observed in Figure 4.36 is the expected one, because the wing presents the same type of deformation that is seen in the reference, and also on the results presented on the Only Skin section of this study. Referring now to the rest of the modes, it can be seen how the wing structure behaves in an erratic way, however this modes are not as interesting as the first one, because those ones are not as likely to occur.

## 4. Results

---

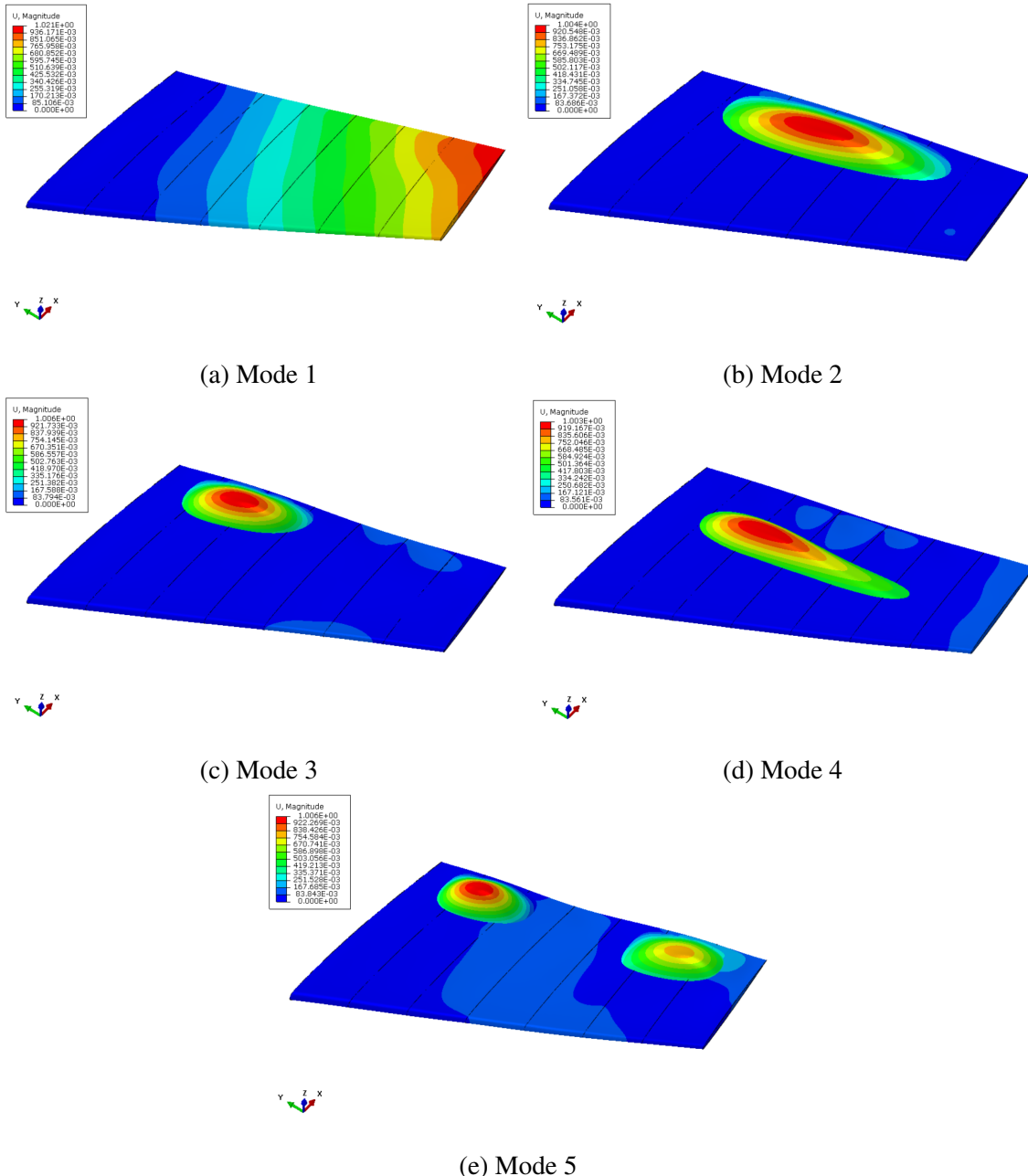


Figure 4.36: Deformations of first modes of Modal Analysis for aluminium alloy

### 4.6.3 Buckling Analysis (Julio)

The buckling analysis will evaluate the stability of the structure under non-linear effects, and establish at which point, the loads applied into the structure will make the structure to collapse. This type of analysis is typically performed for structures under compressing

## 4. Results

---

loads, which is generally not the case for the structure of this study however, also the shear forces contributes to the buckling non-linear effects, and this is why it is interesting to perform the analysis. In Table 4.19 the buckling load factor obtained from each material and for 5 modes are presented.

The load factor value that is presented in Table 4.19 represents the ratio between the critical load and the current load, and as a consequence of this, as higher is this number, safer is the structure in terms of stability.

Table 4.19: Buckling Load Factor for each wing material

Modes	Al 2024 T3	Epoxy Carbon UD	Epoxy E-Glass	Epoxy S-Glass
1	4304,6	1601,7	1312,7	1351,1
2	4336,8	1684,9	1318,8	1359,1
3	5051,3	1688,3	1349,9	1387,1
4	5098,9	1695,6	1496,0	1478,1
5	5740,7	1870,8	1517,0	1549,3

From the results obtained it can be observed, firstly, that the values are high enough to ensure that the structure will not in any case suffer buckling effects. Taking into account now the differences between the materials, it is clear that the aluminium alloy is the one that present less sensitivity to the buckling by almost 4 times in comparison with the other composites materials. It is also remarkable that from the three composites, the carbon-fiber is the one which presents a better behaviour against buckling, and for glass-fiber composites, they both present a very similar value of buckling load factor. However all of this, all the materials will not have problems in terms of buckling.

In the Figure 4.37 the deformations observed for the first 5th modes are presented for the aluminium alloy. Only the results for the aluminium are shown in the present study, due the similarity of the results of the analysis for the rest of materials analyzed, and those ones are representative enough to show how the deformations are produced. As can be seen, the major deformation are present mainly near the root, which is the zone where major stresses are concentrated. It is also remarkable that the deformation that appears has mainly shape of bubbly, which is a typical effect of the buckling in a skin-based structure.

## 4. Results

---

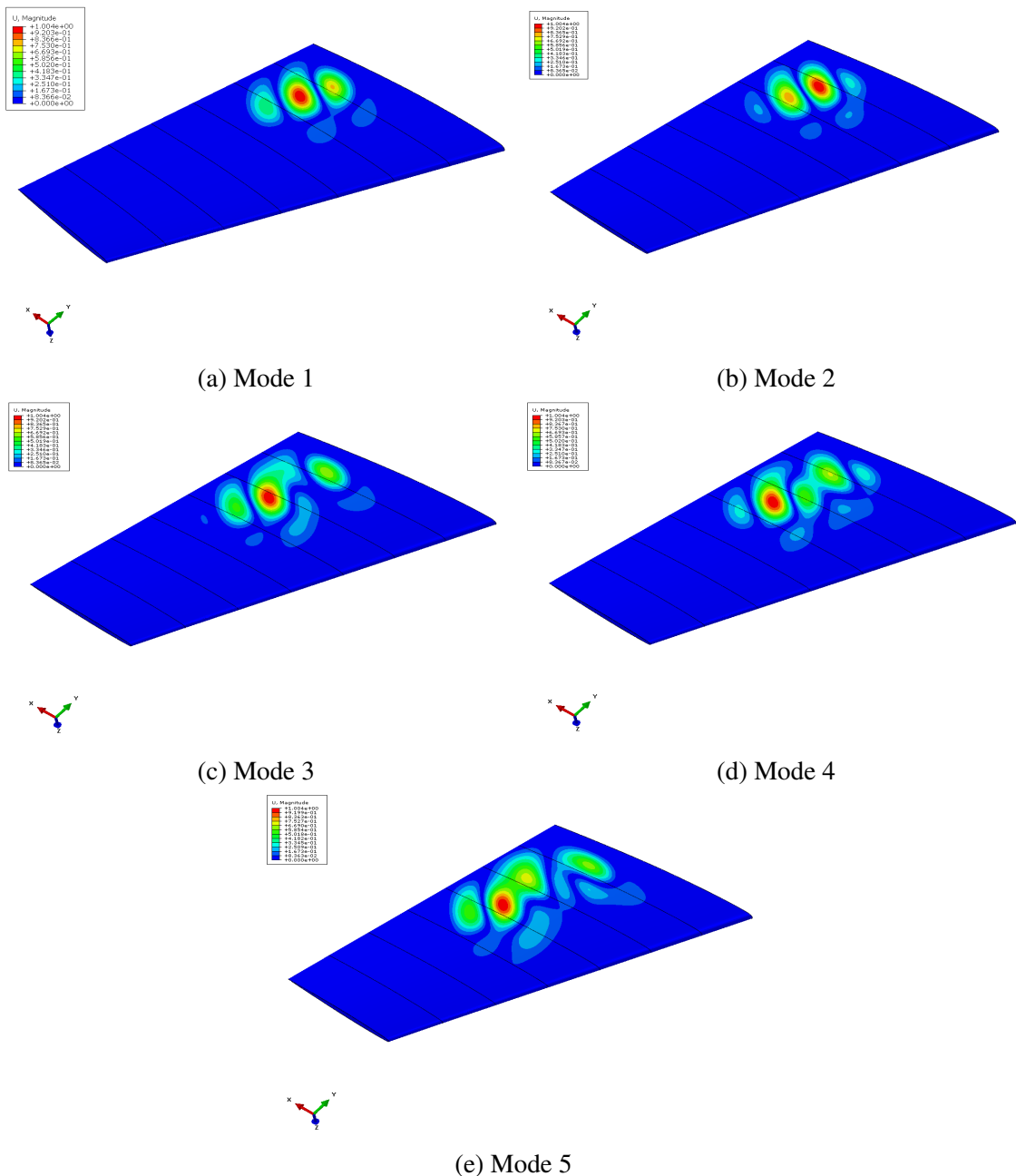


Figure 4.37: Deformations of first modes of Buckling Analysis for aluminium alloy

# Chapter 5

## Conclusions

The main purpose of the investigation has been achieved. A full study of the fluid and structure interaction of the ONERA M6 wing under a transonic environment has been described, simulated and validated with results from different sources. The FEM methodology has been carefully examined. The numerical results come from two different FEM Structural commercial softwares (ABAQUS, ANSYS) providing consistent and coherent results between each other. A Grid Convergence Study has been also carried out for the total deformation magnitude of a section of a wing, withdrawing excellent coherence and approach to the asymptote of unity value. Due to the facts explained, it can be said that all the results gathered within this document are reliable for further investigation.

For the Fluid simulation, five different turbulence models (Spalart-Allmaras, Standard  $k - \varepsilon$ , Realizable  $k - \varepsilon$ , Standard  $k - \omega$  and Shear Stress Transport  $k - \omega$ ) widely applied in the CFD community have been applied and their results contrasted. Their influence, depending on the mathematical formulation and assumptions of each one, show differences which are also noted in the structural simulation. Once their results are validated, the closer approach to the physical problem has been provided by the Shear Stress Transport  $k - \omega$  turbulence model. Good prediction of the flow behaviour is also given by Realizable  $k - \varepsilon$  and Spalart-Allmaras. It is important to mention that, even though the SST  $k - \omega$  demonstrated better performance, the fastest convergence is noticed in the Spalart-Allmaras model as it is a 1-equation semi-empirical model specifically designed for the aerospace environment. Therefore, if quick results are aimed, it stands as a very solid turbulence model to be considered.

Attending to the wing's model, two different CAD geometries have been evaluated computationally. The first one, taken from GRABCAD with the author's permission to run this research, is composed by only the skin of the aircraft. Similar studies such as [2],

## 5. Conclusions

---

[6] have conducted this same research with a similar geometry but only considering the effect on the upper surface in the wing.

Apparently, this approach may be incomplete if we consider the fact that the real structure is held by structural elements such as ribs, spars, and longerons and then the union between those. Thus, a CAD has been designed by our own according to the needed calculus -which have been provided in this document- which incorporates these elements, and in fact, no much literature for this scenario has been found for similar geometries 8 (see [5] ). The Fluid-structure interaction evaluation could not be achieved for this geometry as a result of incompatibilities between both FEM Solvers (ABAQUS, ANSYS) therefore the classic analytical approaches of different study of "equivalent" loads has been correctly performed and explained.

The current aerospace industry is giving special attention to materials which might enhance the aircraft's operation by reducing weight (and accordingly cost) but maintaining high resistance to static and dynamic situations. This is why, the noble materials of : Epoxy-Carbon UD, Epoxy S-Glass and Epoxy E-Glass have been correctly tested as well. Their results show promising properties for future manufacturing, as they overall show mechanical properties enough to face the operation and fatigue resistance (although they are slightly worse than the Aluminium Alloy Al 2024 T3) but specially entail a huge reduction in the weight of the skin.

Now, particular appreciations will be made for the results obtained for each geometry. As it will be seen, the order of magnitudes of both approaches are accordant, yet the influence of the structural elements suppose an essential and needed impediment for the total deformation to advance in the whole geometry and also to attach the skin to stiffer elements to prevent it from further induced deformations. In this sense, the effect of the own-designed CAD is appreciated as it was expected and redounds in a more direct approach to the real fluid-structure interaction of an aircraft's operation.

- **Only Skin CAD**

Looking at the results for the skin-only geometry, similar results were found in literature ([2], [6]).

For the static analysis, as the distribution of the load is different depending on how well the turbulence models may simulate the flow it's clear that these turbulence models impact the deformation, stress and strain, even though the results are almost comparable. The composite materials had in general higher displacement and stress and lower strain than the aluminium alloy.

## 5. Conclusions

---

The results for the modal analysis showed that the composite material had mostly lower natural frequency than the aluminium.

The buckling analysis reveals that the proprieties of the materials have an impact on the deformation of the mode. In our results, the different materials gave same order results but the Epoxy Carbon UD tended to buckle more. Nonetheless, in these simulations, the buckling factors were big enough to ensure that the buckling will not appear.

Through the transient analysis conducted it is possible to state that Epoxy S-glass material reaches a stabilizing point before Aluminium 2024 T3 alloy in the strain and displacement variation graphs, but not in the stress variation. However, it is possible to say that Epoxy S-glass is the better material through the transient analysis as even the stress obtained for Epoxy S-glass is lower than the Aluminium alloy.

Through the Loading analysis conducted on the skin CAD it was not possible to state which loading type study was the better one. But it was possible to see that the difference of displacements, between the Skin CAD and the CAD with element structures, was only by 1 mm. But the stress values were highly different between the CAD drawings, as expected since one didn't have structural elements.

- **Self-designed CAD Conclusions**

Taking into consideration the results presented in Self-designed CAD, the first thing that can be concluded is that the results have been validated due the demonstrated similarities with other studies such as (Hoang; 2015) [4].

In terms of the results obtained for the static analysis, the first important thing to remark, is how the deformation and stresses changes depending the type of load approximation used. And as it have been seen, the punctual load, and uniform distributed load, has worked as a preliminary approximation, giving the order of magnitude of the real results. This approach has been normally used in the flight mechanics and aerodynamic flow theory in order to achieve calculable yet useful results. But, as they are a conservative approach, they overload some parts of the wing, and concluding this way that, the triangular load distribution (where lift is obviously 0 in the wingtip and maximum in the root as the fuselage also acts,in a slight way, as a lifting surface) is the better approach from the ones tested in that section.

In reference to the different materials used for the skin in the static analysis with triangular load distribution, it is clear that composites materials have presented bigger displacements and stresses values, results that were expected as the composites used are more elastic and plastic materials, being the Epoxy Carbon-UD the one that has accordingly shown bigger displacements and stresses. Also, it is interesting to remark that the Epoxy S-Glass, even presenting similar mechanical properties to Epoxy E-Glass, present more

## **5. Conclusions**

---

similar displacements to the carbon fiber, but with lower stresses as a result of its hardening properties. As a consequence of this, it is understandable why the industry is moving towards the composites materials, and using in a lower ratio the aluminium alloys.

The modal analysis, which has also been performed with the same four materials, has been also validated with the results provided by (El Maani et al., 2016) [32] for the frequencies and for the deformation shape. The most noticeable insight is that the aluminium alloy generally presents higher natural frequencies than the composites ones, thing that has also been observed in the only skin CAD results.

Finally, the buckling analysis conducted has shown that the buckling load factor values are high enough to ensure that with the load studied, there is no risk of buckling for any of the studied materials. It is also interesting to mention that, the aluminium alloy is the one that presents lowest sensitivity to buckling by 4 times in comparison with the composites materials.

# Chapter 6

## Future Work (Marc, Julio)

The present study has been done under exceptional circumstances (in plenum COVID-19 outbreak) and has been challenging in terms of communication, time managing and specially resources. All the simulations have been run in low-specifications personal computers therefore the accuracy and resolution targeted could not be as high as it was desired. However, results demonstrate an important and satisfactory approach to the real problem with high fidelity results (validated with literature and by statistical error study) and in this sense the objectives are thought to be achieved.

The work by itself leads to improvement in so many aspects. Here, the most evident will be suggested.

To begin with, this simulation is constructed on theoretical approach and supported by mathematical models, which are not exactly equivalent to reality. Some errors can be made in the modelling or in the treatment of the data. FEM has been shown to be a more than valid approach for structural analysis yet FVM could be applied, with major difficulties, in order to have more mathematical strength.

In terms of the flow problem, the simulation setup has been described above. The procedure of evaluation has been under a Reynolds-Averaged Navier Stokes Equations (RANS) although DNS, LES and hybrid methods would be interesting to investigate. Another setups with different Riemann Solvers, higher order schemes, flux formulation, meshes could be tested and consequently higher evidence of being in the right track would be owned. Nonetheless, when the results of the different flow behaviour predicted by the different turbulence models have been plotted against experimental data [1], great concordance and coherence has been found with reality. From this graphic, the SST  $k-\omega$  and the Spalart-Allmaras models outstood as the most accurate to the real flow problem.

The difficulty of the turbulence mathematical treatment has been stated, as no general method has been developed to correctly model it for any case. As it has been seen, every model has its owns advantages and drawbacks. Given the specific case we are dealing,

## **6. Future Work (Marc, Julio)**

---

modifications in those models could be made such as the improvements in the SST model made by [51] by UDFs (User-Defined Functions) to prioritize those terms and parameters which predominate in this problem. At the same time, a parametric study of the turbulence models could be also carried out and other turbulence models could be examined as well.

In the end, the flow problem is incorporated to the structure as imported load in its surface. This approach, although is apparently the most accurate, can also be modelled with other means and could logically be supported by experimental tests run on a physical prototype. Talking about the structural problem, shells have been used as the main FEM elements. It has been demonstrated that width and length are significantly larger than the thickness dimension, and as a consequence of that, a 2D approximation of the geometry can be assumed. Then, this thickness dimension has been ignored in the analysis performed, and including it, by selecting solid elements such as hexahedral, or tetrahedral, could make the problem more realistic. However, the approach done in this study, is good enough to produce valid results.

In this process, topology optimization techniques have not been used to look for other more convenient geometries as they could affect the aerodynamic problem and significantly harden the industrial construction of the ONERA M6 Wing. Nonetheless, in terms of academic scope, we believe it would entail a positive contribution to this work.

# Bibliography

- [1] Suad Jakirlić, Bernhard Eisfeld, Roland Jester-Zuerker, and Norbert Kroll. Near-wall, reynolds-stress model calculations of transonic flow configurations relevant to aircraft aerodynamics. *International journal of heat and fluid flow*, 28(4):602–615, 2007.
- [2] Bojan Šekutkovski, Ivan Kostić, Aleksandar Simonović, Philip Cardiff, and Vladimir Jazarević. Three-dimensional fluid–structure interaction simulation with a hybrid rans–les turbulence model for applications in transonic flow domain. *Aerospace Science and Technology*, 49:1–16, 2016.
- [3] Stuart Dutton, Donald Kelly, and Alan Baker. *Composite materials for aircraft structures*. American Institute of Aeronautics and Astronautics, 2004.
- [4] Hoang Hoang and Viet Toan. Simplified design of a commercial aircraft wing made of carbon fiber. B.S. thesis, 2015.
- [5] K.Sivamanikandan K.Keerthana K.Balaji G.Vigneshwaran, M.Vijayaraghavan. Fluid structure interaction over an aircraft wing. *International Journal of Engineering Research and Development*, 2017.
- [6] Chowla Sangeetha, Mr Veeranjaneyulu, and MSN Guptha. Fluid structure interaction on agard 445.6 wing at transonic speeds. *Jawaharlal Nehru technological university, Hyderabad*, 2015.
- [7] Daryl L Logan. *A first course in the finite element method*. Cengage Learning, 2011.
- [8] Thomas JR Hughes. *The finite element method: linear static and dynamic finite element analysis*. Courier Corporation, 2012.
- [9] Jiapeng Tang, Ping Xi, Baoyuan Zhang, and Bifu Hu. A finite element parametric modeling technique of aircraft wing structures. *Chinese Journal of Aeronautics*, 26(5):1202–1210, 2013.

## Bibliography

---

- [10] Ravi Kumar B. Investigation on buckling response of the aircraft's wing using finite-element method. *Australian Journal of Mechanical Engineering*, pages 1–10, 2018.
- [11] George Staab. *Laminar composites*. Butterworth-Heinemann, 2015.
- [12] Stephen W Tsai and Edward M Wu. A general theory of strength for anisotropic materials. *Journal of composite materials*, 5(1):58–80, 1971.
- [13] Alfredo Güemes Gordo and Nuria Martín Piris. *Ciencia de materiales para ingenieros*. Pearson Educación, 2012.
- [14] Sandeep Tamrakar. *Characterization of S-glass epoxy composite interface under various rates of loading*. PhD thesis, University of Delaware, 2018.
- [15] Turkay Yildiz. Design and analysis of a lightweight composite shipping container made of carbon fiber laminates. *Logistics*, 3(3):18, 2019.
- [16] John L Sullivan, Geoffrey M Lewis, and Gregory A Keoleian. Effect of mass on multimodal fuel consumption in moving people and freight in the us. *Transportation Research Part D: Transport and Environment*, 63:786–808, 2018.
- [17] NASA. Navier-stokes equations 3-dimensional unsteady. *Glenn Research Center," NASA TM*, 2015. [online] Available at: <https://www.grc.nasa.gov/WWW/K-12/airplane/nseqs.html> [Accessed 2020-54-08].
- [18] J.-B. Cazalbou S. Jamme, F. Torres and P. Chassaing. Parallel direct numerical simulation of shock-turbulence interaction. *Parallel Comput. Fluid Dyn.*, page 163–170, 1998.
- [19] F. Roelofs and A. Shams. Cfd—introduction. *Therm. Hydraul. Asp. Liq. Met. Cool. Nucl. React.*, pages 213–218, 2019.
- [20] Y. Zhiyin. Large-eddy simulation: Past, present and the future. *Chinese J. Aeronaut.*, 28:11–24, 2015.
- [21] M. Hahn, Computing Centre for Fluid Mechanics, and Scientific. Cfd for aerospace applications. 2014.
- [22] Corina Drapaca and Siv Sivaloganathan. Brief review of continuum mechanics theories. 2019. [online] Available at: [https://link.springer.com/chapter/10.1007/978-1-4939-9810-4\\_2](https://link.springer.com/chapter/10.1007/978-1-4939-9810-4_2) [Accessed 2020 – 05 – 11].

## Bibliography

---

- [23] Massachusetts Institute of Technology. Constitutive equations. 2019. [online] Available at: [http://web.mit.edu/Constitutive\\_files/module3withsolutions.pdf](http://web.mit.edu/Constitutive_files/module3withsolutions.pdf) [Accessed 2020–05–11].
- [24] Matthias Heil. Stress, cauchy’s equation and the navier-stokes equations. *University of Manchester*, 2019. [online] Available at: <https://personalpages.manchester.ac.uk/matthias.heil> [Accessed 2020-05-11].
- [25] S P Venkatesan, J Jayaprabakar, N Beemkumar, and P N Kadiresh. Modelling and analysis of aircraft wing with and without winglet. *International Journal of Ambient Energy*, pages 1–20, 10 2018.
- [26] Salu Kumar Das and Sandipan Roy. Finite element analysis of aircraft wing using carbon fiber reinforced polymer and glass fiber reinforced polymer. *IOP Conference Series: Materials Science and Engineering*, 08 2018.
- [27] SIMSCALE. What is von mises stress? [online] Available at: <https://www.simscale.com/docs/content/simwiki/fea/what-is-von-mises-stress.html> [Accessed 2020-04-20].
- [28] Recep Gunes and Kemal Arslan. Development of numerical realistic model for predicting low-velocity impact response of aluminium honeycomb sandwich structures. *Journal of Sandwich Structures and Materials*, 18(1):95–112, 2016.
- [29] Engineersedge. Von mises criterion (maximum distortion energy criterion) strength (mechanics) of materials. [online] Available at: [https://www.engineersedge.com/materials\\_science/von\\_mises.htm](https://www.engineersedge.com/materials_science/von_mises.htm) [Accessed 2020–04–20].
- [30] Nikhil A Khadse and S R Zaweri. Modal analysis of aircraft wing using ansys workbench-software package. *International Journal of Engineering Research Technology (IJERT)*, 04, 07 2015.
- [31] Jai Kumar Charma. Theoretical and experimental modal analysis of beam, lecture notes in electrical engineering, 01 2019.
- [32] Rabii El Maani, Bouchaib Radi, and Abdelkhalak El Hami. Validation numérique d’un modèle aérodynamique : application à une aile d’avion. *ISTE OpenScience*, 1, 12 2016.
- [33] V S Ramamurthy K E Girish Shivaraj, Ranganatha S R. Buckling and linear static analysis of fuselage structure subjected to air load distribution. *IJARSE Journal*, pages 375–381, 2014.
- [34] Shruti Deshpande. Buckling and post buckling of structural components. 2011.

## Bibliography

---

- [35] Xueyan Zhang, Yan Zhao, and Fan Si. Analysis of wing flexure deformation based on ansys. In *2018 IEEE/ION Position, Location and Navigation Symposium (PLANS)*, pages 190–196. IEEE, 2018.
- [36] Miguel Cervera. *Non-linear transient dynamic analysis of three dimensional structures*, pages 320–504. 01 1987.
- [37] Henk Kaarle Versteeg and Weeratunge Malalasekera. *An introduction to computational fluid dynamics: the finite volume method*. Pearson education, 2007.
- [38] Yoshihide Tominaga and Ted Stathopoulos. Cfd simulation of near-field pollutant dispersion in the urban environment: a review of current modeling techniques. *Atmospheric Environment*, 79:716–730, 07 2013.
- [39] Alexander Moen, Lorenzo Mauri, and Vagesh D. Narasimhamurthy. Comparison of k-models in gaseous release and dispersion simulations using the cfd code flacs. *Process Safety and Environmental Protection*, 130:306–316, 08 2019.
- [40] Ansys. 4.4.1 standard k-epsilon model, 2009. [online] Available at: <https://www.afs.enea.it/project/neptunius/docs/fluent/html/th/node58.htm> [Accessed 2020-04-11].
- [41] Ansys. 4.4.3 realizable k-epsilon model, 2009. [online] Available at: <https://www.afs.enea.it/project/neptunius/docs/fluent/html/th/node60.htm> [Accessed 2020-04-11].
- [42] Ansys. 4.4.2 rng k-epsilon model, 2009. [online] Available at: <https://www.afs.enea.it/project/neptunius/docs/fluent/html/th/node59.htm> [Accessed 2020-04-11].
- [43] Ansys. 4.4.5 effects of buoyancy on turbulence in the k-epsilon models, 2009. [online] Available at: <https://www.afs.enea.it/project/neptunius/docs/fluent/html/th/node62.htm> [Accessed 2020-04-11].
- [44] Ansys. 4.4.6 effects of compressibility on turbulence in the k-epsilon models, 2009. [online] Available at: <https://www.afs.enea.it/project/neptunius/docs/fluent/html/th/node63.htm> [Accessed 2020-04-11].
- [45] Ansys. 4.4.7 convective heat and mass transfer modeling in the k-epsilon models, 2009. [online] Available at: <https://www.afs.enea.it/project/neptunius/docs/fluent/html/th/node64.htm> [Accessed 2020-04-11].

## Bibliography

---

- [46] C. David Wilcox. Reassessment of the scale-determining equation for advanced turbulence models. *Aiaa Journal*, pages 1299–1310, 1988.
- [47] Florian R Menter. Improved two-equation k. *Turbulence Models for Aerodynamic Flows," NASA TM*, 103975, 1992.
- [48] CD Argyropoulos and NC Markatos. Recent advances on the numerical modelling of turbulent flows. *Applied Mathematical Modelling*, 39(2):693–732, 2015.
- [49] Florian R Menter. Review of the shear-stress transport turbulence model experience from an industrial perspective. *International journal of computational fluid dynamics*, 23(4):305–316, 2009.
- [50] Pavel E Smirnov and Florian R Menter. Sensitization of the sst turbulence model to rotation and curvature by applying the spalart–shur correction term. *Journal of turbomachinery*, 131(4), 2009.
- [51] Antti Hellsten. Some improvements in menter’s k-omega sst turbulence model. In *29th AIAA, Fluid Dynamics Conference*, page 2554, 1998.
- [52] Richard Courant, Kurt Friedrichs, and Hans Lewy. On the partial difference equations of mathematical physics. *IBM journal of Research and Development*, 11(2):215–234, 1967.
- [53] Qing Fang, Takuya Tsuchiya, and Tetsuro Yamamoto. Finite difference, finite element and finite volume methods applied to two-point boundary value problems. *Journal of Computational and Applied Mathematics*, 139(1):9–19, 2002.
- [54] William Sutherland. Lii. the viscosity of gases and molecular force. *The London, Edinburgh, and Dublin Philosophical Magazine and Journal of Science*, 36(223):507–531, 1893.
- [55] Cailin A Buchanan, Marwan Charara, John L Sullivan, Geoffrey M Lewis, and Gregory A Keoleian. Lightweighting shipping containers: Life cycle impacts on multimodal freight transportation. *Transportation Research Part D: Transport and Environment*, 62:418–432, 2018.
- [56] Lee ching hao, S. Sapuan, and Mohd Roshdi Hassan. A review of the flammability factors of kenaf and allied fibre reinforced polymer composites. *Advances in Materials Science and Engineering*, 2014, 04 2014.
- [57] BR Rose, GR Jinu, and M Manivel. Partly coupled fluid structure interaction analysis of an aircraft wing at subsonic speeds. *International Journal of Mechanical & Mechatronics Engineering*, 14(3):22–29, 2014.

## Bibliography

---

- [58] Intizar Ali, Abdul Hameed Memon, M Tarique Bhatti, Dileep Kumar, Ishfaque Ali Qazi, Sajjad Banghwar, et al. Dynamic fluid-structure interaction analysis of propeller aircraft wing. *American Scientific Research Journal for Engineering, Technology, and Sciences (ASRJETS)*, 45(1):64–74, 2018.
- [59] Thomas Graf and Lukas Degener. Grid convergence of variable-density flow simulations in discretely-fractured porous media. *Institute of Fluid Mechanics in Civil Engineering, Leibniz Universität Hannover, Appelstraße 9A, 30167 Hannover, Germany*, pages 760–769, 04 2011.
- [60] Ansys. 26.18.1 judging convergence, 2009. [online] Available at: <https://www.afs.enea.it/project/neptunius/docs/fluent/html/ug/node833.htm> [Accessed 2020-05-04].
- [61] Viktor P. Zhukov and Klaus P. Heinrich. Evaluation of the grid convergence for a rocket combustion chamber with a porous injector. *Institute of Space Propulsion, German Aerospace Center (DLR), Langer Grund, 74239, Hardthausen, Germany*, pages 438–443, 2019.
- [62] Patrick J Roache. *Computational fluid dynamics*. Number BOOK. Hermosa publishers, 1972.
- [63] MORENO GONZÁLEZ Carlos. *Introducción al cálculo numérico*. Editorial UNED, 2014.
- [64] Ngoc San Ha, Tailie Jin, and Nam Seo Goo. Modal analysis of an artificial wing mimicking an allomyrina dichotoma beetle’s hind wing for flapping-wing micro air vehicles by noncontact measurement techniques. *Optics and Lasers in Engineering*, 51(5):560–570, 05 2013.
- [65] Peter Morgan. *Carbon fibers and their composites*. CRC press, 2005.
- [66] Jane Maria Faulstich de Paiva, Sérgio Mayer, and Mirabel Cerqueira Rezende. Comparison of tensile strength of different carbon fabric reinforced epoxy composites. *Materials Research*, 9(1):83–90, 2006.

# **Chapter 7**

## **Appendix**

### **7.1 Appendix 1: Individual Contribution**

- **Julio Maldonado:**

My individual contribution to the present study has been based in prepare, perform and analyse all the Abaqus simulations done. I have been in charge in all this section, by documenting myself firstly about how to do Abaqus simulation, to later on create the own CAD model with CATIA V5 software. Also, setup the Abaqus software, by implementing the materials, selecting the type of FEM elements, and meshing all the parts of the structure, also I have been in charge of preparing the loads implemented into the model. This leads to one of the main problems I had to deal with, because I tried to implement a FSI with the ANSYS Fluent results, which I didn't succeed due the incompatibility of both software to do it. Afterwards, I decided to analyse the model by using traditional approaches with demonstrated reliability, and once the simulations were performed, the results were introduced into the present report and analysed. It is also worth mentioning that I have also have a taste of the ANSYS Workbench and ANSYS Fluent, by performing the FSI simulations of the Wilcox's Standard  $k-\omega$ , and doing theoretic section of it in the Theory fundamentals section of this report, in which I also wrote the Governing Equations section. Finally, it is also remarkable that I prepared the CAD model drawings that are included in the appendix of this document. Also, both Marc Barceló and I have created the latex document together and have written the Applied Loads and Future Works section together.

I would like to use this lines also to acknowledge Marc, Léa and Erwan for the work they have done during this group project, because without their collaboration, this project wouldn't succeed. I feel really proud of all the work done and presented by this team.

- **Marc Barcelo:**

## 7. Appendix

---

My individual role in this group has been to assume the responsibility of being the leader and therefore working collaboratively in most of the sections with my partners, documenting myself in that ambit and helping as much as I could. Minor duties such as having closer contact with the supervisor and doing the paperwork were also part of this role. All the actions we have made as a team have been approved by the majority of the members and I believe I have put an effort in helping my colleagues and motivating them to work and communicate with the greatest efficiency possible. Talking about the individual contribution made by myself, I started to write a wide initial literature review which also involved fuselage study as initially we were supposed to run this FEM study on an aircraft's fuselage. As it was later on conveniently changed into the ONERA M6 wing study, I carried out the first initial simulations where we achieved results for a coarse mesh, only with skin. Some of the decisions such as creating a CAD with more structural elements, evaluating different aeronautic materials and Grid Convergence Study were thought by myself and approved with my colleagues. We felt really comfortable working together efficiently. I helped Julio with the calculus of the new CAD geometry in order to ensure its adequacy. Then, he started working on the simulation of our own CAD and evaluating its results in ABAQUS while Erwan, Léa and I worked in different aspects of the only skin CAD in ANSYS in order to compare both softwares. As Léa and Erwan were not able to obtain appropriate results with ANSYS because of a failure of the program, I ran all the simulations (flow and structural) for the only skin, and then for a fine mesh, with a CAD downloaded from GRABCAD, simulating for each different turbulence model and material (45 simulations in total). This number only represents the successful ones, as the failed actually rise to a very high number. Meanwhile, Léa and Erwan worked nicely in writing the theory fundamentals of structural analysis. Once I shared my results with everyone, I have been in charge of writing the theory fundamentals of the aerodynamic flow problem, FEM approach, redacting my assigned turbulence model which was the  $k-\omega$  SST, and I have also commented the structural buckling analysis and developed the mathematics of the Grid Convergence Study and the Validation and Verification of our results. Some contribution in the Materials and Appendixes has been done as well.

All the work which was my responsibility has been labeled with my name. The Introduction, Literature Review and Conclusions have been done collaboratively between Léa, Erwan, Julio and me and -as it can be seen- some other sections have been shared as well. I feel proud of the work done by this team and I would not hesitate to repeat it.

- **Léa Valade:**

During this project, I worked more particularly with Erwan, on trying to perform the simulations for the Spalart-Allmaras, and the  $k - \varepsilon$  turbulence models (for the only-skin

## 7. Appendix

---

CAD). However issues with Ansys did not allowed us to get relevant results, hence, we lost much time on it. So, we studied together the structural problem. I focused on the static structural and modal analysis, to find relevant results from literature and to understand the stakes and the fundamentals behind the theory. Reading also allowed us to work on the turbulence models and in my case, I introduced the mathematical meaning and the main effects of the spalart-allmaras and of the standard  $k-\epsilon$  turbulence models. I worked on the grid convergence introduction, to understand its fundamentals and I helped for the writing of the Ansys Workbench section. I compared the results provided by Marc for the modal analysis, to see the influence of the materials on the wing and its behavior depending on the mode. I worked on the literature review and in writing several introduction and conclusion parts. I would like to particularly thank Julio, Erwan and Marc for the huge amount of work they did during this project, for their motivation and their good humour. It was a real pleasure to work with them.

- **Erwan Moudir:**

With Léa we work together on the structural part and I focused my research on understanding the concept and found the governing equations for the buckling analysis and transient dynamic analysis with the presentation of relevant literature for these analyses. Also, for the aerodynamic flow problem, with Léa, we were in charge of introducing the Spalart-Allmaras and three of the  $k-$  turbulence model: the standard  $k-$ , the realizable  $k-$  and the RNG  $k-$ . I work more on the RNG  $k-$  and the realizable  $k-$  models. Moreover, I work on the ANSYS Workbench setup part as I was working with ANSYS for the only-skin CAD model, in order to have the results with the FSI simulation for the static structural analysis even I had some issue with Ansys on my personal laptop which made me waste a lot of time. In addition to this, I help for the Grid convergence study parts. For the Results part, as explain before, I was not able to have relevant results for the static structural problem, so Marc provide me the results he had. Thanks to that, I was able to compare and comment the results for the static structural analysis with the different materials and turbulence model used in this research work. In addition to this, I help for the Grid convergence study parts and write the abstract and the literature review for the fluid structure interaction problem. Moreover I would like to thank Léa, Marc and Julio for all the work they have done during this group design project. It was a pleasure and an honor to work with them.

## **7. Appendix**

---

- **Tharindu Warnakulasuriya:**

My contribution to this project started by performing FSI simulation on the RNG  $k-\varepsilon$  turbulence model on the Skin CAD of the Onera M6 wing in order to move to the structural problem, afterwards that the group had to face. Through this simulation I performed structural analysis and Model analysis and finally the buckling analysis. Initially to work with Ansys workbench for structural analysis problem wasn't easy for me but during this group project I managed to learn how to use the software. However even if the RNG  $K-\varepsilon$  turbulence model was completed the group decided not include it in the report as it was giving results very much similar to  $k-\varepsilon$  realizable turbulence model. After that I performed simulation for transient analysis for all the turbulence models:  $k-\varepsilon$  RNG,  $k-\varepsilon$  realizable, standard  $k-\varepsilon$ , Spalart Allmaras, SST  $k-\omega$  and for the standard  $k-\omega$ . This analysis with all the turbulence models were applied to all 4 materials taken into consideration in this group project. For further work in the group project I conducted a Loading analysis just on the skin of the wing with the usage of Ansys Workbench, by using three types of loads which were punctual load, distributed loads and triangular loads studied on all 4 materials. I also help the group to write the conclusion in the report. To complete these tasks the other group members work was pivotal, and I'm happy to have had worked with my group mates to complete this project

## 7. Appendix

---

### 7.2 Appendix 2: Materials (Marc)

In this section, the materials used in the simulations displayed above, will be further detailed giving evidence of their behaviour. Hence, the Aluminium Al2024 T3 alloy, the Epoxy Carbon Unidirectional (UD), the Epoxy S-Glass and the Epoxy E-Glass will be reviewed carefully giving special importance in the macromechanic facet.

#### 7.2.1 Aluminium 2024 T3

The choice of the aluminium as an interesting material to be used relies in the fact that it is actually the most common metal present in the Earth's surface (in form of oxide,  $Al_2O_3$ ). Even though the pure material is first obtained by Oersted, the industrial processing of this metal did not start until the procedure of Hall-Heroult was defined approximately 60 years later than Oersted.

If the aluminium density is considered, it is seen that compared to most of the other metals it is included inside the group of "light" metals.

The most remarkable features of the pure metal is the fact that it shows good resistance against corrosion, as it is usually covered by the alumina ( $Al_2O_3$ ) that prevents the inner metal to turn into oxide and loose its properties. Also, according to [13], its FCC (Face Centered Cubic) solid state structure is responsible for its good plasticity behaviour.

On the other hand, the temperature dilatation coefficient is high, this is why other metals are merged with aluminium into an alloy in order to overcome this weakness. The Young Modulus of approximately 70 GPa is not outstanding either if it is compared to the 200 GPa of common steels, thence the choice of including other metals to form alloys for this reason as well. This is why, in its pure form it is not used for structural means, however, as it is said, some alloys with aluminium as the principal component are excellent in terms of structural behaviours. This is the case of the Aluminium 2xxx and 7xxx (where x are numerical digits) families that are widely used in the aviation industry, specially the T3, T4, T6 and T8 alloys.

Regarding the 2xxx Aluminium Alloy family in which we are going to focus, the copper (Cu, with 3.8-4.9 % composition of the whole alloy for the Al 2024 T3) is the second most predominant metal as serves to create hardening precipitates, although it worsens the resistance against corrosion. Magnesium (Mg, with 1.2-1.8 % of presence) is used for catalyzing means, contributing to the creation of these hardening precipitates. Similarly, silicon (Si, <0.5 %) in the exact quantity can lead to the same beneficial hardening precipitates yet if it is present in excess, it produces intermetallic phases incurring into tenacity and plasticity decrease. The last important element to mention is the manganese (Mn, 1.2-1.8 %), which is known to be a non-recrystallization agent and thus enhances the mechanical properties. Minor elements such as plumb (Pb) and bismuth (Bi) can facilitate

## **7. Appendix**

---

the machinability of the material.

Only the 7xxx Al alloys seem to have better mechanic characteristics than the 2xxx hence its use in more modern aircrafts, nonetheless, they are worse at evading fatigue crack propagation along the whole structure.

The most obvious drawbacks of the Al 2xxx family is the special sensitivity of the corrosion, induced by the copper as the galvanic battery effect: spoilage of the material by loosing electrons. However, the Al 2024 T3 has shown an acceptable behaviour against corrosion and therefore the use of this alloy for aircraft's surface manufacturing. Here, find attached the results for the mechanical resistance of the Al 2024 T3 from [13].

### **7.2.2 Composite Materials**

The latest advances and investigation in the manufacturing advances have been focused to optimize the operation of the aircraft through aiming smoother aerodynamic surfaces that do represent a favorable ratio of cost/efficiency and also the substitution of the conventional aluminium alloys for new composite materials, which are lighter but still able to safely resist the operation. The comparison between different aircraft researched materials in term of specific modulus and specific strength has been provided by [3] in Figure 7.1.

## 7. Appendix

---

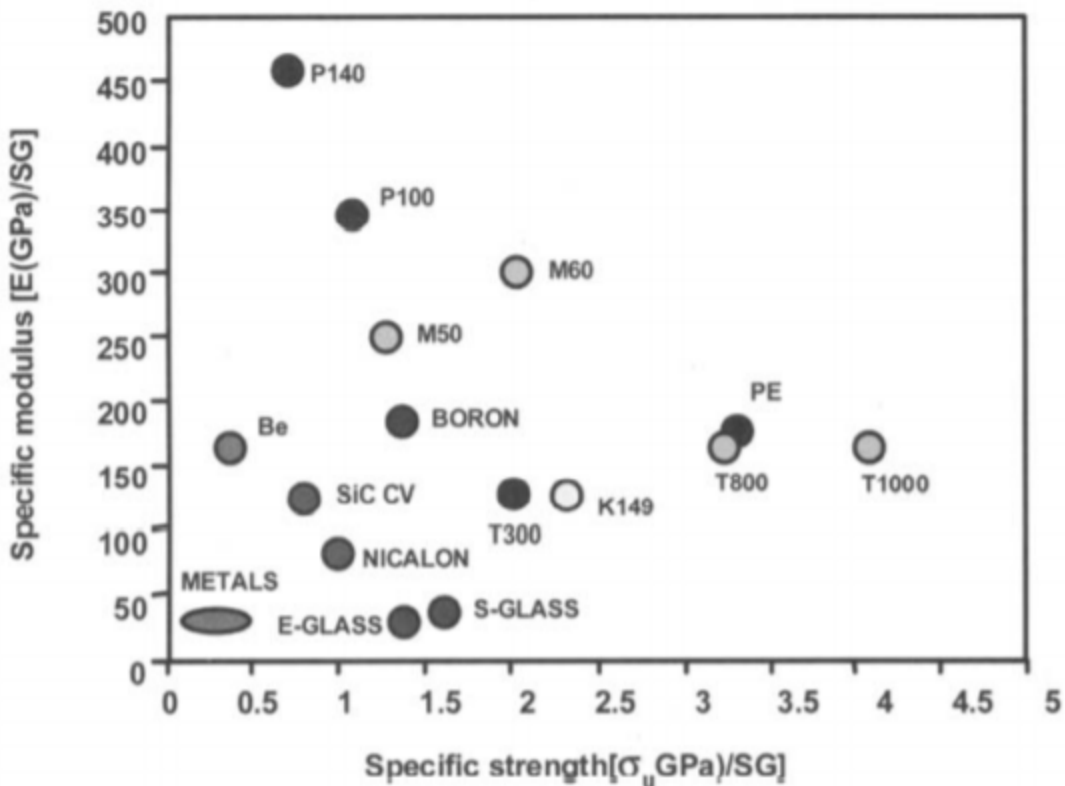


Figure 7.1: Aviation materials evaluated in specific modulus and strength. Source: [3]

Composites, apart from the obvious difference that imply (attend to the density difference with aluminium alloys from Table 4.1) in terms of weight, do have several interesting advantages which will be outlined now. The considerable weight reduction exhibits more ability to increase the range, decrease of fuel needed (up to 15- 20% according to [3]), higher capacity of carrying payload and even better control of the aircraft. Moreover, there's also a significant enhancement of the aerodynamic performance of the aircraft as smoother and finer shapes can be achieved, the aeroelastic properties of the composite material can be seized and specially for military aircrafts, the composite materials do not produce a so evident mismatch with the electric field irradiated by radars hence they are not so easily detected.

However, there are also several withdraws of composites when they are contrasted with the aluminium alloys used for aerospace means. They suppose an initially higher cost, and attending the RD of new materials, there's a huge cost per certification of new composition. In terms of mechanical behaviour that is what is mainly evaluated in this document, there have been seen overall less resistance to mechanic forces and also less resistance to high temperatures.

## **7. Appendix**

---

As it is known, the composite materials do entail a combination of a matrix or base material in which the fibers penetrate and are held. Attending to the effects of both components, it has been seen that the best results are obtained when strong and stiff fibers are merged with a weaker, flexible matrix, which does not provide excessive fragility.

One of the best compositions that can be used as matrix is the epoxy, as it exhibits outstanding mechanical features, merges good with fibers and finally does not possess excessive shrinkage in the operation. This is due to the fact that -according to [3] the composite material inherits from matrix element features of: temperature and environmental resistance, and strengths of longitudinal compression, transverse tensile and shear rather than from the fibers. Attending to the fibers (Carbon, Glass, etc), the final behaviour of the composite will be defined. Here, we will evaluate the influence of the Carbon, S-Glass and E-Glass fibers to the mechanical behaviour of the material.

### **7.2.2.1 Epoxy-Carbon UD**

The Carbon Fibers used for the reinforcement of the Epoxy composite materials are logically produced by submitting organic compounds (Polyacrylonitrile, PAN, specifically used in most of Epoxy-Carbon materials of aerospace) into a carbonization process. In it, according to [65] the aromatic rings are transformed into the monomer of hexagonal pattern of carbons distributed along basal sheets, then it is a two-dimensional predominant structure. The bonding between the layers are subject to weak Van der Waals forces and therefore the derived properties of the carbon fibers. Depending on the objective of the fiber and the mechanical properties, three types of carbon fibers can be distinguished: High modulus (or Type I), high strength (type II) or intermediate properties between both (type III).

The overall characteristics of this reinforcement is to provide high stiffness, high tensile strength, high protection against chemical agents and good behaviour against a wide range of temperatures. According to [15], carbon reinforced composites have higher strength and stiffness ratios (dimension-less by the weight) than the conventional aluminium alloys, which is consistent with [66] and with the results obtained. In the same manner, they possess higher fatigue strength and resistance to corrosion than conventional metallic alloys. They are also light which makes them ideal for many structural purposes, especially in environments such as motorsport and aeronautics where the optimization of the structure prevails before the relatively high economic expense. Compared to Glass Fibers, they tend to be more expensive. The mechanical differences between both can be seen in Table 4.1.

## 7. Appendix

---

### 7.2.2.2 Epoxy-Glass

Glass fibers are mainly composed and based by the silica ( $SiO_2$ ) material, offering overall high strength at a relatively low cost. Between the Epoxy Glass fibers, the dominant are Epoxy E-Glass and Epoxy S-Glass, which will be detailed in the following lines.

The Epoxy E-Glass stands for "Electrical", as it presents high electric permeability whilst holding a low value of dielectric constant. It is used for most common structural applications due to its high strength, up to 3.5 GPa after the manufacturing process, in which it is appreciatively decreased. It is composed by calcium-aluminium-borosilicate in the following approximate proportions in percentage (Si: 53 %,  $Al_2O_3$ : 14%, CaO: 18%,  $B_2O_3$ :10, MgO:5%, and other minor oxides ). Nevertheless, a recent form of calcium-aluminium-silicate has been developed in order to suit the material with higher resistance to chemical agents. The fiber diameters usually take place between 5 and 20  $\mu m$ .

In the other hand, the Epoxy S-Glass is known for its "High Strength", from where it derives its S. Its value rises up to 4.6 GPa, which is an improvement of 31.42 % respectively to the Epoxy E-Glass. This is why it is used for the most demanding structural applications, in which the aerospace sector is included. Apart from the enhancement of strength, it is a little bit more stiff, although this additional stiffness is achieved at a relatively high cost. Finally, a better resistance against high temperatures is sighted. This is why, it is rather used for the aircraft surface. It is made up by magnesium alumino-silicate, with the approximate proportions of the compounds (Si: 65%,  $Al_2O_3$ : 25%, MgO:10%). These material, as a consequence of its extraordinary mechanical properties, has been more researched than the E-Glass ([14]).

## **7. Appendix**

---

### **7.3 Appendix 3: Wing Drawings (Julio)**

This appendix includes the drawings of the CAD designed by the authors of this investigation, which includes the assembled and the individual parts of the wing.

1

2

3

4

D

D

C

C

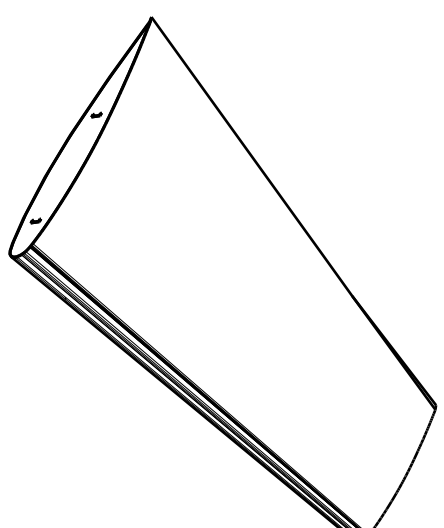
A

B

1196.3

805.9

0°



This drawing is our property.  
It can't be reproduced  
or communicated without  
our written agreement.

## Cranfield University

DRAWING TITLE

Onera M6 Wing - Assembly

DATE

DRAWN BY

Julio Maldonado

DATE

CHECKED BY

DATE

DESIGNED BY

DATE

DATE

SCALE

SIZE

REV

WEIGHT (kg)

SHEET

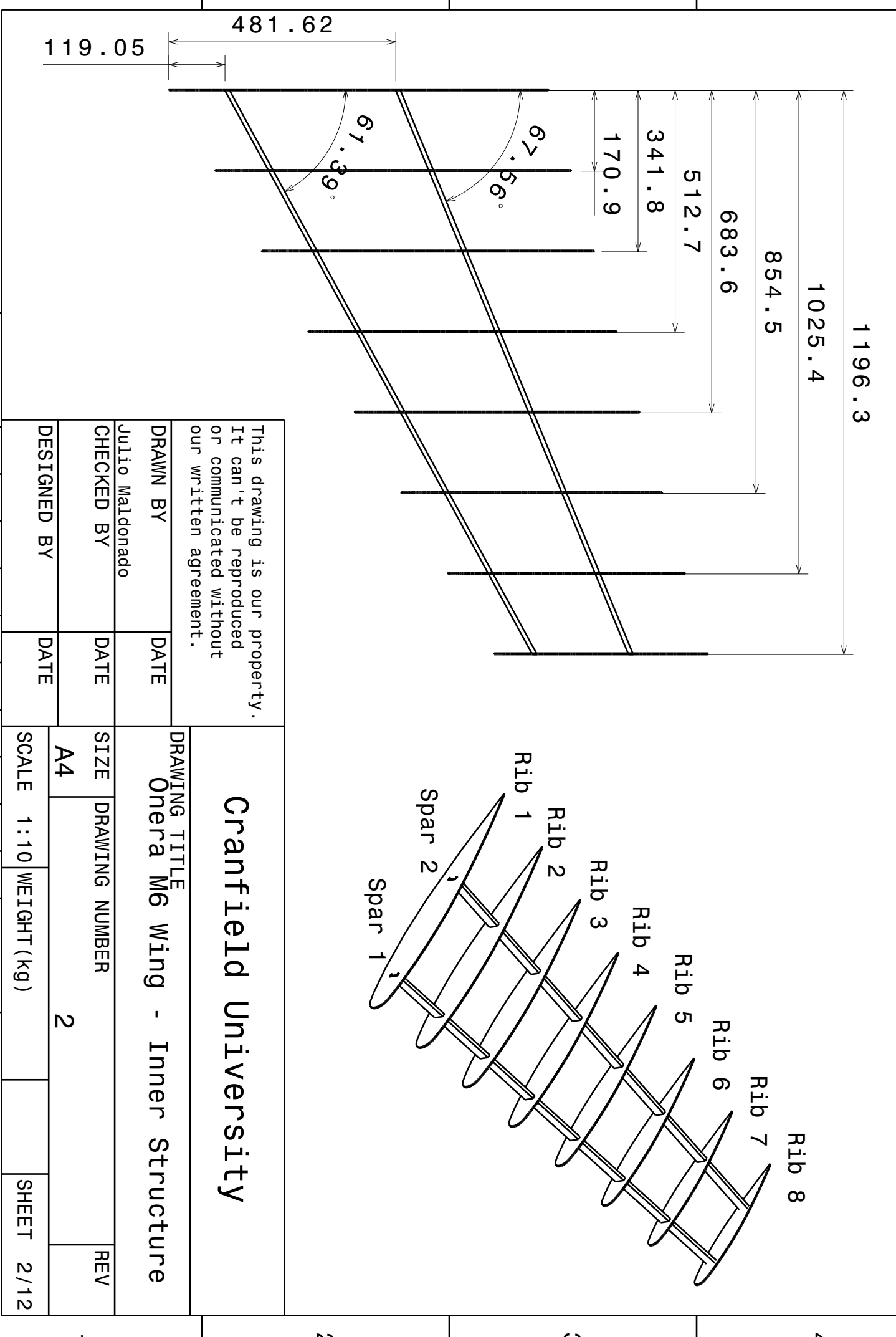
1 / 12

1

2

3

4



1

2

3

4

D

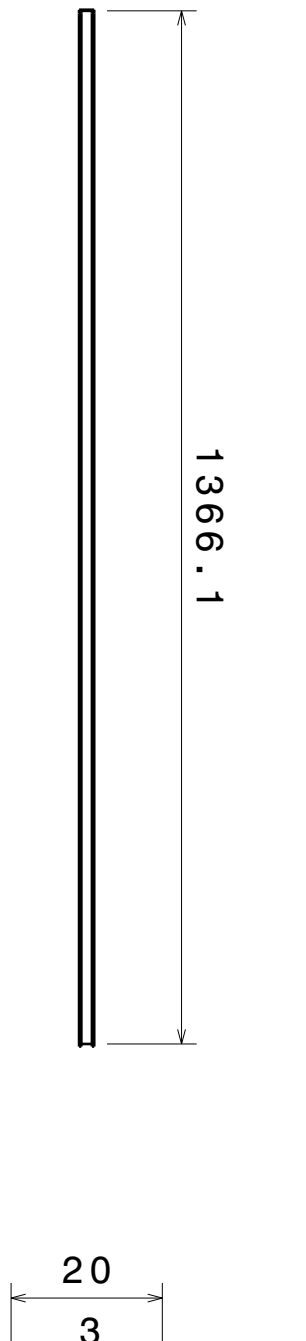
D

C

B

A

Left view  
Scale: 1:1



This drawing is our property.  
It can't be reproduced  
or communicated without  
our written agreement.

## Cranfield University

DRAWING TITLE  
Onera MG Wing - Spar 1

DRAWN BY	DATE	DRAWING NUMBER		REV
Julio Maldonado				
CHECKED BY	DATE	SIZE	SCALE	WEIGHT (kg)
		A4	1:10	
DESIGNED BY	DATE			SHEET 3 / 12

A

1

2

3

4

1

2

3

4

D

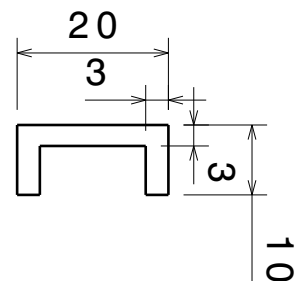
D

C

B

A

1297.52



Left view  
Scale: 1:1

This drawing is our property.  
It can't be reproduced  
or communicated without  
our written agreement.

## Cranfield University

DRAWING TITLE      Onera M6 Wing - Spar 2

DRAWN BY	DATE	DRAWING NUMBER		REV
Julio Maldonado				
CHECKED BY	DATE	SIZE		
		A4	4	
DESIGNED BY	DATE	SCALE	WEIGHT (kg)	SHEET
		1:10		4 / 12

A

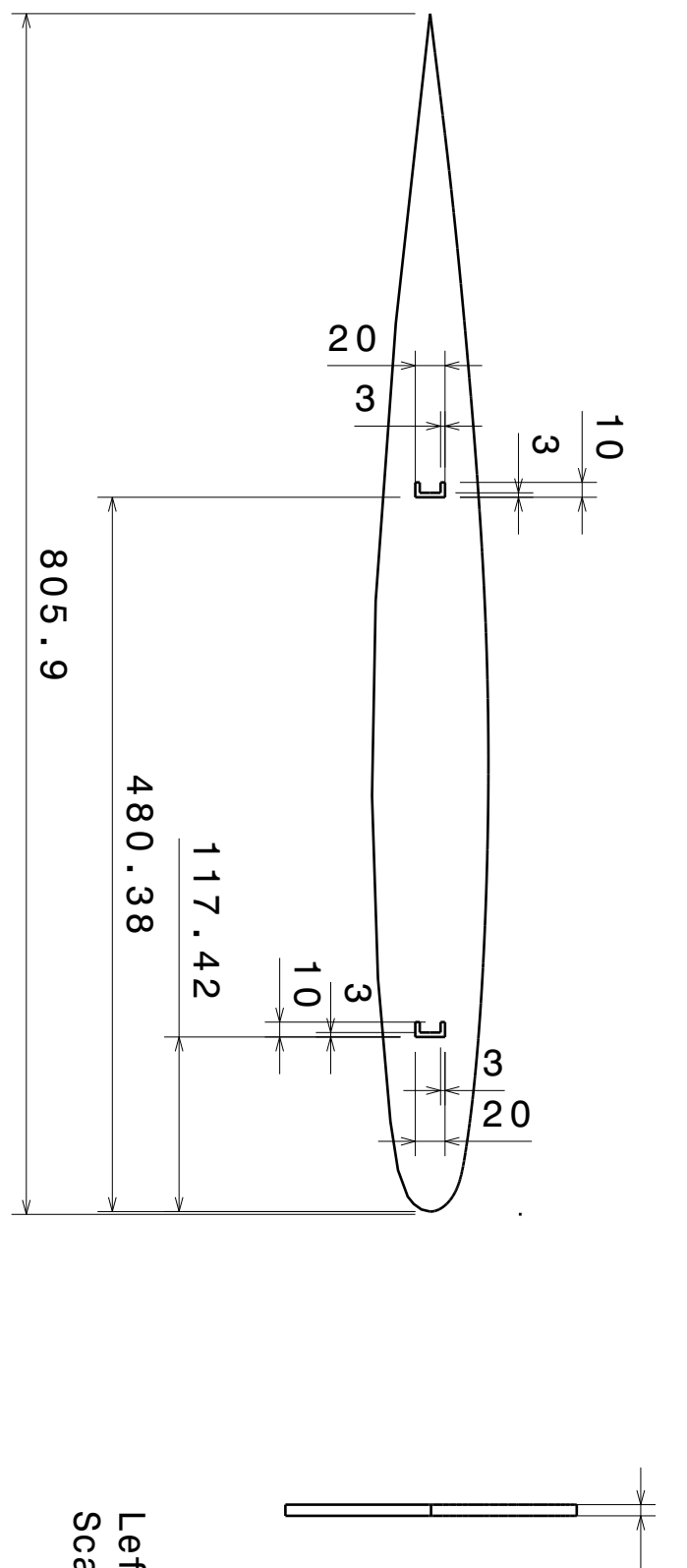
2

3

4

1

This drawing is our property. It can't be reproduced or communicated without our written agreement.	
<b>Cranfield University</b>	
DRAWN BY	DATE
Julio Maldonado	
CHECKED BY	DATE
DESIGNED BY	DATE



Left view  
Scale: 1:2

DRAWING TITLE      Onera M6 Wing - Rib 1

DATE

117 . 42

DATE

480 . 38

DATE

805 . 9

DATE

10 / 12

DATE

1 : 5

DATE

WEIGHT (kg)

SIZE

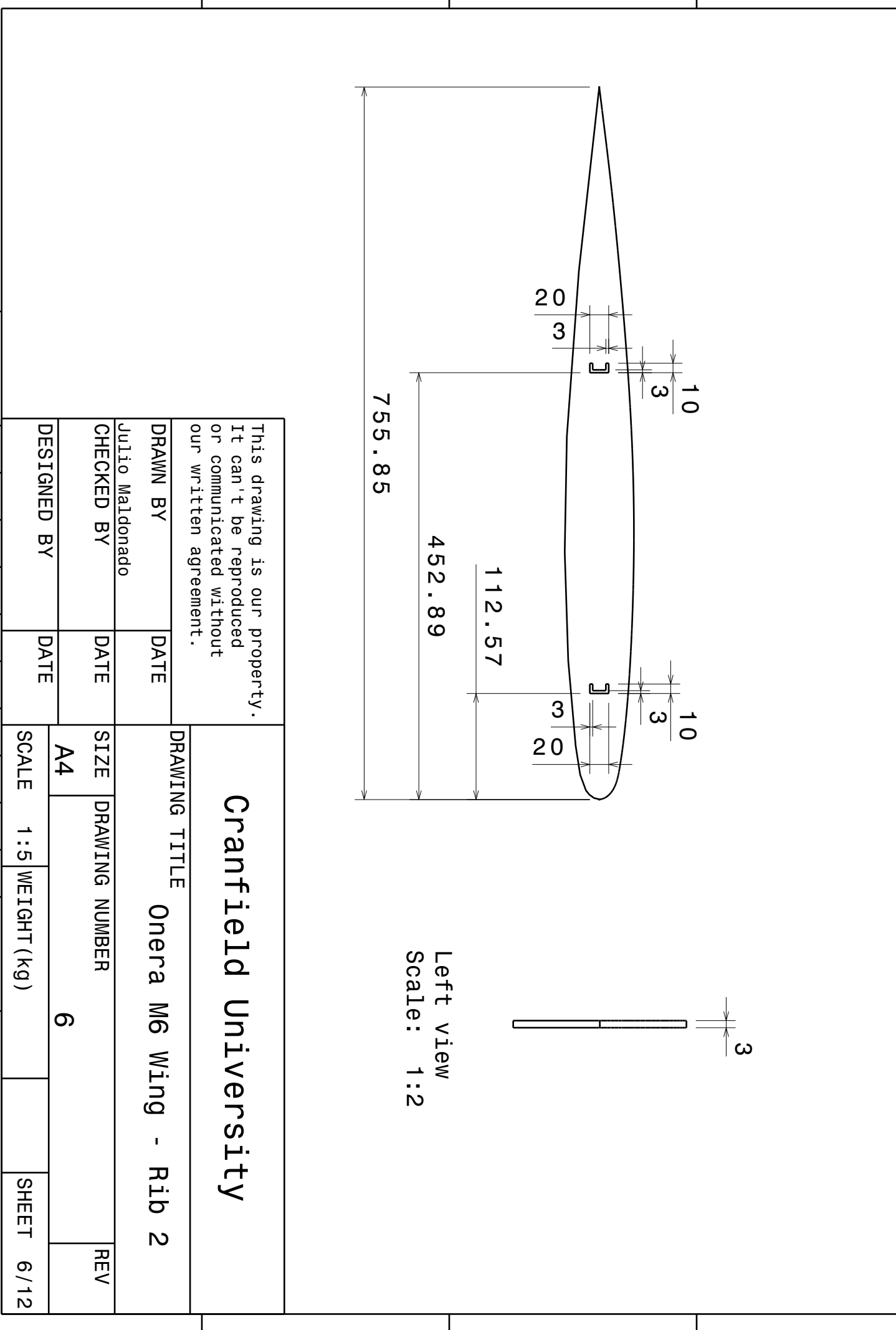
A4

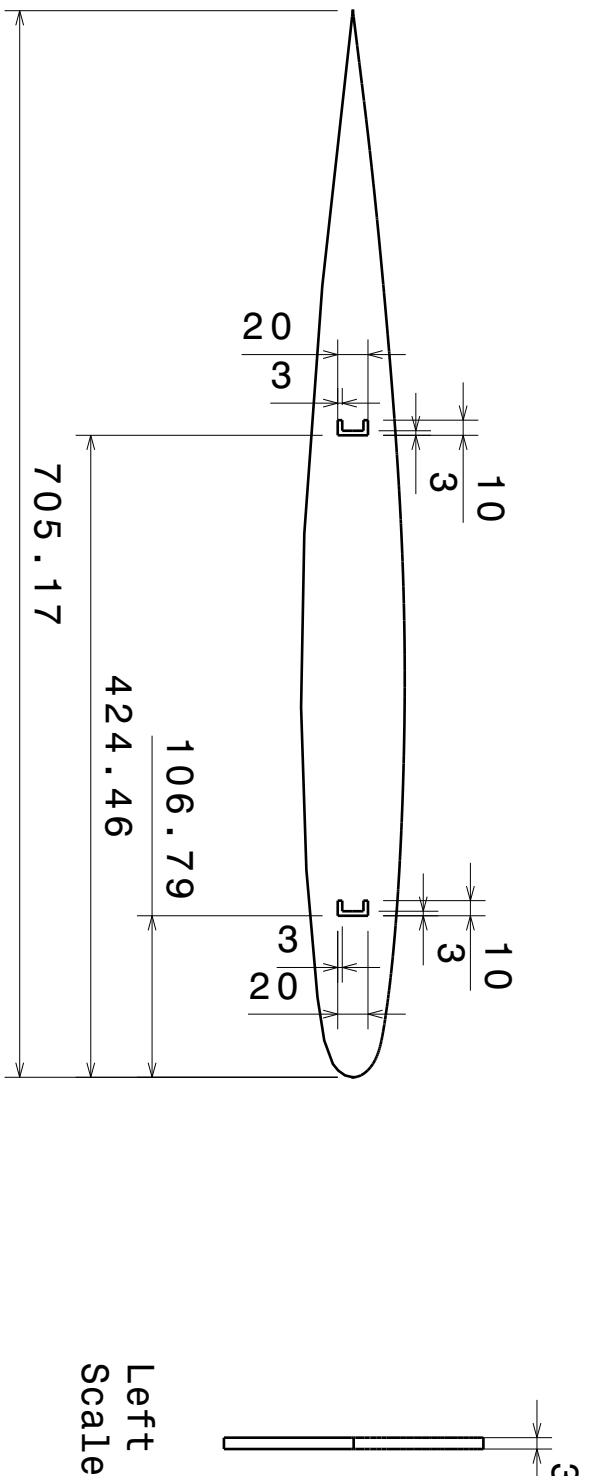
DRAWING NUMBER

5

REV

5 / 12





This drawing is our property.  
It can't be reproduced  
or communicated without  
our written agreement.

## Cranfield University

DRAWING TITLE      Onera M6 Wing - Rib 3

DRAWN BY      Julio Maldonado

DATE

SIZE

DRAWING NUMBER

7

REV

1:5

WEIGHT (kg)

SHEET 7/12

DESIGNED BY

DATE

SCALE

1

D

2

1

3

4

D

C

B

A

1

2

3

4

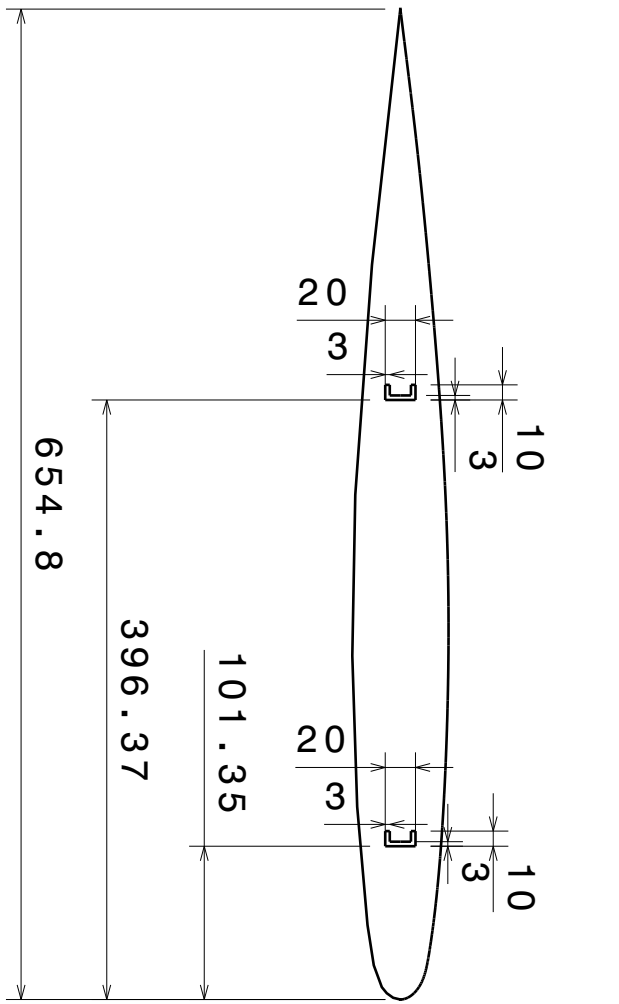
D

D

C

B

A



Left view  
Scale: 1:2

This drawing is our property.  
It can't be reproduced  
or communicated without  
our written agreement.

## Cranfield University

DRAWING TITLE      Onera M6 Wing - Rib 4

DRAWN BY      Julio Maldonado

DATE

CHECKED BY

DATE

DESIGNED BY

DATE

REV

SCALE

SHEET

WEIGHT (kg)

8 / 12

A

2

3

4

1

1

2

3

4

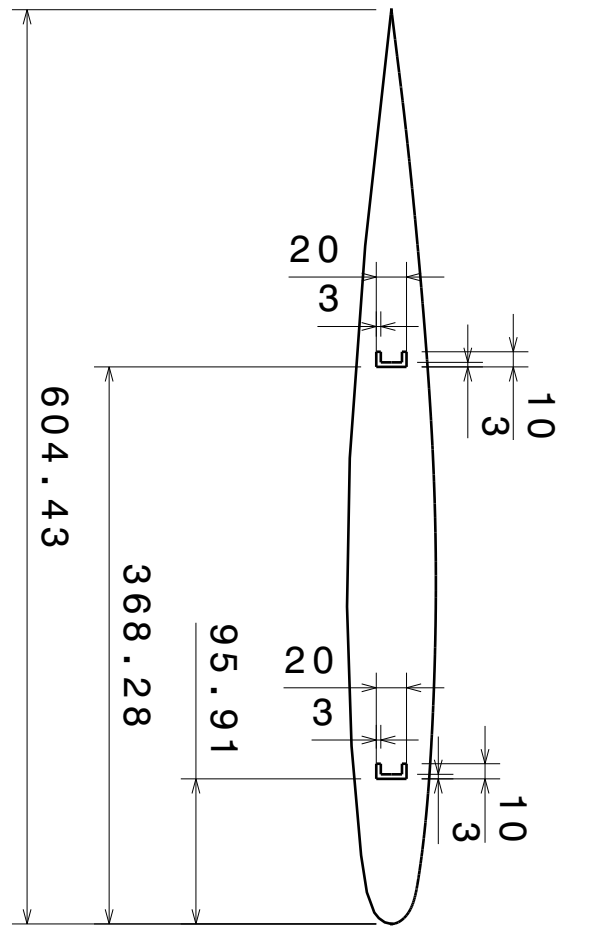
D

D

C

B

A



Left view  
Scale: 1:2

This drawing is our property.  
It can't be reproduced  
or communicated without  
our written agreement.

## Cranfield University

DRAWING TITLE      Onera M6 Wing - Rib 5

DRAWN BY	DATE	DRAWING NUMBER		REV
Julio Maldonado				
CHECKED BY	DATE	SIZE	SCALE	WEIGHT (kg)
		A4	1:5	
DESIGNED BY	DATE			SHEET 9/12

1

2

3

4

1

2

3

4

D

D

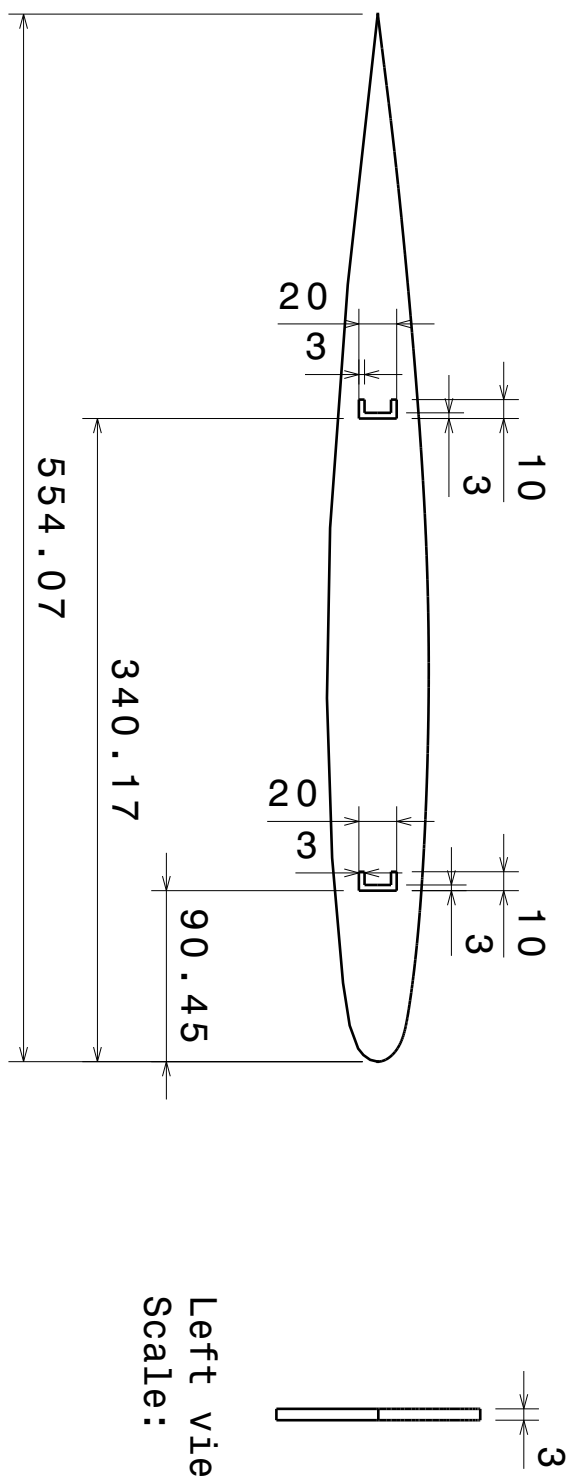
C

C

A

B

A



This drawing is our property.  
It can't be reproduced  
or communicated without  
our written agreement.

## Cranfield University

DRAWING TITLE      Onera M6 Wing - Rib 6

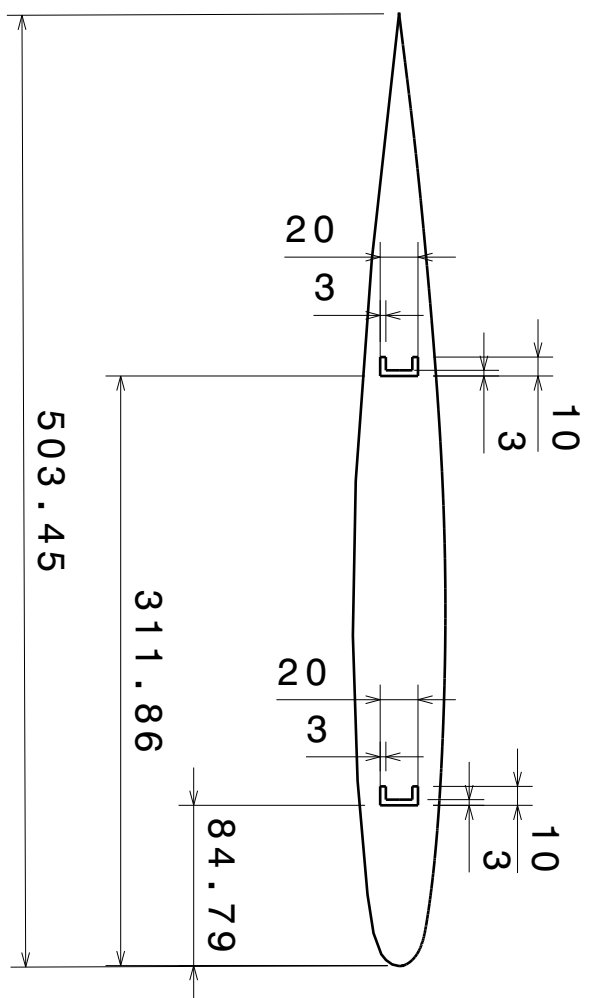
DRAWN BY	DATE	SIZE	DRAWING NUMBER	REV
Julio Maldonado		A4	10	
CHECKED BY	DATE	SCALE	WEIGHT (kg)	SHEET 10/12
DESIGNED BY		1:4		

1

2

3

4



Left view  
Scale: 1:2

This drawing is our property.  
It can't be reproduced  
or communicated without  
our written agreement.

## Cranfield University

DRAWING TITLE      Onera M6 Wing - Rib 7

DRAWN BY	DATE	SIZE	DRAWING NUMBER	REV
Julio Maldonado		A4	11	
CHECKED BY	DATE	SCALE	WEIGHT (kg)	SHEET 11 / 12
DESIGNED BY	DATE	1:4		

D

2

1

3

4

D

C

B

A

